UNIVERSITAT DE BARCELONA

Peptide functionalized polymeric nanocarriers: Towards selective targeting of prostate cancer

Madhura Murar

ADVERTIMENT. La consulta d'aquesta tesi queda condicionada a l'acceptació de les següents condicions d'ús: La difusió d'aquesta tesi per mitjà del servei TDX (**www.tdx.cat**) i a través del Dipòsit Digital de la UB (**diposit.ub.edu**) ha estat autoritzada pels titulars dels drets de propietat intel·lectual únicament per a usos privats emmarcats en activitats d'investigació i docència. No s'autoritza la seva reproducció amb finalitats de lucre ni la seva difusió i posada a disposició des d'un lloc aliè al servei TDX ni al Dipòsit Digital de la UB. No s'autoritza la presentació del seu contingut en una finestra o marc aliè a TDX o al Dipòsit Digital de la UB (framing). Aquesta reserva de drets afecta tant al resum de presentació de la tesi com als seus continguts. En la utilització o cita de parts de la tesi és obligat indicar el nom de la persona autora.

ADVERTENCIA. La consulta de esta tesis queda condicionada a la aceptación de las siguientes condiciones de uso: La difusión de esta tesis por medio del servicio TDR (**www.tdx.cat**) y a través del Repositorio Digital de la UB (**diposit.ub.edu**) ha sido autorizada por los titulares de los derechos de propiedad intelectual únicamente para usos privados enmarcados en actividades de investigación y docencia. No se autoriza su reproducción con finalidades de lucro ni su difusión y puesta a disposición desde un sitio ajeno al servicio TDR o al Repositorio Digital de la UB. No se autoriza la presentación de su contenido en una ventana o marco ajeno a TDR o al Repositorio Digital de la UB (framing). Esta reserva de derechos afecta tanto al resumen de presentación de la tesis como a sus contenidos. En la utilización o cita de partes de la tesis es obligado indicar el nombre de la persona autora.

WARNING. On having consulted this thesis you're accepting the following use conditions: Spreading this thesis by the TDX (**www.tdx.cat**) service and by the UB Digital Repository (**diposit.ub.edu**) has been authorized by the titular of the intellectual property rights only for private uses placed in investigation and teaching activities. Reproduction with lucrative aims is not authorized nor its spreading and availability from a site foreign to the TDX service or to the UB Digital Repository. Introducing its content in a window or frame foreign to the TDX service or to the UB Digital Repository is not authorized (framing). Those rights affect to the presentation summary of the thesis as well as to its contents. In the using or citation of parts of the thesis it's obliged to indicate the name of the author.

Doctoral thesis

Peptide functionalized polymeric nanocarriers: Towards selective targeting of prostate cancer

Author:

Madhura Murar

Thesis co-supervisors:

Dr. Lorenzo Albertazzi & Dr. Sílvia Pujals Riatós

Barcelona, 2022

UNIVERSITAT DE BARCELONA

Tesis doctoral

Peptide functionalized polymeric nanocarriers: Towards selective targeting of prostate cancer

Programa de doctorado en Nanociencias

Autora:

Madhura Murar

Directores:

Dr. Lorenzo Albertazzi & Dra. Sílvia Pujals Riatós

Tutor:

Dr. Josep Samitier Martí

Barcelona, 2022

UNIVERSITAT DE BARCELONA

Tesi doctoral

Peptide functionalized polymeric nanocarriers: Towards selective targeting of prostate cancer

Memòria presentada per optar al grau de doctor per la Universitat de Barcelona

Programa de doctorat en Nanociencias

Autora:

Madhura Murar

Directors:

Dr. Lorenzo Albertazzi & Dra. Sílvia Pujals Riatós

Tutor:

Dr. Jose Samitier Martí

Barcelona, 2022

UNIVERSITAT DE BARCELONA

¨In the end, it’s the journey that matters, not the destination¨

-Greg Anderson.

¨The key to success is not through achievement, but through enthusiasm¨

-Malcolm Forbes.

Table of Contents

ABSTRACT **8**

RESUMEN EN CASTELLANO **10**

CHAPTER 1| ACTIVE TARGETING OF CANCER NANOMEDICINES: ROLE OF CONTROLLED DESIGN OF SURFACE PARAMETERS FOR SELECTIVE CELLULAR UPTAKE **12**

1.1 THE LANDSCAPE OF CANCER NANOMEDICINE **13**

1.2 STRATEGIES FOR NANOMEDICINE TARGETING OF TUMORS 16

1.2.1 Passive tumor targeting *18*

1.2.2 Active tumor targeting *19*

1.3 IMPACT OF NANOMATERIAL PROPERTIES ON TUMOR TARGETING 21

1.3.1 An arsenal of surface ligands for active targeting *23*

1.3.2 Importance of surface characterization *30*

1.3.3 Interplay of different surface ligand parameters *33*

1.4 DUAL-LIGAND MEDIATED NANOPARTICLE TARGETING: TOWARDS SUPER-SELECTIVITY 35

1.4.1 Concept of super-selectivity in nanomedicine targeting *35*

1.4.2 Design principles for dual ligand mediated selective tumor targeting *38*

1.5 THESIS AIM AND CONTENTS 42

1.6 REFERENCES 44

CHAPTER 2| A QUANTITATIVE ASSESSMENT OF GE11 PEPTIDE-MEDIATED NP CONJUGATION STRATEGIES: IMPACT ON SELECTIVE EGFR TARGETING **60**

2.1 INTRODUCTION 60

2.2 RESULTS AND DISCUSSION 62

2.2.1 Pre- and post-GE11 conjugation strategies *62*

2.2.2 Pre-GE11 conjugation, NP formulation and characterisation *64*

2.2.3 Surface peptide quantification by specific enzymatic digestion *66*

2.2.4 EGFR expression and NP cytotoxicity analyses *68*

2.2.5 Pre- versus post-GE11 NP mediated cellular uptake by CLSM and flow cytometry *70*

2.3 CONCLUSIONS 73

2.4 EXPERIMENTAL SECTION 73

2.5 REFERENCES 79

CHAPTER 3| MULTIVALENT EFFECT OF WQP-PEPTIDE FUNCTIONALIZED 82

POLYMERIC NANOPARTICLES TOWARDS SELECTIVE PSMA TARGETING 82

3.1 INTRODUCTION 82

3.2 RESULTS AND DISCUSSION 84

3.2.1 Mono- and multivalent WQP formulation 84

3.2.2 WQP-Cy5 monomer synthesis, purification and characterization 85

3.2.3 Polymer-peptide conjugation, multivalent NP formulation and characterization 86

3.2.4 Quantification of WQP on NP surface by specific enzymatic degradation 88

3.2.5 Receptor expression and multivalent NP cytotoxicity analyses 90

3.2.6 Effect of mono- versus multivalent WQP-mediated uptake in PCa cell lines by CLSM and flow cytometry 92

3.3 CONCLUSIONS 94

3.4 EXPERIMENTAL SECTION 95

3.5 REFERENCES 100

CHAPTER 4| CO-OPERATIVE DUAL PEPTIDE-MEDIATED STRATEGY FOR SELECTIVE TARGETING OF PROSTATE CANCER 103

4.1 INTRODUCTION 104

4.2 RESULTS AND DISCUSSION 106

4.2.1 Design of dual-peptide NPs for selective targeting of prostate cancer 106

4.2.2 Evaluation of PSMA and EGFR expression across prostate cell lines 107

4.2.3 Characterization and optimization of dual-peptide NP surface valency for cooperative cellular uptake 108

4.2.4 Characterization and optimization of dual-peptide NPs having different surface ratios: Impact on cellular uptake 111

4.2.5 Establishing the targeting specificity and selectivity of dual-peptide NPs having different surface ratios by flow cytometry 113

4.3 CONCLUSIONS 115

4.4 EXPERIMENTAL SECTION 116

4.5 REFERENCES 120

CHAPTER 5| DISCUSSION 123

CONCLUSIONS 131

OUTLOOK 135

APPENDIX 1 ..... **138**

APPENDIX 2 ..... **144**

APPENDIX 3 ..... **149**

APPENDIX 4 ..... **156**

GLOSSARY **161**

ACKNOWLEDGEMENTS **163**

SCIENTIFIC ACTIVITY **165**

CURRICULUM VITAE **166**

Statement of Originality

The author of this thesis, Madhura Murar, hereby declares the contents of the thesis to be original and in compliance with the necessary ethical codes and good laboratory practices without containing plagiarism.

Signed:

26/09/22, Barcelona, Spain.

Abstract

Prostate cancer is one of the most frequently encountered malignancies, with 1.4 million new cases in the past year, marking the second leading cause of deaths in men worldwide. Although it is known to be treatable when diagnosed early, advanced stages of the disease often witness an overall increase in the incidence and mortality rates. Current treatment regimens beyond surgery include chemo/radiotherapies that are limited by many adverse effects because of non-specific targeting of cancer cells, reducing the overall quality of life.

One of the key goals of cancer nanomedicine is to offer localized delivery of therapeutic molecules, in an attempt to reduce serious toxicity profiles of existing therapies. However, it has had a poor clinical translation so far. While nanomaterials provide an excellent candidate for a safe and effective delivery system, their biological performance is heavily governed by different physicochemical properties, which require a comprehensive understanding and a

controlled design. Active nanoparticle targeting involves the functionalization of nanoparticles with targeting ligands such as antibodies, peptides, aptamers, among others to guide specific interactions with the diseased cells, leaving the healthy cells unaffected. It relies on a multitude of parameters, which if overlooked, pose several problems of low efficacy, safety, and overall performance. To this end, the properties of targeting ligands play a crucial role in the design of effective nanocarriers, and therefore call for thorough studies characterizing their potential at the nanoscale. However, there is currently a lack of robust techniques to assess and quantify the impact of surface parameters on imparting selectivity to nanoparticle targeting. Furthermore, the use of one ligand type for active cancer targeting often fails to provide sufficient selectivity, owing to the intrinsically heterogenous nature of the disease, limiting the success for clinical approval of targeted nanomedicines.

Within this context, we employ two cell targeting peptides having varying binding affinities for two known prostate cancer biomarkers using polymeric nanocarriers. Different surface ligand properties like affinity, avidity and multivalency are presented and explored using each of the peptides, with a view to enhance NP targeting selectivity. The role of different NP ligand conjugation methods is investigated, highlighting the importance of surface characterization in a controlled design. Finally, a dual peptide-based targeting platform is designed, and the role of surface ligand density and stoichiometric ratios is established and optimized for achieving maximum selectivity for targeting cells simultaneously overexpressing both target receptors. We believe that these new insights provide a platform for the development of smart nanocarriers for selective prostate cancer targeting, bringing us a step closer towards the long-lasting goal of precision nanomedicines.

Resumen en castellano

El cáncer de próstata es una de las neoplasias malignas más frecuentes, con 1,4 millones de nuevos casos en el último año, lo que marca la segunda causa principal de muerte en hombres en todo el mundo. Aunque se sabe que es tratable cuando se diagnostica temprano, las etapas avanzadas de la enfermedad a menudo son testigos de un aumento general en las tasas de incidencia y mortalidad. Los regímenes de tratamiento actuales más allá de la cirugía incluyen quimioterapia / radioterapias que están limitadas por muchos efectos adversos debido a la orientación inespecífica de las células cancerosas, lo que reduce la calidad de vida general. Uno de los objetivos clave de la nanomedicina contra el cáncer es ofrecer la administración localizada de moléculas terapéuticas, en un intento de reducir los perfiles de toxicidad graves de las terapias existentes. Sin embargo, ha tenido una mala traducción clínica hasta ahora. Si bien los nanomateriales proporcionan un excelente candidato para un sistema de administración seguro y efectivo, su rendimiento biológico se rige en gran medida por diferentes propiedades fisicoquímicas, que requieren una comprensión integral y un diseño controlado. La focalización activa de nanopartículas implica la funcionalización de nanopartículas con ligandos dirigidos como anticuerpos, péptidos, aptámeros, entre otros para guiar interacciones específicas con las células enfermas, dejando a las células sanas sin afectar. Se basa en una multitud de parámetros, que si se pasan por alto, plantean varios problemas de baja eficacia, seguridad y rendimiento general. Con este fin, las propiedades de los ligandos dirigidos desempeñan un papel crucial en el diseño de nanoportadores efectivos y, por lo tanto, requieren estudios exhaustivos que caractericen su potencial a nano escala. Sin embargo, actualmente hay una falta de técnicas robustas para evaluar y cuantificar el impacto de los parámetros de superficie en la impartición de selectividad a la orientación de nanopartículas. Además, el uso de un tipo de ligando para la focalización activa del cáncer a menudo no proporciona suficiente selectividad, debido a la naturaleza intrínsecamente heterogénea de la enfermedad, lo que limita el éxito de la aprobación clínica de nano medicamentos dirigidos.

En este contexto, empleamos dos péptidos dirigidos a células que tienen afinidades de unión variables para dos biomarcadores conocidos de cáncer de próstata utilizando nanoportadores poliméricos. Se presentan y exploran diferentes propiedades del ligando de superficie como la afinidad, la avidez y la multivalencia utilizando cada uno de los péptidos, con el fin de mejorar la selectividad de la orientación NP. Se investiga el papel de los diferentes métodos de conjugación NP-ligando, destacando la importancia de la caracterización de la superficie en un diseño controlado. Finalmente, se diseña una plataforma de orientación basada en péptidos duales, y se establece y optimiza el papel de la densidad del ligando de superficie y las relaciones estequiométricas para lograr la máxima selectividad para dirigirse a las células que sobre expresan simultáneamente ambos receptores objetivo. Creemos que estos nuevos conocimientos proporcionan una plataforma para el desarrollo de nanoportadores inteligentes para la orientación selectiva del cáncer de próstata, acercándonos un paso más hacia el objetivo duradero de las nanomedicaciones de precisión.

Chapter 1| Active targeting of cancer nanomedicines: Role of controlled design of surface parameters for selective cellular uptake

This chapter provides an introduction to active targeting of nanomedicines in the context of their role in treatment of cancer. It focuses on the impact of different surface ligands on their biological behavior and highlights the importance of their robust characterization. Finally, it introduces the dual ligand targeting strategy for selective targeting of tumors, as a path towards development of precision treatments.

Nanomedicine is an interdisciplinary field, which involves the interaction of nanotechnology, nanoengineering, and nanoscience with biomedical sciences. It has diverse applications primarily spanning from targeted drug delivery, development of diagnostics and therapeutics in a single system, also known as theranostics, to vaccine development[1]. Nanocarriers are essentially nanoparticles (NPs) that range between 1-100 nm in diameter and are predominantly used for the encapsulation and delivery of therapeutics, owing to their unique advantages over conventional medicines. These include i) improved pharmaceutical characteristics like better tumor accumulation, enhanced solubility and stability, and increased half-life of drug [2–6] ii) improved therapeutic efficacy and reduced toxicity [4,7–9] iii) codelivery of multiple drugs for enhanced efficiency and/or overcome drug resistance[10,11] and iv) selective delivery of drugs to target cells or tissues[12].

About four decades ago, the idea of application of nanocarriers for targeted drug delivery opened doors for a multitude of opportunities in the field of nanomedicine. This resulted in an evident surge in the number of publications in the field, ending up with the first clinically approved nanocarrier in 1995[13]. Over the years, the advantages of nanocarriers for drug delivery applications have been recognized in a wide range of fields, like cardiovascular diseases[14,15], infectious diseases[16], neurological diseases[17], etc. However, the potential applications of nanomedicine targeting have been most widely explored in the field of oncology[18–20]. As the main field of application focused on in this thesis is prostate cancer, the use of nanomedicines in the context of solid tumors will be discussed extensively in the upcoming sections.

1.1 The landscape of cancer nanomedicine

Cancer remains one of the main causes of mortalities globally[21], with its prevalence continually increasing due to increased life expectancy[22]. Furthermore, according to the global cancer survey by World Health Organization (2020), prostate cancer (PCa) marks the second

leading cause of cancer deaths in men worldwide[21]. This is predominantly caused by a lack of effective therapeutics to treat advanced stages of the disease, despite the recent advances in immuno- and gene therapy[18,23]. The clinical success of these emerging treatment regimens continues to be limited by multiple challenges, like non-specificity of drugs for tumors, their rapid clearance and degradation, and severely toxic side effects that are closely associated with cancer drug delivery[24–26]. Even though new targets and therapeutic modalities can advance cancer treatments, the dynamic nature of cancer allows it to persist[27]. Therefore, there is a need for a paradigm shift of anti-cancer strategies: from discovery of new therapies to improvement of existing ones in new, innovative, and plausible ways. The growing interest in the use of nanocarriers in anti-cancer strategies is largely attributable to their unique and appealing features for controlled drug delivery, diagnosis and imaging, development of synthetic vaccines and miniature medical devices as described earlier, along with the therapeutic potential of some NPs themselves[26,28–31]. In the context of PCa, the last decade witnessed a few nano formulations that entered preclinical and clinical trials[32–34], however, none of them have yet been approved[35,36].

The clinical translation of cancer nanomedicines dates to the mid-90s, when Doxil – a liposomal formulation of doxorubicin – was approved by the FDA for AIDS-related Kaposi sarcoma[13]. Ever since, this landscape has evolved steadily, with a substantial increase in the number of nano-based anti-cancer therapies and products for selective delivery, imaging and diagnostics entering the market in the recent years[20] (Figure 1.1). Most of these are nanocarriers of existing approved drugs, allowing for lesser time required by the regulatory agencies for their approval. Consequently, reduced toxicity over the free drug (e.g., Doxil and Abraxane encapsulating the cytotoxic chemo drugs Doxorubicin and Paclitaxel, respectively) has been the main clinical benefit of these formulation, in place of an improved efficiency. However, several formulations currently in clinical trials are showing promising results with enhanced efficacy, that are expected to receive regulatory approval[37].

An ever-evolving cancer nanomedicine landscape has allowed us to also gradually realize the challenges and opportunities that lie ahead[38,39]. Foremost, despite the translational potential of nanomedicines being recognized, there exists an extremely low number of approved NPs compared to the tremendous monetary investments made for pre-clinical studies, highlighting a crucial issue in the field. In the past decade, the interest in the field has grown significantly, as exemplified by increased number of publications from being roughly 100 per year to more than 5000 in 2021. However, this increase did not correlate linearly to an upturn in clinical translations[40]. This imbalance in investigations and clinically translated systems demonstrates the importance of identifying and overcoming the key bottlenecks limiting the nanomedicine application.

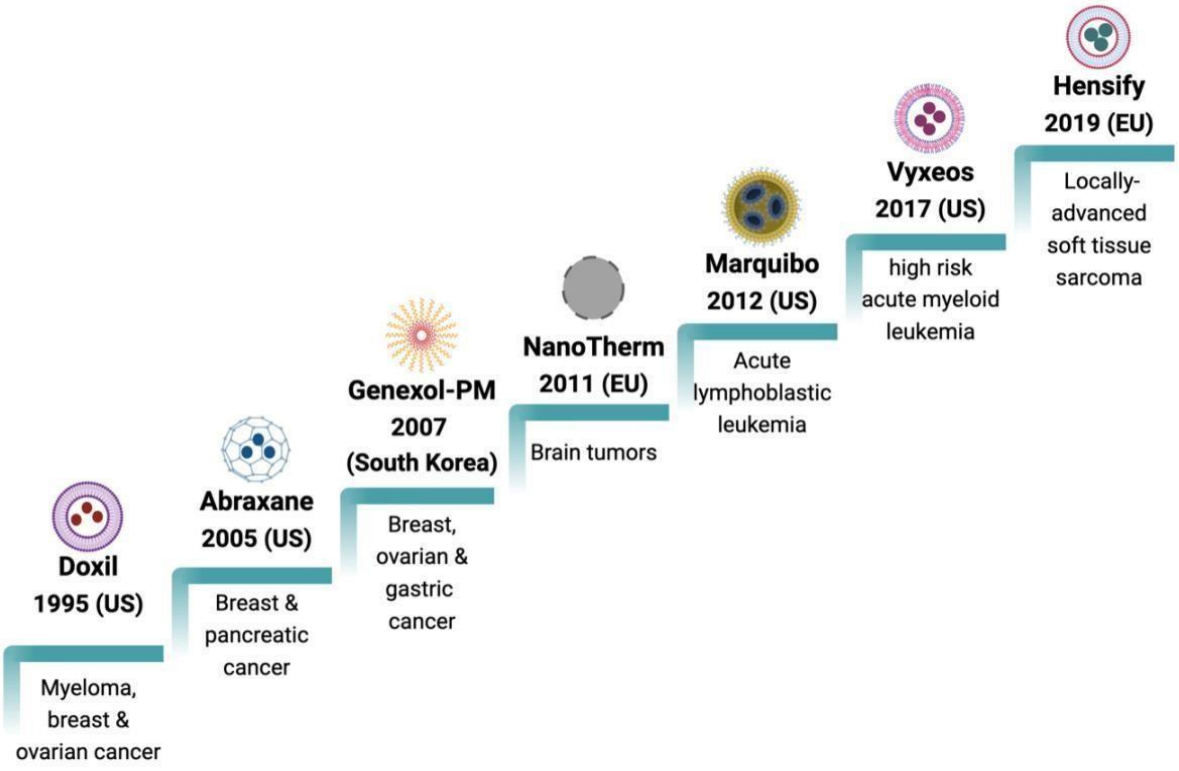

Figure 1.1 Evolution of the cancer nanomedicine landscape. *Historical timeline depicting the developments of different nano-formulated therapeutics approved in different parts of the world for clinical use against various types of cancers[20]. Created with Biorender.com.*

1.2 Strategies for nanomedicine targeting of tumors

In general, NPs can disperse both hydrophilic and hydrophobic drugs stably in aqueous conditions with no aggregation by allowing for efficient encapsulation[43]. Owing to their tunable physicochemical properties, such as size and surface charge, they can easily prolong the release of drugs, thus allowing sufficient time for the necessary therapeutic action. Notably, they also facilitate controlled release of drugs, which in some cases can be tailored to respond to specific stimuli such as pH, light, heat, or enzymes[44]. Even though there exist several different types of nanomaterials for targeted drug delivery applications, polymeric NPs are widely applicable due to their simple synthesis and the availability of extensive data regarding their efficacy and safety[43]. They can be either natural (e.g., proteins and glycans) or synthetic materials (e.g., poly(lactide) and polyesters) and can be formulated as polymeric NPs, micelles, polyplexes, polymersomes or polymer drug conjugates. Drug delivery is possible via different mechanisms, for example encapsulated in the core, in the polymer matrix or conjugated to the surface of the nanoparticle, allowing both hydrophobic and hydrophilic payloads to be used[43]. Thus, they make for ideal drug-delivery candidates owing to their biodegradability, solubility, biocompatibility, and malleable surface chemistries allowing for additional targeting[45].

The sites of drug administration and its consequent therapeutic action are usually quite distant from each other, laying foundation for the need for studies on targeted drug delivery. As described earlier, nanocarriers play a pivotal role in the targeted delivery of anticancer drugs. By the year 2021, there are around 15 cancer NP formulations on the market[20], and approximately 75 in pre-clinical and clinical trials[41]. The first clinically approved formulations

such as Doxil and Abraxane provide excellent examples of passively targeted NP systems that helped to improve therapy and patient outcomes[13,42]. In terms of tumor targeting capabilities of nanocarriers, they utilize two crucial processes, namely ´passive targeting´ and ´active targeting´[45,46], that facilitate their delivery specifically at the site of tumor and selectively inside cancerous cells as depicted in Figure 1.2. Subsequently, the intracellular trafficking of these nanocarriers is crucial for determining the fate of the cargo (drug) with regards to its processing and transportation.

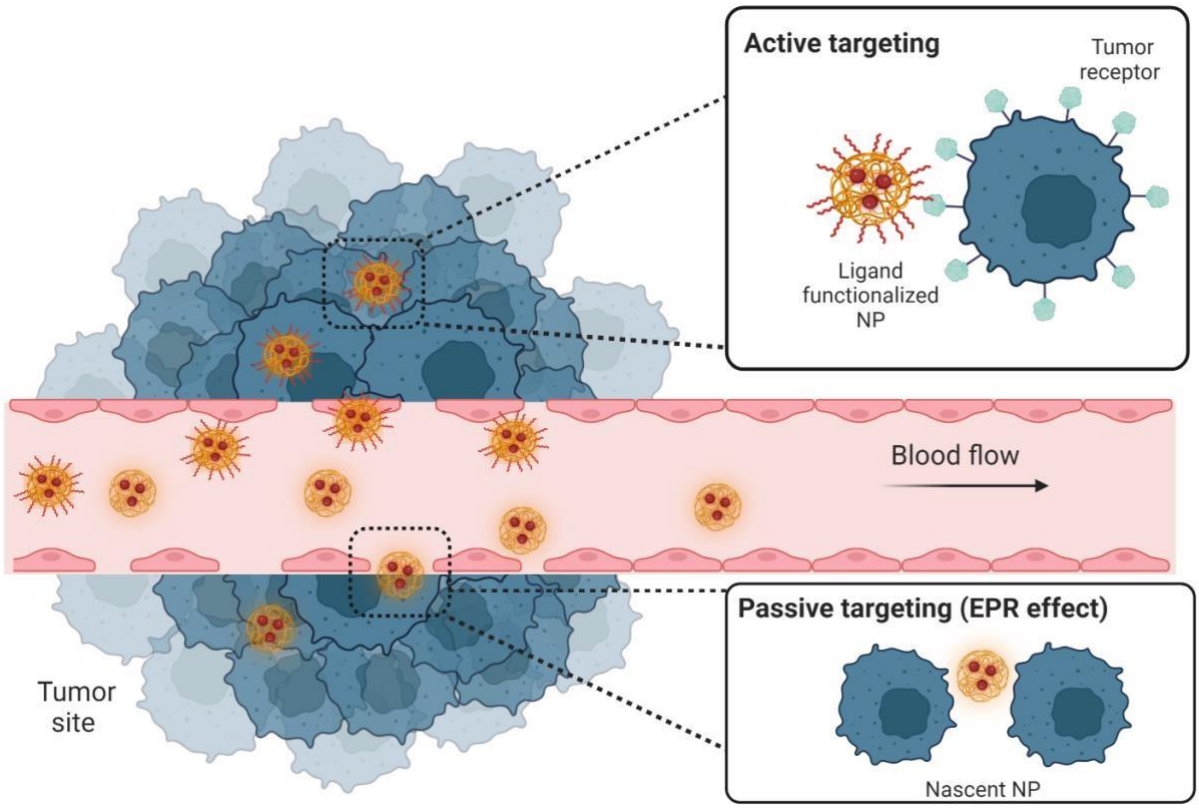

Figure 1.2 Nanomedicine targeting strategies. *Schematic representation of active and passive tumor targeting strategies for tumor targeting of nanomedicines. Figure adapted from the reference 1 and modified with Biorender.com. Copyright © 2017 American Chemical Society.*

1.2.1 Passive tumor targeting

As the name suggests, this type of targeting strategy involves ¨passive¨ accumulation of nanocarriers at the site of tumor, on account of a leaky vasculature, a phenomenon popularly known as enhanced permeability and retention (EPR). It was described by Maeda and coworkers in 1980s[47] and revolves around the fact that the tumor vasculature is morphologically defective. Normal blood vessels usually show presence of tight junctions between endothelial cells, causing restriction of molecular permeability. However, these structures are disrupted in case of tumor vessels due to rapid and abnormal angiogenesis during cancer progression, creating gaps (fenestrae) between endothelial cells with sizes varying from tenths of nm to few microns (~1.5 um)[48]. Owing to their sizes in the range of the endothelium fenestrations, nanocarriers can extravasate specifically to tumor sites whilst sparing the healthy tissues. There have been studies in animal models with solid tumors showing the ability of nanocarriers (up to 200 nm size range) to extravasate[49]. Additionally, the poor lymphatic drainage in the tumor microenvironment induces retention of the nanocarriers in the tissue. Overall, it is believed that the EPR effect favors the enhanced accumulation of NPs in the tumor site, thereby improving their therapeutic potential[50]. Despite passive targeting strategy in nanocarriers design has aided in lowering the side effects of the conventional therapies[51], the insufficient accumulation of NPs in solid tumors continues to pose a challenge. Even though the leaky tumor vasculature allows for extravasation, administered NPs do not penetrate sufficiently at the tumor site. Often, tumor blood vessels have irregular or obstructed blood flow, which further complicates drug delivery along with the presence of extracellular matrix (ECM) and intratumoral pressure[52]. Furthermore, studies with solid tumors from Chan et al recently found that up to 97% of NPs are transported by a transcytosis process by endothelial cells, rather than through inter-endothelial fenestrations, and also showed that the frequency of gaps between cells is too low to facilitate sufficient NP accumulation[53,54].These obstacles along with the significant heterogeneity of the EPR effect

among cancer patients, promote the investigation and development of more efficient targeting strategies[49].

1.2.2 Active tumor targeting

Active targeting strategy has been defined as the holy grail of targeted drug delivery using nanoparticulate systems[55,56], holding greater promise of facilitating specific cellular uptake of NPs, thus providing an improvement over the passive targeting approach. It involves decorating the NP surface with ligands that bind specifically to antigens or receptors found exclusively overexpressed on the surface of cancer cells, thereby directing them selectively to the tumor site[57]. This strategy is postulated to be the ¨magic bullet¨ to effectively distinguish between cancer cells and the healthy ones, consequently reducing the adverse effects of current treatments and provide precision therapies[58].

There exist multiple types of ligands that have been identified and explored for active targeting[59,60]. Often, these biological ligands have a strong binding affinity for specific receptors on target cells, which drives their specific uptake and increases therapeutic efficacy[59]. Depending on this affinity, in comparison to targeting solely with a weak-binding ligand, NPs allow for an increased valency of ligands which is beneficial for improving the binding and cellular uptake via the multivalency effect[61]. Several types of ligands have been employed for this purpose, including monoclonal antibodies (and their fragments), proteins and polysaccharides, nucleic acids, peptides, and small molecules[62–66], taking into account the characteristics of the target receptor (details discussed in in the next section). Targeting moieties can be functionalized to NPs using two main strategies: They can either be chemically conjugated or physically adsorbed on the NPs after formation of NPs[59]. Chemical conjugation involves covalent binding of ligands to the NP surface. It can be achieved either by direct

conjugation to active groups present on the NP surface (e.g., by maleimide-thiol chemistry) or to a surface-coating polymer linker like PEG[40,67,68].

The popularity of active targeting approach has led to a large number of studies dedicated in the past decade and by the year 2019, thirteen targeted nanomedicines are found in clinical trials[69]. Despite this, there has been no approved targeted formulation in the market so far[41,70]. The primary reason for this is attributed to the complexity of this strategy, which is not as straightforward as it was first proposed. The complexity primarily pertains to heterogeneities involved on two levels: One is the actual number of ligands that are available to interact with the target receptor, due masking of the ligands by adsorption of molecules in blood such as serum proteins, decreasing the efficiency of the targeting[71–73]. The other reason is due to heterogeneity at the receptor level, caused by ubiquitous expression of target receptors, making it undesirable for specific targeting[27,74]. More often than not, healthy cells also express the target receptors, albeit to a lesser extent, making it difficult for the active nanocarrier to differentiate the cancer cells. In addition, the heterogeneity of target receptor levels between different stages of cancer (intra-) and amongst patients (inter-) further complicates the possibility to optimize these carriers. These challenges revolving around clinical translation are currently raising a concerning question about the value of benefits provided by actively targeted nanomedicines in comparison to their non-targeted counterparts[35,75,76]. It is often seen that targeted nanomedicines tend to have positive outcomes at Phase I clinical trials because of their good safety profiles but almost always fail at Phase II trials due to unimproved clinical efficacy[41,77,78]. Recently, a critical analysis by Chan et al revealed that out of the 117 individual studies carried out using targeted nanomedicines, only a median of 0.7% of administered NPs were found to be accumulated at the site of the tumor[79]. When compared to their passively targeted counterparts, the targeting efficiency was only slightly increased from 0.6% to 0.9%. Furthermore, this efficiency showed no

improvements over a time span of a decade, thereby questioning the overall progress of the field.

The complex nature of nano-bio interactions still remains to be poorly understood, failing to provide their full-proof optimization for specific targeting. This further lays the conundrum of the magic bullet paradigm being oversimplified. Even though active targeting has been already implemented for some clinical applications like antibody-drug conjugates[80,81], use of bispecific antibodies[82], etc. the conjugation of targeting ligands to NPs provides an additional layer of complexity to the process. NPs are bigger, have distinct physicochemical properties depending on their material, and the number and accessibility of conjugated targeting ligands on their surface are not thoroughly characterized owing to a lack of specific methods thereof. In the next sections, the impact of different NP surface parameters on the active targeting efficiency is discussed in detail and certain methods that are being developed to promote super-selectivity are described.

1.3 Impact of nanomaterial properties on tumor targeting

As explained in the previous sections, the development and implementation of active NPtumor targeting strategy was prompted to overcome the intrinsic limitations of the conventional passive targeting strategies. However, the main obstacles to it becoming a new paradigm in cancer nanomedicine stem mainly from the complexity and heterogeneity involved with tumor biology, an inadequate understanding of nano–bio interactions and the challenges pertaining to NP surface chemistry, reproducibility of manufacturing and controls required for clinical translation and commercialization[26,45,50]. Thus, there is a clear need to uncover a more real picture of active targeting, and recent advances in the field are currently trending towards it.

The idealistic view of active targeted nanomedicines is rather different from the real one, primarily owing to the formation of protein corona, which is a ring-like formation caused by adsorption of serum protein around the NP surface, when it encounters the components in blood, in addition to the heterogeneities arising from the NPs themselves as well as the properties of the tumor environment[56]. Foremost, before arriving at the tumor site, targeted NPs are faced with numerous physiological barriers inside the body that they need to overcome[26,83,84]. At the cellular level, we know that the expression of target receptors is not a black and white condition: There exist inter- (cell-to-cell) and intra- (within the same cell) cellular heterogeneities in the expression levels of target receptors, translating into a difference of therapeutic efficiencies of the administered drug[85–87]. In addition, the inherent variability of spatio-temporal expression of the target receptor between patients adds another layer of complexity for choosing the right target[85,88,89], thereby limiting the overall clinical success of the nanomedicine[86,90]. At the NP level too, recent studies have demonstrated the inter- and intra- particle heterogeneities occurring in the size, charge, and number of targeting ligands between independent formulations and within the same NP batch, respectively[73,91]. The most important NP properties and its surface ligand parameters that influence its cellular binding, uptake and biodistribution are demonstrated in Figure 1.3.

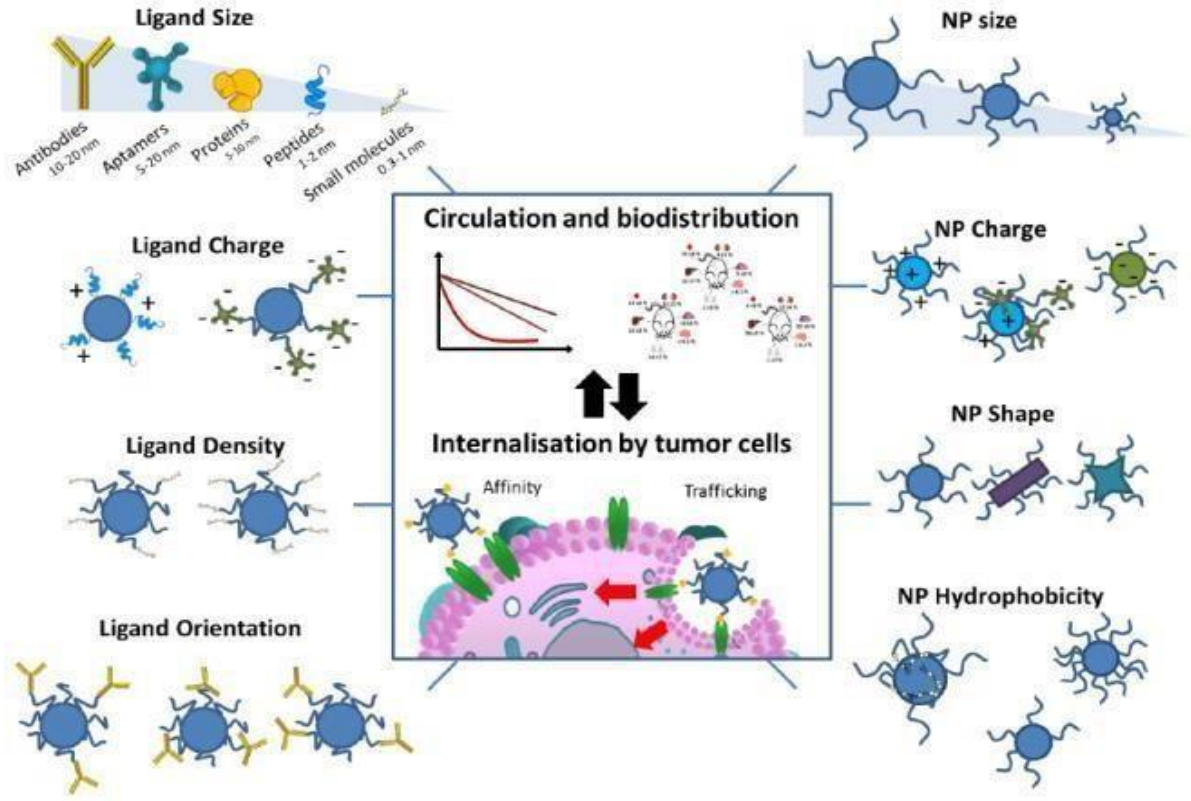

Figure 1.3 Properties of NPs and ligands affecting their biological function. *Schematic representation of key parameters of NPs and surface ligands that influence their biodistribution and cellular uptake. Reproduced from the reference 50. Copyright © 2013 Elsevier B.V.*

As such, the properties of NP itself (such as size, composition, shape, etc.) also have direct biological implications as explored extensively by Rabanel and colleagues[73], however, since that is beyond the scope of this thesis, the impact of NP surface properties, particularly, the types of ligands and their characterization, on their targeting potential are detailed in the following sections.

1.3.1 An arsenal of surface ligands for active targeting

Active targeting drug nanocarriers are the hope for more efficient anticancer therapy. As such, the choice of targeting ligand becomes a key characteristic in the design of NPs for selective

tumor targeting[62]. There exists an arsenal of different types of ligands that have been studied and explored extensively for active targeting applications. Figure 1.4 highlights the main ones, each with their own strengths and weaknesses, which must be consciously considered while making this choice.

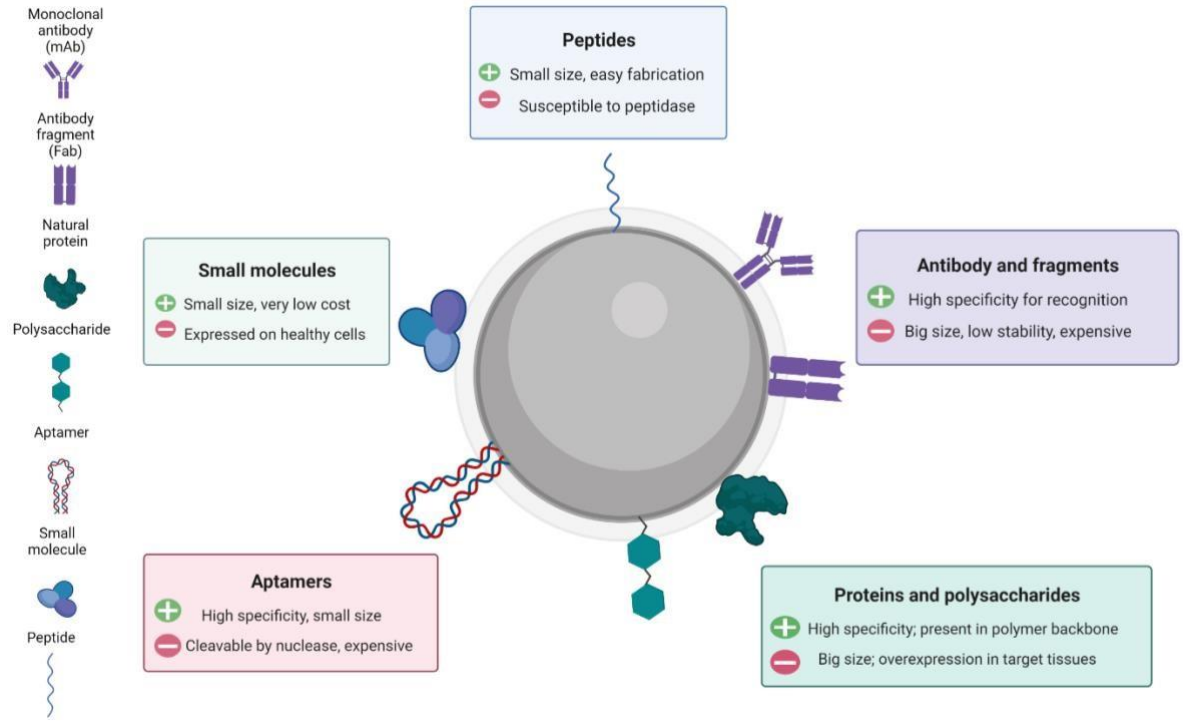

Figure 1.4 Types of surface ligands for active NP targeting. *Schematic representation of the various types of surface ligands used for active targeting of nanocarriers, enlisting their advantages and disadvantages. Figure adapted from 92 and modified using Biorender.com*

Monoclonal antibodies

One of the most widely studied biological ligands for active uptake of NPs are monoclonal antibodies (mAbs), owing to their strong binding affinity, specificity, and stability, thereby having the longest history with respect to targeting specific receptors[93]. A recent study involving anti-HER2 mAbs functionalized with PLGA NPs reported an elevated selective uptake in breast cancer (MDA-MB-453) cell lines in comparison to their bare NP counterparts and

negative control cell lines[94]. While antibodies are very useful molecules to improve specific NPs uptake, they are usually big in size, having molecular weights in tens of kilodaltons range (~150kDa), which poses a potential issue for their functionalization to smaller sized NPs (<10 nm)[93,95]. Therefore, the use of antibody antigen-binding fragments (Fabs) for active targeting with NPs is a viable alternative, as demonstrated by a recent study involving dual delivery of paclitaxel and everolimus encapsulated within PLGA-PEG NPs functionalized with anti-HER2 and anti-EGFR Fabs to selectively target breast cancer cells[96]. In addition, the generation of antibodies in animals further gives rise to potential ethical considerations, making them a less viable candidate for targeting[95].

Proteins and polysaccharides

The use of natural proteins that interact with cancer cell receptors is an alternative that has been widely explored, primarily owing to their high specificity and a ubiquitous presence in the polymer backbone, compared to monoclonal antibodies[62]. Among them, transferrin (Tf) is one of the most commonly used iron-binding glycoproteins that is responsible for iron transport in the body[97]. Recent studies employed active targeting of Tf-modified NPs in human epithelial cervical cancer and blood-brain-barrier, respectively[98,99]. In both cases, the results showed a remarkable increase in the cellular uptake of Tf-modified NPs and therapeutic delivery (release), highlighting the implications of using Tf as a biological ligand in other diseases. Employment of biomolecules to increase active uptake also includes the use of carbohydrates[62]. Among these, hyaluronic acid (HA) is the most explored one. It enhances the NPs uptake through its interaction with CD44 protein, which is often overexpressed on tumor cells and is also a known representative biomarker of cancer stem cells[100]. Recent studies by Li et al. employed the functionalization of HA to carbon dots loaded with doxorubicin to enhance their uptake in CD44 overexpressing 4T1 cells while competing with free HA[101].

Aptamers

Aptamers are a class of short nucleic acid sequences (DNA or RNA) consisting of many nucleotides. They are small, easy to synthesize, highly sensitive, biodegradable, less immunogenic, and relatively cheaper, making them good candidates for active targeting ligands over monoclonal antibodies[66]. They have a specific 3D structure with high binding specificity and affinity to target cancer cell receptors. A10 is a commercially available aptamer that is widely studied for active targeting of prostate specific membrane antigen (PSMA)[102], as demonstrated in a study involving the A10 aptamer and Dox, which were used for developing a polylactide nanoconjugate known as A10 Dox-PLA NCs (Figure 1.5). *In vivo* experiments showed a desirable safety profile, good tolerance post an intravenous infusion of a high-dose in mice, and no observed histological organ toxicity of A10 Dox-PLA NCs, on account of controlled drug release kinetics and selective tumor-associated endothelial cell targeting[103]. This highlights the utility of aptamer-functionalized NPs for active targeting of prostate cancer, which can be further explored for other cancer types.

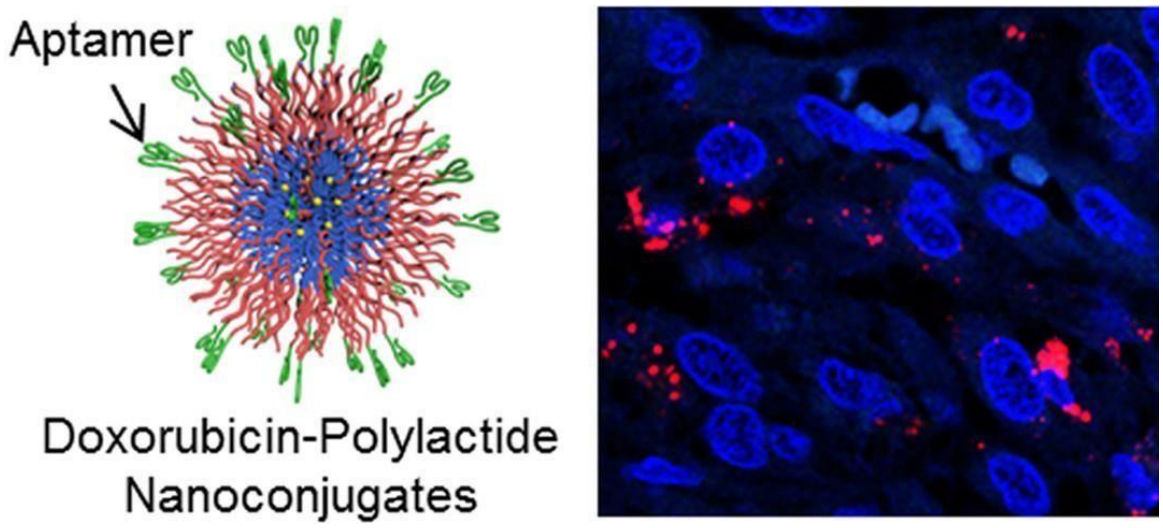

Figure 1.5 A10 aptamer conjugate for active PSMA targeting. *Schematic representation of A10 functionalized PLA-NCs and their selective uptake by PSMA expressing SB-HSA endothelial cells growing in SCID/ Beige mice. Reproduced from the reference 103. Copyright © 2015 American Chemical Society.*

Small molecules

In addition to the molecules already mentioned, certain small molecules have been useful for studying active uptake of NPs, primarily owing to their small size and low cost of production compared to monoclonal antibodies. Folate (FA) receptors are known biomarkers for certain solid tumor cells and macrophages, making them attractive targets for many active NP targeting studies[104–106]. Other examples of small molecules include anisamide (AA), which is a benzamide known to bind sigma-1 receptors overexpressed in cancer cells[107] and phenylboronic acid (PBA) which binds to sialic acid (SA) that is abundantly present on tumor cells[108]. Recent studies involved a successful investigation of these molecules[109,110], wherein the results showed high uptake levels of AA-functionalized NPs and PBA-NPs in HT-29 (sigma receptor positive) cells and HepG2 (SA positive) cells, respectively, emphasizing on the feasibility of these small molecules as active targeting ligands.

Peptides

Among targeting ligands discussed so far, peptides offer a viable alternative, having several advantages such as small size, low cost of production, good stability, low immunogenicity, and ease of conjugation to the surface of NPs at a high density[111]. Indeed, cell targeting peptides (CTPs) are selected by screening the libraries of phages displaying different binding sequences from proteins and isolating those with highest binding affinities using threedimensional (3D) structural analysis[95].

One of the most studied CTPs for active targeting is the small peptide GE11 (sequence: YHWYGYTPQNVI), which is known to bind with high affinity to EGFR, overexpressed in different tumor types (Figure 1.6)[112]. A recent study involved functionalizing this peptide to a micelle and encapsulating evodiamine (GE11-Evo-NPs) to enhance the selective uptake of the drug in colorectal cancer cells *in vivo*[113]. Prior studies involving the GE11 tagged PLGA-PEG NPs successfully showed not only their enhanced cellular uptake over non-tagged NPs in breast cancer cells[114], but also their smart potential to deliver hydrophilic drugs, which otherwise pose many challenges for effective delivery, selectively to lung cancer cells[115], highlighting their importance in the design of smart delivery systems.

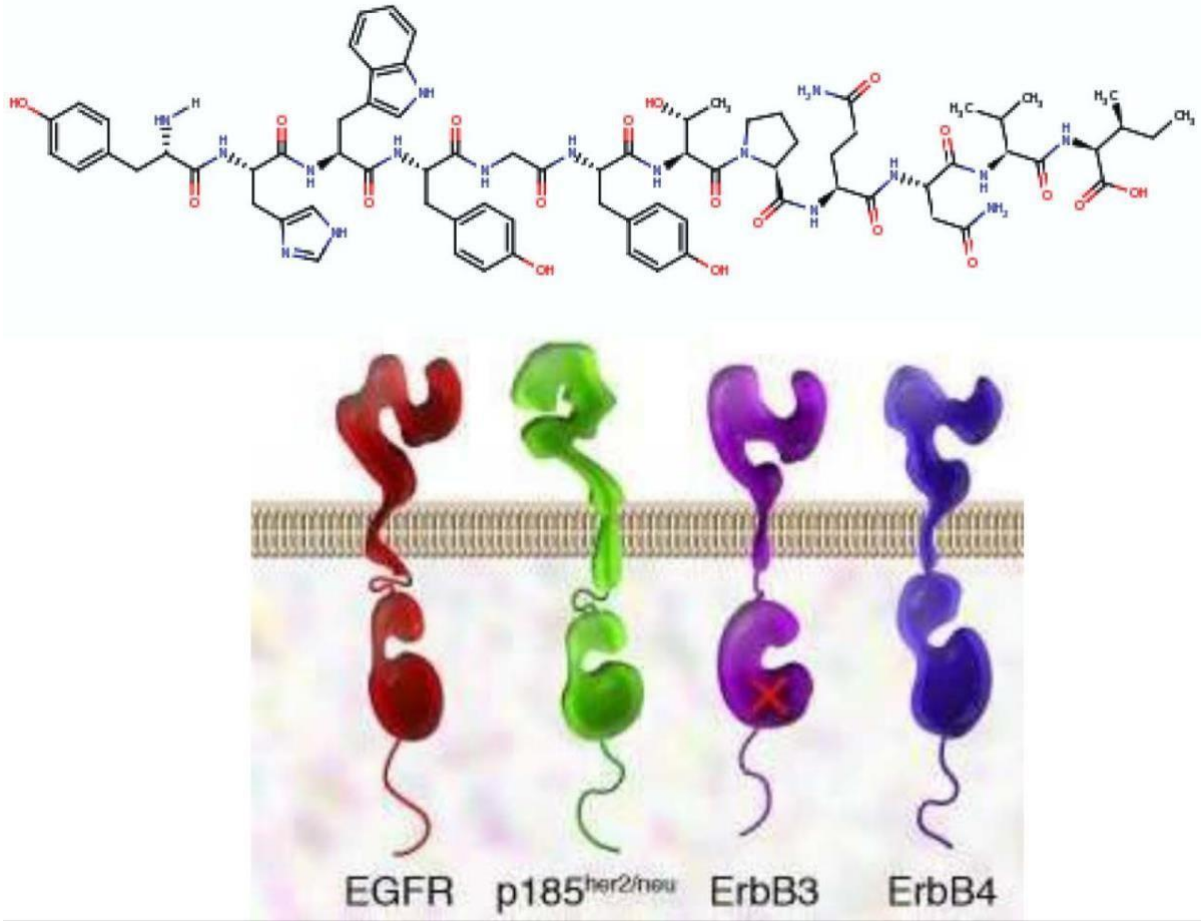

Figure 1.6 GE11 peptide as a targeting agent for EGFR. *Chemical structure of GE11 peptide and schematic representation of its target EGF receptor. Reproduced from the reference 112. Copyright © 2017 by Genta et al.*

Although there exists a myriad of studies employing the active targeting potential various CTPs on account of their strong target receptor binding affinities, their clinical translation has not yet been successful[116], primarily owing to the heterogeneities explained in the earlier section. Nowadays, the trend is moving towards the use of CTPs having moderate/low target receptor binding affinity to achieve super-selectivity in targeting by the virtue of multivalency of the weak binding CTPs on NP surface[56]. This strategy is believed to be next logical step in the development of effective targeted nanosystems, as a mean to overcome the biological barrier of heterogenous target receptor expression levels and achieve targeting selectivity.

1.3.2 Importance of surface characterization.

The clinical success of NPs calls for a comprehensive NP surface characterization and analysis of their physicochemical properties. These are crucial for further determining their biological fate as well as the shelf stability. Notably, all formulation techniques result in mixed populations of NPs leading to heterogeneity in their size and the number of surface ligands along with their functionality. At the NP level, these heterogeneities were found to be divided into two groups as depicted in figure 1.7. To overcome these heterogeneities, a thorough characterization in the surface robust quantification of the NP surface parameters becomes imperative.

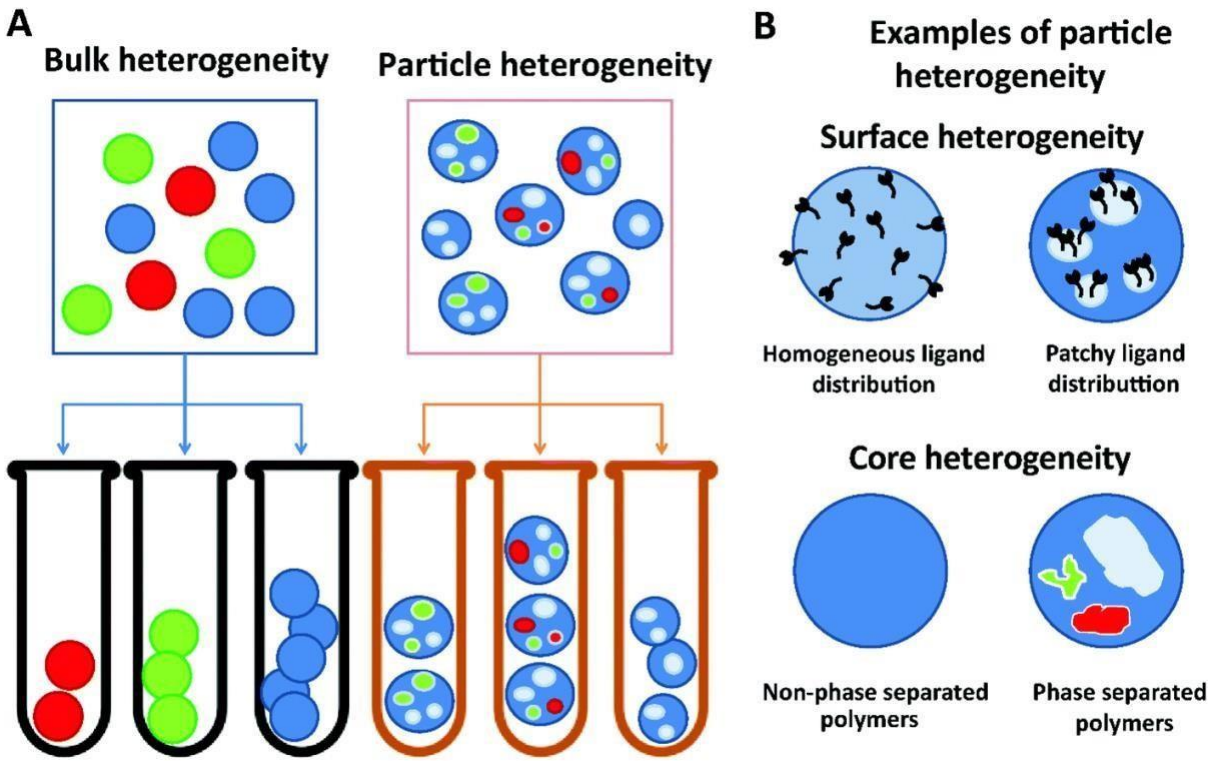

Figure 1.7 Nanoparticle heterogeneity. *Schematic representation of NP heterogeneities occurring at* ***A)*** *surface level where heterogeneity exists within subpopulations of the same batch leading to difference in efficacies of different NP subpopulations, and* ***B)*** *nanoparticle level, where heterogeneity exists either within the core or the surface of individual particles. Reproduced from the reference 73.*

Copyright © 2018 Rabanel et al. with the permission from The Royal Society of Chemistry.

The quantification of NP surface ligands involves two key methods: one that provides total number of surface ligands, and the other that determines the number of functional ligands[117–119]. The total ligand number largely defines the surface charge (zeta potential), consequently shedding light on the colloidal stability, dispersibility, and hydrophobicity/ hydrophilicity of the NPs. While the number of functional surface ligands defines the number of groups having the correct orientation of the ligand available for interaction with (bio)molecules such as the target receptors on cells, highlighting its importance in determining their targeting efficiency. Furthermore, the quantification of both total and functional ligands, in turn, depend on a variety of factors such as signal generation principle (label-based or label-free detection), type of bond between the NP surface and the targeting ligand, concentration of both NPs and the targeting ligands, surface area, etc.[119], often requiring the use of multiple techniques providing different information. There exist many analytical techniques that characterize the NP surface in terms of ligand binding, composition, density, arrangement, mass, and surface composition. A summary of some of the most commonly employed spectroscopic methods for NP surface characterization is provided in Table 1.1.

Analytical method	Parameter(s) characterized
Nuclear Magnetic Resonance (NMR)	Ligand density and arrangement, electronic core structure, atomic composition, influence of ligands on NP shape.
Fourier Transform InfraRed (FTIR)	Surface composition, ligand binding

X-Ray Photoelectron Spectroscopy (XPS)	Electronic structure, elemental composition, oxidation states, ligand binding (surfacesensitive)
Ferromagnetic Resonance (FMR)	NP size, size distribution, shape, crystallographic imperfection, surface composition

Table 1.1 *A summary of the most employed analytical spectroscopic methods for NP surface characterization*[120].

The field of nanomedicine is quite broad and relatively new in the context of life sciences application. As a result, the standardization of many procedures and formulation methods is not established very well, thus complicating their effective development. In addition, the variability of methods employed in different research groups and institutions further complicates this process, consequently affecting their clinical translation[121]. Although now there are efforts underway to unify the reporting practices as a measure of improving our understanding of materials and their biological behavior, thereby adding value to the current literature[122,123]. Even though there exist multiple different methods that are routinely employed for NP characterization, majority of them provide information on the bulk material.

This allows for obtaining only the average values, failing to account for the underlying heterogeneities[73]. Their statistical relevance in particle size, surface charge, drug loading or number and orientation of surface ligands is crucial for determining the overall performance of NPs[124]. Furthermore, for NP surface characterization in particular, an ensemble of techniques is utilized, once again failing to provide exact quantification. Therefore, the choice of NP surface characterization approach should be well established to allow controlled tuning of surface parameters for an improved efficiency of targeting nanosystems.

1.3.3 Interplay of different surface ligand parameters.

While there are consistent efforts being made to better characterize NP surface ligands and evaluate their impact on downstream biological functions of NPs in a robust manner, fewer attempts are being made to understand the interplay of different surface ligand parameters. It is believed that NP surface parameters such as the ligand density, spatial distribution and orientation, and intrinsic affinity are interrelated and play a key role in cellular targeting. Notably, it is anticipated that the surface ligand density interplays with certain NP properties (like size, shape, etc.), invariably affecting their *in vivo* distributions depending on the interrelationship between various parameters. A thorough understanding of the multiparametric role of NP surface physicochemical properties would provide vital information to advance the design of smarter nanocarriers[125]. An overview of the interplay of different surface ligand parameters is demonstrated in Figure 1.8.

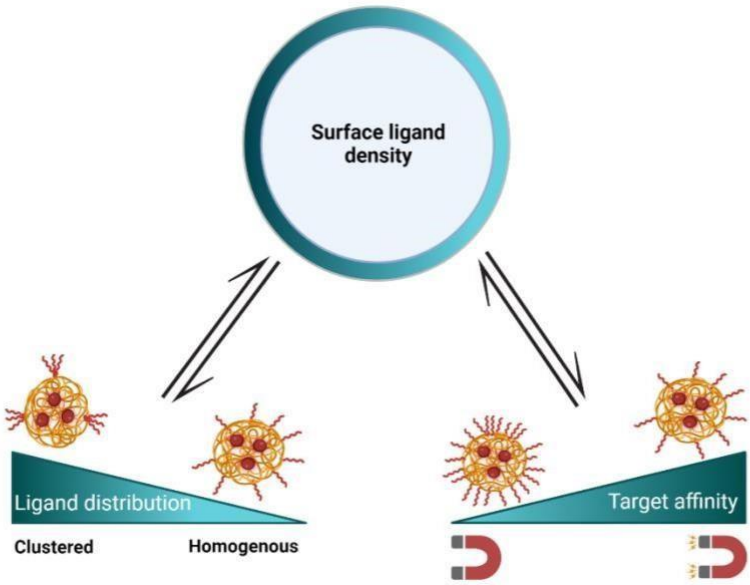

Figure 1.8 Interplay of NP surface parameters. *Schematic representation of the inter-relationship between NP surface parameters primarily influencing their biological behavior. Created with Biorender.com*

Of particular importance is the interplay between surface ligand density and its binding affinity to the target receptor. Somewhat counterintuitively, it is envisaged that for efficient NP targeting, the use of ultrahigh binding affinity ligands may not be always optimal and may show no significant differences in cellular uptake[125], as was observed in a study that evaluated the impact of a broad range of intrinsic affinities (K_D = 264–0.9 nM) of scFv antibody fragments conjugated to liposomes on their cellular uptake[126]. The main reason behind this is the ubiquitous expression of target receptors on healthy cells, as explained in earlier sections, which often results in non-specific binding.

Another parameter that potentially interplays with the surface ligand density is the surface distribution or spatial presentation of targeting ligands, as demonstrated in an interesting study, which reported a clear dependence of the tumor targeting and cellular uptake of mixed micelles displaying folate ligands in the form of "patchy clusters" compared to their counterparts having same total number of folate molecules distributed homogenously over the surface[127]. Another study showed similar improvement in cellular uptake of polystyrene NPs displaying clustered folate molecules co-assembled from albumin tagged with folate together with the untagged albumin[128]. These examples emphasize the importance of accounting for the spatial distribution or clustering effect of surface ligands along with the overall surface ligand density to improve our understand their nano-bio interactions[125,127].

In addition to the aforementioned parameters, the stoichiometry of surface ligands represented by varying the ratios of pre-conjugated ligand-polymer conjugate and the polymer alone allows for controlling the surface ligand density, which consequently impacts the cellular uptake[129]. Even though there are considerable efforts being made to explore the

effect of inter-dependence of NP surface ligand parameters on their cellular uptake, recent strategies are now moving towards employing two or more ligands to simultaneously target multiple receptors, not only on tumor cells, but also their microenvironment, as a mean for enabling enhanced selectivity in targeting.

1.4 Dual-ligand mediated nanoparticle targeting: Towards super-selectivity.

Cancer is a heterogenous disease, involving multiple parameters in a dynamic state that need to be considered when designing treatment regimens. It is already established that the tumor cell receptors undergo continuous changes along with the tumor progression[130,131]. Furthermore, some receptors are also expressed by healthy cells, causing non-selective uptake of targeted nanomedicines by these cells. In addition, cancer cells typically are known to over-express more than one surface receptors, thereby rendering the single ligand targeted strategies insufficient and rather ineffective, ultimately resulting in the failure of their clinical translation. As a result, dual-ligand targeting strategies have garnered a lot of interest in the past years and are now being explored widely for improving NP targeting selectivity[132–138]. However, they remain controversial as they involve an intricate interplay of a multitude of NP physicochemical properties[139,140]. As two types of ligands are functionalized simultaneously to the NP surface, the overall arrangement of the dual ligands along with their different physicochemical properties has a direct impact on the biological interactions of the NPs[140]. Thus, there is a great need to unravel the underlying molecular mechanisms involved in the selective cellular uptake of dual-ligand-functionalized NPs, in order to improve our understanding for a rational design of super-selective targeted nanoparticulate systems.

1.4.1 Concept of super-selectivity in nanomedicine targeting

A key bottleneck in the active targeting field that is often overlooked is the selectivity, which is the ability to distinguish cancer cells from the healthy ones, which show ubiquitous

expression of the same target receptor, although at different levels[141]. One of the widely explored mechanisms to achieve selectivity of targeted nanocarriers is through simultaneous attachment of multiple ligands NP surface to multiple receptors on cell surface, described earlier as multivalent targeting, to enhance the targeting efficiency compared to their monovalent counterparts[142,143]. Of special interest here is the use of ligands having a weak binding affinity, which allow the interplay of surface ligand density and binding affinity along with that of receptor density, resulting in maximal selectivity as illustrated in a study employing a model system that mimics cell receptor-NP binding[144] in Figure 1.9.

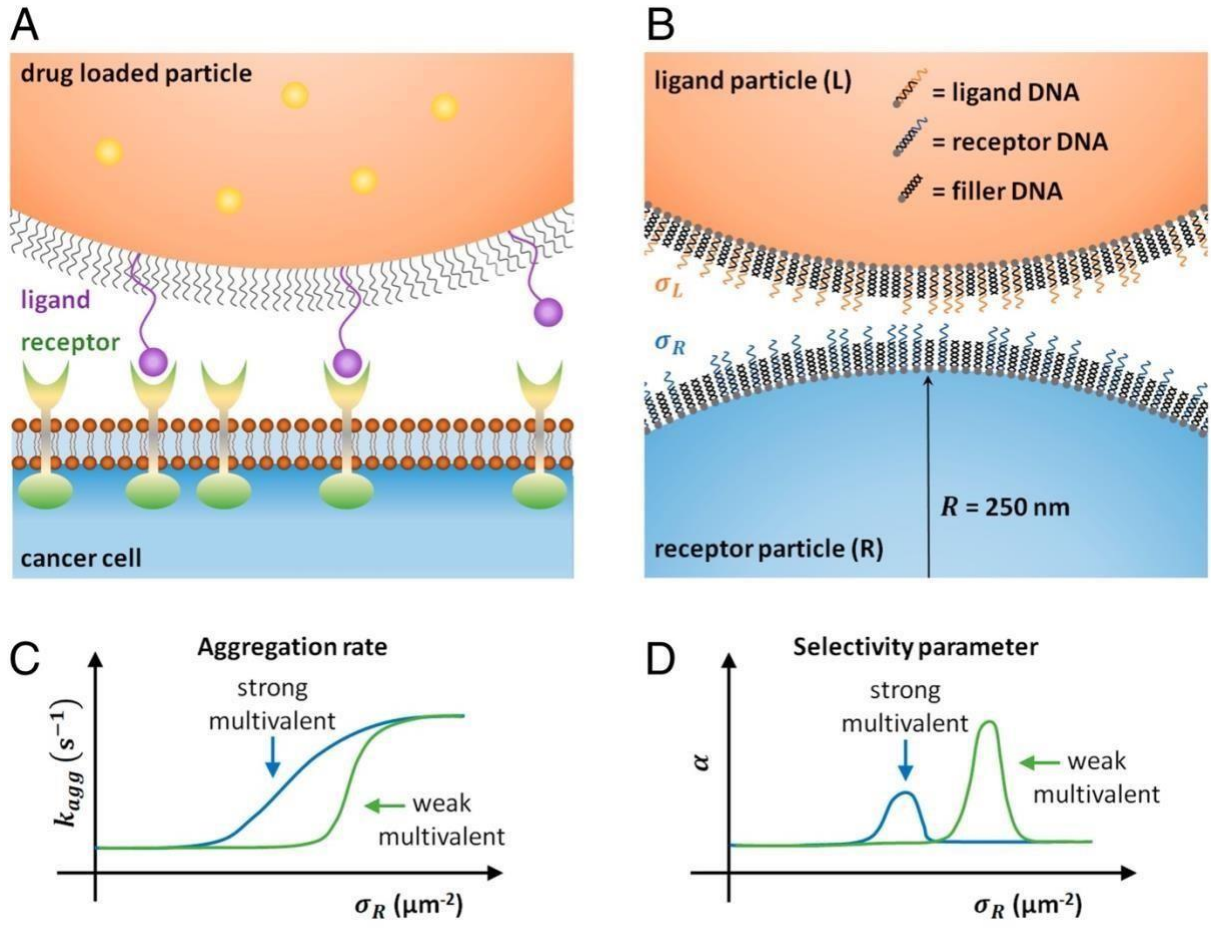

Figure 1.9 Weak multivalent binding for maximal selectivity. *Model system mimicking cell-particle interaction using particle-particle interactions showing schematic representations of:* ***A)*** *ligand functionalized NPs to cell receptors.* ***B)*** *ligand particle functionalized with short DNA constructs*

interacting with receptor particle functionalized with complementary DNA strands, which determines the strength of binding. ***C)*** *Rate of aggregation measured by keeping the ligand density constant, while varying the receptor density.* ***D)*** *Selectivity (α) calculated as a function of aggregation rate depending on receptor density. Reproduced from Reference 144. Copyright © 2020 Scheepers er al. Published by PNAS.*

Nowadays, there is a great deal of interest in the design of smart NPs binding only to regions of high receptor density, while sparing the low receptor density regions, rendering them unaffected[145]. However, even if it is crucial for targeting systems to be maximally selective for diseased cells over normal cells depending on the difference of expression levels of target receptors, recent efforts are being made to take this a step further. Of particular importance is attaining differential binding affinity exceeding the differences in expression levels, thereby inducing a switch-like transition of binding between expression levels of normal and diseased cells. This sharp disparity between receptor density and binding is generally defined as superselectivity. For most types of cancer, identifying receptors that are entirely unique to the diseased state poses a great challenge. Therefore, it is highly advantageous to choose a strategy that selects between normal and diseased cells depending on the target receptor density[146–148]. It generally revolves around employing multivalent interactions either via a single or multiple different target receptor, with the ultimate aim of inducing a switch-like transition in the binding efficiency offering selective regimes of multivalent NP targeting[149]. Such a characteristic is deemed ideal for physiological scenarios that require a high contrast and resolution for effective targeting, as well as to decrease adverse off-site effects of binding to normal cells. Both numerical simulations and experimental analysis have shown that superselective regimes are easily made possible by using multivalent interactions[141]. However, single ligand approaches allow lesser control over the diversity of receptor expression, and so the past decade has witnessed many attempts being made towards employment of two or more ligands, known as heterologous multivalency, targeting multiple receptors on same or different cells, with a view to further enhance super-selectivity as shown in Figure 1.10.

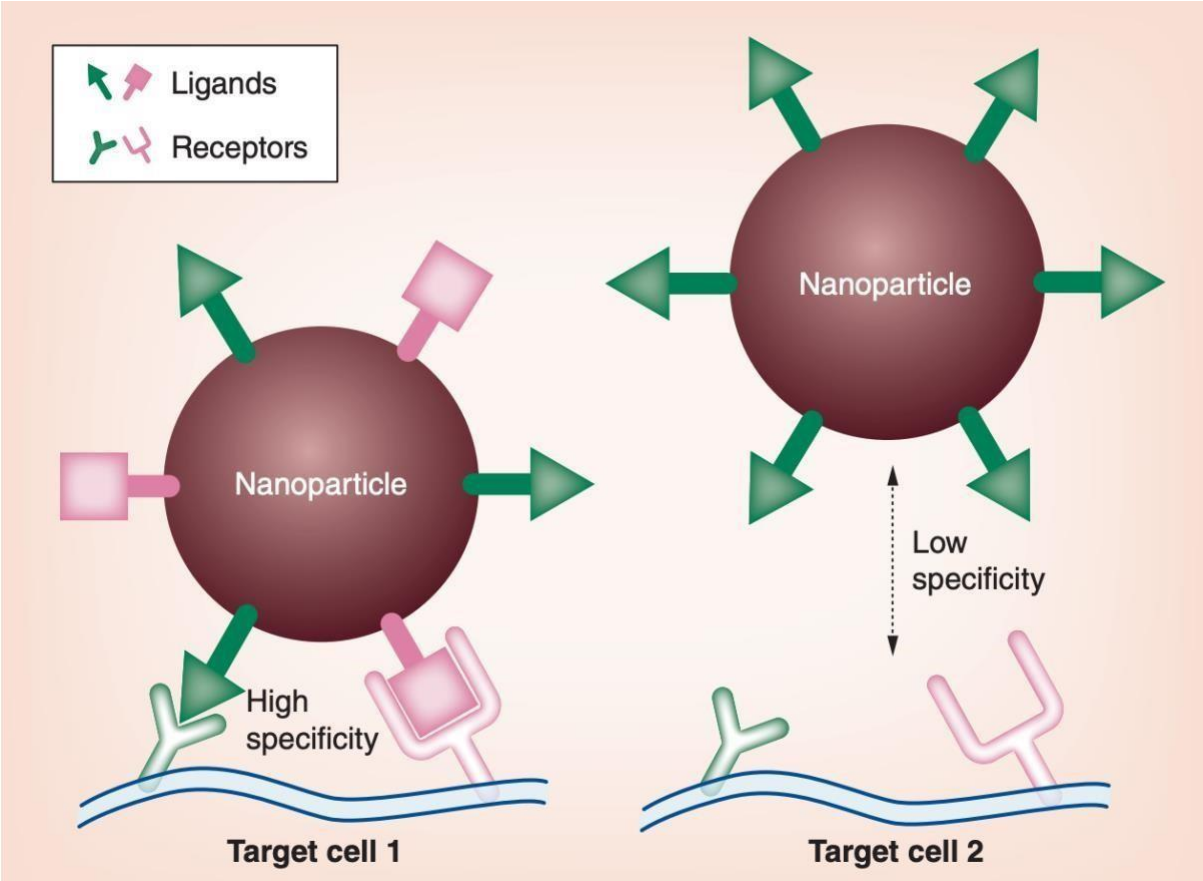

Figure 1.10 Heterologous multivalency for enhanced super-selectivity. *Schematic representation of dual targeting ligand functionalized NPs with optimized surface ligand ratios offering heterologous multivalent binding to dual target receptors, providing regimes of super-selectivity through enhanced specificity. Reproduced from the reference 150. Copyright © 2014 Future Medicine Ltd.*

1.4.2 Design principles for dual ligand mediated selective tumor targeting.

Since active targeting involves the recognition and binding of ligands to tumor cell surface receptors, the targeting efficiency is inevitably affected by the expression levels of target receptor. Furthermore, the recycling and synthesis of receptors takes place over time, leading

to saturation of the receptor-ligand association[151]. In addition, multiple different receptors are often overexpressed on tumor cells, leading to drug resistance caused by overexpression of alternative receptors along with the dynamic switching of molecular pathways between two receptors[152,153]. All these factors cause the targeting efficiency of single-ligand nanomedicines to alter, thereby reducing the efficacy of the targeted drug[154]. In comparison, dual ligand targeting strategies, endowed with versatile functions, hold promise to overcome these heterogeneities and improve cell selectivity in cancer treatments.

In principle, dual molecular targeting is a strategy involving two ligands that target different receptors, expressed either by similar or dissimilar cells. The combinations of ligands employed are distinguished into three different categories based on the kind of targeted cells and their corresponding sites of action: First, where the two ligands target two different receptors overexpressed simultaneously on the same cell; second, where two ligands target receptors overexpressed on two different cells; while the third, where one ligand targets a cell membrane receptor, and the other an intracellular organelle (nucleus or mitochondria)[154]. Each of these categories have their own merits, but their choice varies based on the level of selectivity required to be achieved for the chosen target(s). Furthermore, in the case of peptide ligands, four distinct types of dual-peptide NPs can be obtained, depending on how they are formulated. For instance, they can be either grafted onto the NP by three different conjugation methods or simply self-assembled, depending on the nature of the particles used as well as the peptide itself, shown in Figure 1.10.

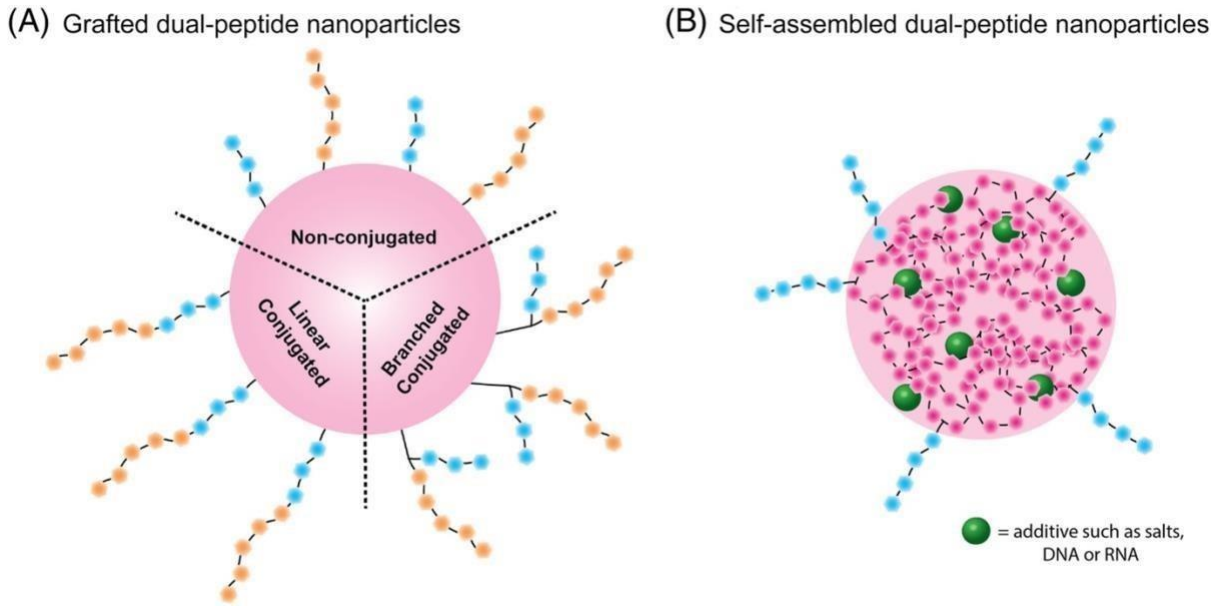

Figure 1.11 Dual peptide NPs formulation strategies. A) *Three types of dual peptide NPs obtained by grafting the peptides to a NPs, typically differing in the mode of connection between the two peptides (blue and orange): (a) non-conjugated: individual peptides are conjugated directly to NP surface, independent of each other (b) linear conjugated: typically using a short peptide spacer and (c) branched conjugated: usually using either lysine or cysteine sequences.* ***B)*** *Self-assembly of two peptides for dual NP formulation, differing in hydro- phili/phobicity, the hydrophobic one comprising the NP core (magenta) and the hydrophilic one covering the NP surface (blue). Reproduced from the reference 155. Copyright © 2020 Wiley Periodicals LLC.*

Consequently, the past decade has witnessed many different dual ligand NP systems being designed for targeting different cells or cellular compartments[154,155]. However, given the extremely non-trivial nature of this strategy, it is yet to reach the stage where all its potential benefits can be realized and exploited. Especially in complex *in vivo* models, dual ligand targeting systems have failed to provide significant advantages over their single ligand counterparts[140,150,156]. These failures often stem from a lack of thorough optimization of the physicochemical properties like particle size, charge, ligand density, target receptor affinity, stoichiometric ratios, etc., which might prove beneficial for future advancements[157].

In addition, the choice of target tumor receptors or biomarkers and targeting ligands is paramount to the optimal design. The choice of target receptors primarily depends on their expression levels and recycling kinetics in addition to their location[158]. The choice of the ligands is based on their size, molecular weight, binding affinity, and structural configuration[159]. For example, even though antibodies have been predominantly employed in targeting studies, their applications are limited by certain disadvantages like big size and cost of production[160]. In contrast, small peptides, aptamers, and small molecules offer a preferable choice for the design of multi-ligand targeting vehicles. Of special interest for the scope of this thesis is the paradigm of employing two ligands, differing in binding affinities towards two target receptors, allowing for their respective affinity and avidity to act synergistically, as a mean to improve the targeting potential of the polymeric nanosystems on account of super-selectivity.

1.5 Thesis aim and contents.

This chapter introduces and highlights some of the most important challenges for active nanoparticle targeting within the landscape of cancer nanomedicine. One of the key goals of nanomedicine is to provide specific and selective drug delivery at target site, to avoid undesirable side effects, yet, it has not been so straight-forward to achieve. While nanomaterials provide an excellent candidate for a safe and effective carrier system, their biological performance is heavily governed by different physicochemical properties, which must be thoroughly understood and well controlled. Furthermore, active nanoparticle targeting relies on a multitude of parameters, which if overlooked, pose several problems for their efficacy, safety, and overall performance. These are presented in detail in the previous sections and particularly include the properties of targeting ligands which play a vital role in the design of smart nanocarriers. In addition, there is currently a lack of robust characterization methods to assess and quantify the impact of each of these parameters on imparting selectivity to nanoparticle targeting. Given the dynamic nature of cancer, the use of single ligands for active targeting often fails to provide selectivity, in turn resulting in poor clinical translation of targeted nanomedicines.

Within this framework, in this thesis, the **main objective** was to target two known cancer biomarkers with small peptide ligands on the surface of polymeric nanocarriers to obtain more efficient and selective targeting using a panel of prostate cancer cell lines. Two cell targeting peptides having varying binding affinities are employed, and the concepts of affinity, avidity and multivalency of targeting ligands are presented and explored with each of the peptides, with a view to enhance NP targeting selectivity. The role of different NP-ligand conjugation methods is investigated, highlighting the importance of surface characterization in controlled design. Finally, a dual peptide-based targeting platform is designed, and the role of surface ligand density and stoichiometric ratios is established and optimized for achieving maximum selectivity for targeting cells simultaneously overexpressing both target receptors.

A schematic representation of the overall scope of this thesis is demonstrated in Figure 1.12. The following are the primary objectives of this thesis:

In **Chapter 2** the objective was to employ the strong binding affinity of GE11 peptide to EGFR to study the role of two different peptide-nanoparticle conjugation methods on the selective targeting of EGFR overexpressed on prostate cancer cells. Herein, we introduced a method optimized for nanoparticle surface quantification for number of GE11 peptides on NP surface obtained by each of the conjugation methods, using site-specific enzymatic digestion. The impact of the conjugation methods on NP surface valency is established and a preferred choice of conjugation method is defined. Consequently, the potential of pre- and post-functionalized GE11 NPs for selective EGFR targeting across a panel of prostate cancer cell lines, is determined.

In **Chapter 3**, the objective was to study the avidity of WQP, a small peptide having weak/moderate binding affinity to PSMA overexpressed on prostate cancer cells, for multivalent targeting of PSMA. The multivalent effect of WQP-functionalized nanoparticles is investigated in comparison to the peptide monomer on their cellular uptake in different prostate cancer cell lines. Thanks to the robustness of the surface characterization method employed before, the quantification of the number of WQPs obtained on multivalent NPs with differing surface valency is carried out. Overall, the impact of multivalent WQP binding on selective PSMA targeting is established.

Finally, having established the contribution of affinity and avidity for targeting selectivity regimes for each of the peptides, in **Chapter 4**, the objective was to design a synthetic strategy based on dual peptide ligands for selectively targeting cells overexpressing both receptors. In particular, surface ligand properties like density and stoichiometric ratios are explored for their impact on selectivity. Overall, the impact of co-operativity of the two peptides offering selective targeting regimes for prostate cancer cells is corroborated.

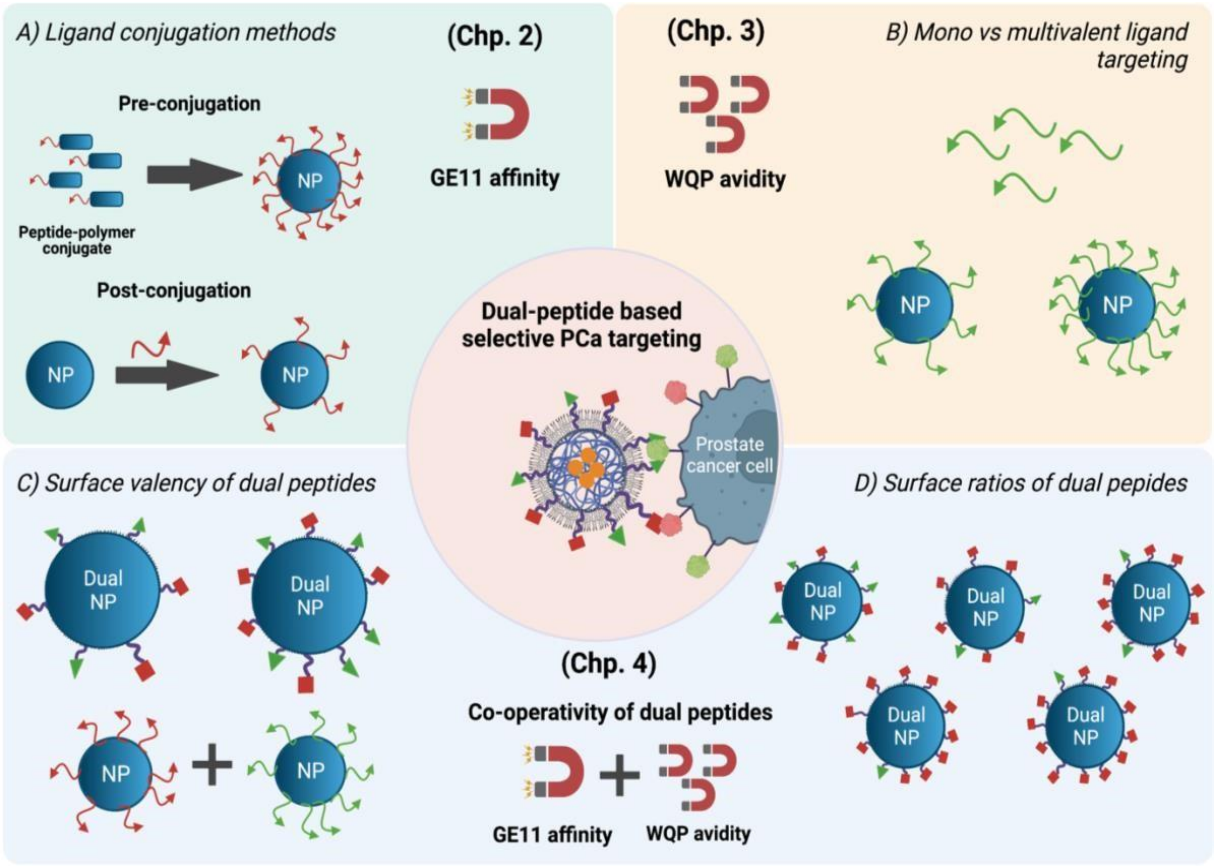

Figure 1.12 Scope of the thesis. *Schematic representation of the overall scope of the thesis, including various surface ligand parameters explored in individual chapters (Chp). Created with Biorender.com*

1.6 References.

1. Pelaz, B. *et al.* Diverse Applications of Nanomedicine. *ACS Nano* **11**, 2313–2381 (2017).
2. Nanoparticle-Based Medicines: A Review of FDA-Approved Materials and Clinical Trials to Date | SpringerLink. https://link.springer.com/article/10.1007/s11095-016-1958-5.
3. Havel, H. *et al.* Nanomedicines: From Bench to Bedside and Beyond. *AAPS J* **18**, 1373–1378 (2016).
4. Sainz, V. *et al.* Regulatory aspects on nanomedicines. *Biochemical and Biophysical Research Communications* **468**, 504–510 (2015).

5. Ventola, C. L. The nanomedicine revolution: part 1: emerging concepts. *P T* **37**, 512–525 (2012).
6. Kumar, S., Dilbaghi, N., Saharan, R. & Bhanjana, G. Nanotechnology as Emerging Tool for Enhancing Solubility of Poorly Water-Soluble Drugs. *BioNanoSci.* **2**, 227–250 (2012).
7. Wolfram, J. *et al.* Safety of nanoparticles in medicine. *Curr Drug Targets* **16**, 1671–1681 (2015).
8. Nanoparticle systems reduce systemic toxicity in cancer treatment | Nanomedicine. https://www.futuremedicine.com/doi/10.2217/nnm.15.166.
9. Allen, T. M. Ligand-targeted therapeutics in anticancer therapy. *Nat Rev Cancer* **2**, 750– 763 (2002).
10. *Nanotoxicity*. vol. 926 (Humana Press, 2012).
11. Yao, Y. *et al.* Nanoparticle-Based Drug Delivery in Cancer Therapy and Its Role in Overcoming Drug Resistance. *Frontiers in Molecular Biosciences* **7**, (2020).
12. Mitchell, M. J. *et al.* Engineering precision nanoparticles for drug delivery. *Nat Rev Drug Discov* **20**, 101–124 (2021).
13. Barenholz, Y. Doxil®--the first FDA-approved nano-drug: lessons learned. *J Control Release* **160**, 117–134 (2012).
14. Duivenvoorden, R. *et al.* Nanoimmunotherapy to treat ischaemic heart disease. *Nat Rev Cardiol* **16**, 21–32 (2019).
15. Biomimetic nanoparticle technology for cardiovascular disease detection and treatment -Nanoscale Horizons (RSC Publishing). https://pubs.rsc.org/en/content/articlelanding/2020/nh/c9nh00291j.
16. Current applications of nanoparticles in infectious diseases - ScienceDirect. https://www.sciencedirect.com/science/article/abs/pii/S0168365916300074?via%3Dih ub.

17. Nanotechnology—novel therapeutics for CNS disorders | Nature Reviews Neurology. https://www.nature.com/articles/nrneurol.2012.76.

18. Guo, P., Huang, J. & Moses, M. A. Cancer Nanomedicines in an Evolving Oncology Landscape. *Trends Pharmacol Sci* **41**, 730–742 (2020).

19. Delivering nanomedicine to solid tumors | Nature Reviews Clinical Oncology. https://www.nature.com/articles/nrclinonc.2010.139.

20. Kemp, J. A. & Kwon, Y. J. Cancer nanotechnology: current status and perspectives. *Nano Convergence* **8**, 34 (2021).

21. Sung, H. *et al.* Global Cancer Statistics 2020: GLOBOCAN Estimates of Incidence and Mortality Worldwide for 36 Cancers in 185 Countries. *CA: A Cancer Journal for Clinicians* **71**, 209–249 (2021).

22. Franceschi, S. & La Vecchia, C. Cancer epidemiology in the elderly. *Crit Rev Oncol Hematol* **39**, 219–226 (2001).

23. Sumanasuriya, S. & De Bono, J. Treatment of Advanced Prostate Cancer—A Review of Current Therapies and Future Promise. *Cold Spring Harb Perspect Med* **8**, a030635 (2018).

24. Chen, H., Zhang, W., Zhu, G., Xie, J. & Chen, X. Rethinking cancer nanotheranostics. *Nature Reviews Materials* **2**, 17024 (2017).

25. Engineering and physical sciences in oncology: challenges and opportunities | Nature Reviews Cancer. https://www.nature.com/articles/nrc.2017.83.

26. Shi, J., Kantoff, P. W., Wooster, R. & Farokhzad, O. C. Cancer nanomedicine: progress, challenges and opportunities. *Nature Reviews Cancer* **17**, 20–37 (2017).

27. Burrell, R. A., McGranahan, N., Bartek, J. & Swanton, C. The causes and consequences of genetic heterogeneity in cancer evolution. *Nature* **501**, 338–345 (2013).

28. Ferrari, M. Cancer nanotechnology: opportunities and challenges. *Nat Rev Cancer* **5**, 161– 171 (2005).

29. Peer, D. *et al.* Nanocarriers as an emerging platform for cancer therapy. *Nature Nanotech* **2**, 751–760 (2007).

30. Shi, J., Votruba, A. R., Farokhzad, O. C. & Langer, R. Nanotechnology in Drug Delivery and Tissue Engineering: From Discovery to Applications. *Nano Lett.* **10**, 3223–3230 (2010).

31. Swartz, M. A., Hirosue, S. & Hubbell, J. A. Engineering Approaches to Immunotherapy. *Science Translational Medicine* **4**, 148rv9-148rv9 (2012).

32. Nanospectra Biosciences, Inc. A Pilot Study of AuroLase(tm) Therapy in Patients With Refractory and/or Recurrent Tumors of the Head and Neck. https://clinicaltrials.gov/ct2/show/NCT00848042 (2016).

33. Merrimack Pharmaceuticals. A Phase-1 Study Evaluating the Safety, Pharmacology and Preliminary Activity of MM-310 in Patients With Solid Tumors. https://clinicaltrials.gov/ct2/show/NCT03076372 (2018).

34. ImmunoVaccine Technologies, Inc. (IMV Inc.). A Phase I Study of Two Different Doses of the Subcutaneous Administration of an Immunotherapeutic Vaccine, DPX-0907 in Advanced Stage Patients With Ovarian, Breast or Prostate Cancer. https://clinicaltrials.gov/ct2/show/study/NCT01095848 (2015).

35. Nayak, P. P., S., N., Narayanan, A., Badekila, A. K. & Kini, S. Nanomedicine in Cancer Clinics: Are We There Yet? *Curr Pathobiol Rep* **9**, 43–55 (2021).

36. Vicente-Ruiz, S., Serrano-Martí, A., Armiñán, A. & Vicent, M. J. Nanomedicine for the Treatment of Advanced Prostate Cancer. *Advanced Therapeutics* **4**, 2000136 (2021).

37. Caster, J. M., Patel, A. N., Zhang, T. & Wang, A. Investigational nanomedicines in 2016: a review of nanotherapeutics currently undergoing clinical trials. *WIREs Nanomedicine and Nanobiotechnology* **9**, e1416 (2017).

38. Salvioni, L. *et al.* Thirty Years of Cancer Nanomedicine: Success, Frustration, and Hope. *Cancers (Basel)* **11**, E1855 (2019).

39. Bhatia, S. N., Chen, X., Dobrovolskaia, M. A. & Lammers, T. Cancer nanomedicine. *Nat Rev Cancer* 1–7 (2022) doi:10.1038/s41568-022-00496-9.

40. Li, Z., Tan, S., Li, S., Shen, Q. & Wang, K. Cancer drug delivery in the nano era: An overview and perspectives (Review). *Oncol Rep* **38**, 611–624 (2017).

41. He, H., Liu, L., Morin, E. E., Liu, M. & Schwendeman, A. Survey of Clinical Translation of Cancer Nanomedicines—Lessons Learned from Successes and Failures. *Acc. Chem. Res.* **52**, 2445–2461 (2019).

42. Anselmo, A. C., Prabhakarpandian, B., Pant, K. & Mitragotri, S. Clinical and commercial translation of advanced polymeric nanoparticle systems: opportunities and material challenges. *Transl. Mater. Res.* **4**, 014001 (2017).

43. Göke, K. *et al.* Novel strategies for the formulation and processing of poorly watersoluble drugs. *European Journal of Pharmaceutics and Biopharmaceutics* **126**, 40–56 (2018).

44. Yue, X., Zhang, Q. & Dai, Z. Near-infrared light-activatable polymeric nanoformulations for combined therapy and imaging of cancer. *Advanced Drug Delivery Reviews* **115**, 155–170 (2017).

45. Attia, M. F., Anton, N., Wallyn, J., Omran, Z. & Vandamme, T. F. An overview of active and passive targeting strategies to improve the nanocarriers efficiency to tumour sites. *Journal of Pharmacy and Pharmacology* **71**, 1185–1198 (2019).

46. Rosenblum, D., Joshi, N., Tao, W., Karp, J. M. & Peer, D. Progress and challenges towards targeted delivery of cancer therapeutics. *Nat Commun* **9**, 1410 (2018).

47. A new concept for macromolecular therapeutics in cancer chemotherapy: mechanism of tumoritropic accumulation of proteins and the antitumor agent smancs - PubMed. https://pubmed.ncbi.nlm.nih.gov/2946403/.

48. Openings between defective endothelial cells explain tumor vessel leakiness - PubMed. https://pubmed.ncbi.nlm.nih.gov/10751361/.

49. Golombek, S. K. *et al.* Tumor targeting via EPR: Strategies to enhance patient responses. *Advanced Drug Delivery Reviews* **130**, 17–38 (2018).

50. Bertrand, N., Wu, J., Xu, X., Kamaly, N. & Farokhzad, O. C. Cancer nanotechnology: The impact of passive and active targeting in the era of modern cancer biology. *Advanced Drug Delivery Reviews* **66**, 2–25 (2014).

51. Subhan, M. A., Yalamarty, S. S. K., Filipczak, N., Parveen, F. & Torchilin, V. P. Recent Advances in Tumor Targeting via EPR Effect for Cancer Treatment. *J Pers Med* **11**, 571 (2021).

Upponi, J. R. & Torchilin, V. P. Passive vs. Active Targeting: An Update of the EPR Role in Drug Delivery to Tumors. in *Nano-Oncologicals: New Targeting and Delivery Approaches* (eds. Alonso, M. J. & Garcia-Fuentes, M.) 3–45 (Springer International Publishing, 2014). doi:10.1007/978-3-319-08084-0_1.

52. Challenging paradigms in tumour drug delivery. *Nat. Mater.* **19**, 477–477 (2020).

53. Sindhwani, S. *et al.* The entry of nanoparticles into solid tumours. *Nat. Mater.* (2020) doi:10.1038/s41563-019-0566-2.

54. Zhao, Z., Ukidve, A., Kim, J. & Mitragotri, S. Targeting Strategies for Tissue-Specific Drug Delivery. *Cell* **181**, 151–167 (2020).

55. Woythe, L., Tito, N. B. & Albertazzi, L. A quantitative view on multivalent nanomedicine targeting. *Advanced Drug Delivery Reviews* **169**, 1–21 (2021).

56. Torchilin, V. P. Passive and active drug targeting: drug delivery to tumors as an example. *Handb Exp Pharmacol* 3–53 (2010) doi:10.1007/978-3-642-00477-3_1.

57. Ahmad, A., Khan, F., Mishra, R. K. & Khan, R. Precision Cancer Nanotherapy: Evolving Role of Multifunctional Nanoparticles for Cancer Active Targeting. *Journal of Medicinal Chemistry* **62**, 10475 (2019).

58. Yoo, J., Park, C., Yi, G., Lee, D. & Koo, H. Active Targeting Strategies Using Biological Ligands for Nanoparticle Drug Delivery Systems. *Cancers* **11**, 640 (2019).

59. Byrne, J. D., Betancourt, T. & Brannon-Peppas, L. Active targeting schemes for nanoparticle systems in cancer therapeutics. *Advanced Drug Delivery Reviews* **60**, 1615– 1626 (2008).

60. Multivalent Effects of RGD Peptides Obtained by Nanoparticle Display | Journal of Medicinal Chemistry. https://pubs.acs.org/doi/10.1021/jm060515m.

61. Salahpour Anarjan, F. Active targeting drug delivery nanocarriers: Ligands. *NanoStructures & Nano-Objects* **19**, 100370 (2019).

62. Delivery of therapeutic oligonucleotides | Nucleic Acids Research | Oxford Academic. https://academic-oup-com.sire.ub.edu/nar/article/44/14/6518/2468139.

63. Srinivasarao, M., Galliford, C. V. & Low, P. S. Principles in the design of ligand-targeted cancer therapeutics and imaging agents. *Nat Rev Drug Discov* **14**, 203–219 (2015).

64. Wang, Y. *et al.* Peptide–drug conjugates as effective prodrug strategies for targeted delivery. *Advanced Drug Delivery Reviews* **110–111**, 112–126 (2017).

65. Jo, H. & Ban, C. Aptamer–nanoparticle complexes as powerful diagnostic and therapeutic tools. *Exp Mol Med* **48**, e230–e230 (2016).

66. Martínez-Jothar, L. *et al.* Insights into maleimide-thiol conjugation chemistry: Conditions for efficient surface functionalization of nanoparticles for receptor targeting. *Journal of Controlled Release* **282**, 101–109 (2018).

67. Brückner, M., Simon, J., Landfester, K. & Mailänder, V. The conjugation strategy affects antibody orientation and targeting properties of nanocarriers. *Nanoscale* **13**, 9816–9824 (2021).

68. Pearce, A. K. & O'Reilly, R. K. Insights into Active Targeting of Nanoparticles in Drug Delivery: Advances in Clinical Studies and Design Considerations for Cancer Nanomedicine. *Bioconjug Chem* **30**, 2300–2311 (2019).

69. Huang, H., Feng, W., Chen, Y. & Shi, J. Inorganic nanoparticles in clinical trials and translations. *Nano Today* **35**, 100972 (2020).

70. Barrán-Berdón, A. L. *et al.* Time Evolution of Nanoparticle–Protein Corona in Human Plasma: Relevance for Targeted Drug Delivery. *Langmuir* **29**, 6485–6494 (2013).

71. Andrian, T., Delcanale, P., Pujals, S. & Albertazzi, L. Correlating Super-Resolution Microscopy and Transmission Electron Microscopy Reveals Multiparametric Heterogeneity in Nanoparticles. *Nano Lett.* **21**, 5360–5368 (2021).

72. Rabanel, J.-M. *et al.* Nanoparticle heterogeneity: an emerging structural parameter influencing particle fate in biological media? *Nanoscale* **11**, 383–406 (2019).

73. Rees, P., Wills, J. W., Brown, M. R., Barnes, C. M. & Summers, H. D. The origin of heterogeneous nanoparticle uptake by cells. *Nat Commun* **10**, 2341 (2019).

74. Crommelin, D. J. A., van Hoogevest, P. & Storm, G. The role of liposomes in clinical nanomedicine development. What now? Now what? *J Control Release* **318**, 256–263 (2020).

75. Dai, Q. *et al.* Quantifying the Ligand-Coated Nanoparticle Delivery to Cancer Cells in Solid Tumors. *ACS Nano* **12**, 8423–8435 (2018).

76. Youn, Y. S. & Bae, Y. H. Perspectives on the past, present, and future of cancer nanomedicine. *Adv Drug Deliv Rev* **130**, 3–11 (2018).

77. Nano-Oncologicals: A Tortoise Trail Reaching New Avenues - Dacoba - 2021 - Advanced Functional Materials - Wiley Online Library. https://onlinelibrary.wiley.com/doi/full/10.1002/adfm.202009860.

78. Wilhelm, S. *et al.* Analysis of nanoparticle delivery to tumours. *Nat Rev Mater* **1**, 16014 (2016).

79. Conjugation site modulates the in vivo stability and therapeutic activity of antibodydrug conjugates | Nature Biotechnology. https://www.nature.com/articles/nbt.2108.

80. Beck, A., Goetsch, L., Dumontet, C. & Corvaïa, N. Strategies and challenges for the next generation of antibody–drug conjugates. *Nat Rev Drug Discov* **16**, 315–337 (2017).

81. Wu, Y., Yi, M., Zhu, S., Wang, H. & Wu, K. Recent advances and challenges of bispecific antibodies in solid tumors. *Experimental Hematology & Oncology* **10**, 56 (2021).

82. Ferrari, M. Frontiers in cancer nanomedicine: directing mass transport through biological barriers. *Trends Biotechnol* **28**, 181–188 (2010).

83. Blanco, E., Shen, H. & Ferrari, M. Principles of nanoparticle design for overcoming biological barriers to drug delivery. *Nat Biotechnol* **33**, 941–951 (2015).

84. Seoane, J. & De Mattos-Arruda, L. The challenge of intratumour heterogeneity in precision medicine. *J Intern Med* **276**, 41–51 (2014).

85. Bae, Y. H. & Park, K. Targeted drug delivery to tumors: myths, reality and possibility. *J Control Release* **153**, 198–205 (2011).

86. Bedard, P. L., Hansen, A. R., Ratain, M. J. & Siu, L. L. Tumour heterogeneity in the clinic. *Nature* **501**, 355–364 (2013).

87. Dexter, D. L. & Calabresi, P. Intraneoplastic diversity. *Biochimica et Biophysica Acta (BBA) - Reviews on Cancer* **695**, 97–112 (1982).

88. Heppner, G. H. & Miller, B. E. Tumor heterogeneity: biological implications and therapeutic consequences. *Cancer Metastasis Rev* **2**, 5–23 (1983).

89. Kim, J. W. & Cochran, J. R. Targeting ligand-receptor interactions for development of cancer therapeutics. *Curr Opin Chem Biol* **38**, 62–69 (2017).

90. Feiner-Gracia, N. *et al.* Super-Resolution Microscopy Unveils Dynamic Heterogeneities in Nanoparticle Protein Corona. *Small* **13**, (2017).

91. Frontiers | Nanoparticle Surface Functionalization: How to Improve Biocompatibility and Cellular Internalization. https://www.frontiersin.org/articles/10.3389/fmolb.2020.587012/full#B65.

92. Alibakhshi, A. *et al.* Targeted cancer therapy through antibody fragments-decorated nanomedicines. *Journal of Controlled Release* **268**, 323–334 (2017).

93. Fathian kolahkaj, F. *et al.* Active targeting carrier for breast cancer treatment: Monoclonal antibody conjugated epirubicin loaded nanoparticle. *Journal of Drug Delivery Science and Technology* **53**, 101136 (2019).

94. Sanità, G., Carrese, B. & Lamberti, A. Nanoparticle Surface Functionalization: How to Improve Biocompatibility and Cellular Internalization. *Front. Mol. Biosci.* **7**, (2020).

95. Houdaihed, L., Evans, J. C. & Allen, C. Dual-Targeted Delivery of Nanoparticles Encapsulating Paclitaxel and Everolimus: a Novel Strategy to Overcome Breast Cancer Receptor Heterogeneity. *Pharm Res* **37**, 39 (2020).

96. Remacha, A. F., Sarda, M. P., Parellada, M., Ubeda, J. & Manteiga, R. The role of serum transferrin receptor in the diagnosis of iron deficiency. *Haematologica* **83**, 963–966 (1998).

97. Scheeren, L. E. *et al.* Transferrin-conjugated doxorubicin-loaded PLGA nanoparticles with pH-responsive behavior: a synergistic approach for cancer therapy. *J Nanopart Res* **22**, 72 (2020).

98. Clark, A. J. & Davis, M. E. Increased brain uptake of targeted nanoparticles by adding an acid-cleavable linkage between transferrin and the nanoparticle core. *Proceedings of the National Academy of Sciences* **112**, 12486–12491 (2015).

99. Aruffo, A., Stamenkovic, I., Melnick, M., Underhill, C. B. & Seed, B. CD44 is the principal cell surface receptor for hyaluronate. *Cell* **61**, 1303–1313 (1990).

100. Li, J. *et al.* Facile strategy by hyaluronic acid functional carbon dot-doxorubicin nanoparticles for CD44 targeted drug delivery and enhanced breast cancer therapy. *Int J Pharm* **578**, 119122 (2020).

101. Wang, X. *et al.* Insights into Aptamer–Drug Delivery Systems against Prostate Cancer. *Molecules* **27**, 3446 (2022).

102. Tang, L. *et al.* Targeting tumor vasculature with aptamer-functionalized doxorubicinpolylactide nanoconjugates for enhanced cancer therapy. *ACS Nano* **9**, 5072–5081 (2015).

103. Khan, M. M. *et al.* Folate targeted lipid chitosan hybrid nanoparticles for enhanced anti-tumor efficacy. *Nanomedicine* **28**, 102228 (2020).

104. Intraoperative tumor-specific fluorescence imaging in ovarian cancer by folate receptor-α targeting: first in-human results | Nature Medicine. https://www.nature.com/articles/nm.2472.

105. Folate-modified PLGA nanoparticles for tumor-targeted delivery of pheophorbide a in vivo - ScienceDirect. https://www.sciencedirect.com/science/article/abs/pii/S0006291X1830487X?via%3Dih ub.

106. Fitzgerald, K. A. *et al.* A novel, anisamide-targeted cyclodextrin nanoformulation for siRNA delivery to prostate cancer cells expressing the sigma-1 receptor. *International Journal of Pharmaceutics* **499**, 131–145 (2016).

107. Deshayes, S. *et al.* Phenylboronic Acid-Installed Polymeric Micelles for Targeting Sialylated Epitopes in Solid Tumors. *J. Am. Chem. Soc.* **135**, 15501–15507 (2013).

108. Qian, X. *et al.* Targeting and microenvironment-improving of phenylboronic acid decorated soy protein nanoparticles with different sizes to tumor. *Theranostics* **9**, 7417– 7430 (2019).

109. Ramzy, L., Metwally, A. A., Nasr, M. & Awad, G. A. S. Novel thymoquinone lipidic core nanocapsules with anisamide-polymethacrylate shell for colon cancer cells overexpressing sigma receptors. *Sci Rep* **10**, 10987 (2020).

110. Target-specific delivery of peptide-based probes for PET imaging - ScienceDirect. https://wwwsciencedirectcom.sire.ub.edu/science/article/pii/S0169409X10001821?via%3Dihub. 111. Genta, I. *et al.* GE11 Peptide as an Active Targeting Agent in Antitumor Therapy: A Minireview. *Pharmaceutics* **10**, 2 (2017).

112. Li, C. *et al.* Development of EGFR-targeted evodiamine nanoparticles for the treatment of colorectal cancer. *Biomater Sci* **7**, 3627–3639 (2019).

113. Jin, H. *et al.* EGFR-targeting PLGA-PEG nanoparticles as a curcumin delivery system for breast cancer therapy. *Nanoscale* **9**, 16365–16374 (2017).

114. Colzani, B. *et al.* Design of smart GE11-PLGA/PEG-PLGA blend nanoparticulate platforms for parenteral administration of hydrophilic macromolecular drugs: synthesis, preparation and in vitro/ex vivo characterization. *Int J Pharm* **511**, 1112–1123 (2016). 115. Brown, K. C. Peptidic Tumor Targeting Agents: The Road from Phage Display Peptide Selections to Clinical Applications. *Current Pharmaceutical Design* **16**, 1040–1054.

116. Hennig, A. *et al.* Scope and limitations of surface functional group quantification methods: exploratory study with poly(acrylic acid)-grafted micro- and nanoparticles. *J Am Chem Soc* **134**, 8268–8276 (2012).

117. Moser, M., Nirmalananthan, N., Behnke, T., Geißler, D. & Resch-Genger, U. Multimodal Cleavable Reporters versus Conventional Labels for Optical Quantification of Accessible Amino and Carboxy Groups on Nano- and Microparticles. *Anal Chem* **90**, 5887– 5895 (2018).

118. Geißler, D., Nirmalananthan-Budau, N., Scholtz, L., Tavernaro, I. & Resch-Genger, U. Analyzing the surface of functional nanomaterials—how to quantify the total and derivatizable number of functional groups and ligands. *Microchim Acta* **188**, 321 (2021).

119. Mourdikoudis, S., Pallares, R. M. & Thanh, N. T. K. Characterization techniques for nanoparticles: comparison and complementarity upon studying nanoparticle properties.

Nanoscale **10**, 12871–12934 (2018).

120. Baer, D. R. *et al.* Surface characterization of nanomaterials and nanoparticles: Important needs and challenging opportunities. *Journal of Vacuum Science & Technology A:*

Vacuum, Surfaces, and Films **31**, 050820 (2013).

121. Faria, M. *et al.* Minimum information reporting in bio-nano experimental literature. *Nat Nanotechnol* **13**, 777–785 (2018).

122. Mulvaney, P., Parak, W. J., Caruso, F. & Weiss, P. S. Standardizing Nanomaterials. *ACS Nano* **10**, 9763–9764 (2016).

123. Mullen, D. G. & Banaszak Holl, M. M. Heterogeneous Ligand–Nanoparticle Distributions: A Major Obstacle to Scientific Understanding and Commercial Translation. *Acc. Chem. Res.* **44**, 1135–1145 (2011).

124. Alkilany, A. M. *et al.* Ligand density on nanoparticles: A parameter with critical impact on nanomedicine. *Advanced Drug Delivery Reviews* **143**, 22–36 (2019).

125. Zhou, Y. *et al.* Impact of Single-chain Fv Antibody Fragment Affinity on Nanoparticle Targeting of Epidermal Growth Factor Receptor-expressing Tumor Cells. *Journal of Molecular Biology* **371**, 934–947 (2007).

126. Poon, Z. *et al.* Ligand-Clustered "Patchy" Nanoparticles for Modulated Cellular Uptake and In Vivo Tumor Targeting. *Angewandte Chemie International Edition* **49**, 7266–7270 (2010).

127. Moradi, E., Vllasaliu, D., Garnett, M., Falcone, F. & Stolnik, S. Ligand density and clustering effects on endocytosis of folate modified nanoparticles. *RSC Adv.* **2**, 3025–3033 (2012).

128. Gu, F. *et al.* Precise engineering of targeted nanoparticles by using self-assembled biointegrated block copolymers. *Proc Natl Acad Sci U S A* **105**, 2586–2591 (2008).

129. Di Lorenzo, G. *et al.* Expression of epidermal growth factor receptor correlates with disease relapse and progression to androgen-independence in human prostate cancer. *Clinical Cancer Research* **8**, 3438–3444 (2002).

130. Platet, N., Cathiard, A. M., Gleizes, M. & Garcia, M. Estrogens and their receptors in breast cancer progression: a dual role in cancer proliferation and invasion. 13 (2004).

131. Doolittle, E. *et al.* Spatiotemporal Targeting of a Dual-Ligand Nanoparticle to Cancer Metastasis. *ACS Nano* **9**, 8012–8021 (2015).

132. Covarrubias, G. *et al.* Effective treatment of cancer metastasis using a dual-ligand nanoparticle. *PLoS One* **14**, e0220474 (2019).

133. Xu, Q. *et al.* Anti-tumor activity of paclitaxel through dual-targeting carrier of cyclic RGD and transferrin conjugated hyperbranched copolymer nanoparticles. *Biomaterials* **33**, 1627–1639 (2012).

134. Bhattacharyya, S. *et al.* Efficient Delivery of Gold Nanoparticles by Dual Receptor Targeting. *Advanced Materials* **23**, 5034–5038 (2011).

135. Jang, C., Lee, J. H., Sahu, A. & Tae, G. The synergistic effect of folate and RGD dual ligand of nanographene oxide on tumor targeting and photothermal therapy in vivo. *Nanoscale* **7**, 18584–18594 (2015).

136. Ying, X. *et al.* Dual-targeting daunorubicin liposomes improve the therapeutic efficacy of brain glioma in animals. *J Control Release* **141**, 183–192 (2010).

137. Li, X. *et al.* Enhancement of cell recognition in vitro by dual-ligand cancer targeting gold nanoparticles. *Biomaterials* **32**, 2540–2545 (2011).

138. Peiris, P. M. *et al.* Precise targeting of cancer metastasis using multi-ligand nanoparticles incorporating four different ligands. *Nanoscale* **10**, 6861–6871 (2018).

139. Xia, Q., Ding, H. & Ma, Y. Can dual-ligand targeting enhance cellular uptake of nanoparticles? *Nanoscale* **9**, 8982–8989 (2017).

140. Makhani, E. Y., Zhang, A. & Haun, J. B. Quantifying and controlling bond multivalency for advanced nanoparticle targeting to cells. *Nano Convergence* **8**, 38 (2021).

141. Colombo, M. *et al.* Tumour homing and therapeutic effect of colloidal nanoparticles depend on the number of attached antibodies. *Nat Commun* **7**, 13818 (2016).

142. Binding Affinity and Kinetic Analysis of Targeted Small Molecule-Modified Nanoparticles | Bioconjugate Chemistry. https://pubsacsorg.sire.ub.edu/doi/10.1021/bc900438a.

143. Scheepers, M. R. W., van IJzendoorn, L. J. & Prins, M. W. J. Multivalent weak interactions enhance selectivity of interparticle binding. *Proc Natl Acad Sci USA* **117**, 22690–22697 (2020).

144. Martinez-Veracoechea, F. J. & Frenkel, D. Designing super selectivity in multivalent nano-particle binding. *Proceedings of the National Academy of Sciences* **108**, 10963– 10968 (2011).

145. Curk, T., Dobnikar, J. & Frenkel, D. Optimal multivalent targeting of membranes with many distinct receptors. *Proc Natl Acad Sci USA* **114**, 7210–7215 (2017).

146. Trister, A. D. & Hammer, D. A. Role of gp120 Trimerization on HIV Binding Elucidated with Brownian Adhesive Dynamics. *Biophysical Journal* **95**, 40–53 (2008).

147. English, T. J. & Hammer, D. A. Brownian Adhesive Dynamics (BRAD) for Simulating the Receptor-Mediated Binding of Viruses. *Biophysical Journal* **86**, 3359–3372 (2004).

148. Tito, N. B. & Frenkel, D. Switch-like surface binding of competing multivalent particles. *Eur. Phys. J. Spec. Top.* **225**, 1673–1682 (2016).

149. Wang, B., Galliford, C. V. & Low, P. S. Guiding principles in the design of ligand-targeted nanomedicines. *Nanomedicine (Lond)* **9**, 313–330 (2014).

150. Koenig, J. A. & Edwardson, J. M. Endocytosis and recycling of G protein-coupled receptors. *Trends in Pharmacological Sciences* **18**, 276–287 (1997).

151. Resistance to epidermal growth factor receptor-targeted therapy - ScienceDirect. https://www-sciencedirect-com.sire.ub.edu/science/article/pii/S1368764605000634.

152. Jones, H. E. *et al.* Growth factor receptor interplay and resistance in cancer. *EndocrineRelated Cancer* **13**, S45–S51 (2006).

153. Zhu, Y., Feijen, J. & Zhong, Z. Dual-targeted nanomedicines for enhanced tumor treatment. *Nano Today* **18**, 65–85 (2018).

154. Forest, C. R., Silva, C. A. C. & Thordarson, P. Dual-peptide functionalized nanoparticles for therapeutic use. *Peptide Science* **n/a**, e24205.

155. Sawant, R. R., Jhaveri, A. M., Koshkaryev, A., Qureshi, F. & Torchilin, V. P. The effect of dual ligand-targeted micelles on the delivery and efficacy of poorly soluble drug for cancer therapy. *Journal of Drug Targeting* **21**, 630–638 (2013).

156. Liu, Y. *et al.* Synergetic Combinations of Dual-Targeting Ligands for Enhanced In Vitro and In Vivo Tumor Targeting. *Advanced Healthcare Materials* **7**, 1800106 (2018).

157. Taghipour, Y. D. *et al.* An update on dual targeting strategy for cancer treatment. *Journal of Controlled Release* **349**, 67–96 (2022).

158. Zinger, A. *et al.* Collagenase Nanoparticles Enhance the Penetration of Drugs into Pancreatic Tumors. *ACS Nano* **13**, 11008–11021 (2019).

159. Chudasama, V., Maruani, A. & Caddick, S. Recent advances in the construction of antibody–drug conjugates. *Nature Chem* **8**, 114–119 (2016).

Chapter 2| A quantitative assessment of GE11 peptide-mediated NP conjugation strategies: Impact on selective EGFR targeting.

Cancer nanomedicine involves the development of delivery systems that selectively target cancer cells to reduce undesired off-target responses of current therapies. To this end, studies on surface coating of nanoparticles (NPs) with targeting ligands in a robust, quantitative manner are necessary. Different conjugation strategies have been employed, but their direct impact on selectivity of the nanosystems is not well understood. A key bottleneck towards this goal is the lack of robust methods for quantifying the exact number of surface ligands.

In this chapter, we carry out a comparative analysis of two commonly employed (pre- and post-) conjugation strategies using the GE11 peptide and polymeric (PLGA-PEG) NPs by quantifying the number of surface GE11 in a robust manner and consequently investigating their impact on selective targeting of cells over-expressing EGFR. A method for the quantification of the number of WQPs on NPs having different surface valencies in a robust manner is developed using specific enzymatic digestion. Our findings highlight the importance of thorough understanding of the influence of conjugation strategies for designing optimal nanosystems for selective prostate cancer targeting.

Supportive information for this chapter can be found in **Appendix 1.*

2.1 Introduction

As described in detail in the previous chapter, the development of delivery systems that selectively target tumor cells has been a key goal of nanomedicine[1]. To this end, the active targeting strategy is widely employed, to enhance the internalization of NPs at the target site,

thus avoiding the side effects of current treatment regimens and consequently improving patient outcomes[2]. Among the many targeting ligands extensively studied for active NP targeting[3], CTPs are known offer some distinct advantages and are being widely explored for targeted drug delivery systems[4,5]. Although there exist several different types of nanomaterials, polymeric NPs offer excellent biocompatibility and are particularly explored for the design of carriers involving self-assembly of individual components along with the encapsulation of the therapeutic moiety.

The number of NP surface ligands is an essential parameter that needs to be accounted for in the development of active targeted nanosystems[7]. Controlling the ligand number on the nanoparticle surface in a more precise manner allows for an improved therapeutic efficacy[8,9]. Although there exist different conjugation methods depending on the type of ligands in the literature[8–12], the most commonly employed strategies rely on the conjugation of the ligand to the NP surface before or after the NP formulation, known as the pre-conjugation strategy and the post-conjugation strategy, respectively[8,9]. The post-conjugation strategy involves conjugation of the ligand to NP surface after their formulation. This is a relatively straightforward conjugation approach, protecting the bioactivity of the ligand from having to undergo the NP formulation process, and is therefore widely used[8,13]. However, it usually requires an excess amount of ligands to drive the chemical reaction, making it difficult to regulate the properties of the NP surface in a reproducible manner, thereby offering a limited control of the ligand density on the NP surface[8]. On the other hand, pre-conjugation involves conjugating the ligand to the polymer prior to NP formulation. This kind of strategy offers a higher control over the ligand density on NP surface and is therefore, being widely explored[8,14]. The quantification of surface ligand number on NP surface is quite challenging owing to their nanometric size and their often low abundance, making them barely detectable by standard characterization techniques[15,16]. Furthermore, most of these characterization methods rely on bulk results, failing to take into account the inter- and intra-particle

heterogeneity in surface ligand number and distribution, which has a direct consequence on its biological response.[17,18] Therefore, there is a clear need for characterization techniques that allow robust quantification of surface ligand.

Here, we designed a study to assess the impact of pre- and post-conjugation strategies using polymeric NPs on the selective targeting of prostate cancer (PCa). We chose the GE11 peptide as targeting ligand, as it is a very well-known CTP, as demonstrated in the earlier chapter, having strong binding affinity towards epithelial growth factor receptor (EGFR), a known biomarker for a variety of solid tumors[20– 22]. There have been numerous studies with GE11 peptide in for breast cancer[19,23,24], so we wanted to test its utility in the context of PCa, the second most prevalent malignancy worldwide[25]. Of particular interest, we developed a method of site-specific enzymatic digestion to robustly quantify the number of GE11 on NP surface and consequently studied their effect on the cellular uptake in PCa cell lines having varying expression levels of EGFR.

2.2 Results and discussion

2.2.1 Pre- and post-GE11 conjugation strategies.

A brief overview of the workflow of the two conjugation strategies employed is shown in Figure 2.1. Pre-conjugation, as the name suggests, involved conjugation of the thiolcontaining GE11 peptide to the PLGA-PEG-maleimide polymer by maleimide-thiol chemistry in an organic solvent overnight under stirring conditions. The conjugate formed was then purified from unreacted polymer and peptide by the processes of precipitation and dialysis, respectively. Next, it was combined with PLGA-PEG and PLGA polymers to formulate 30% PLGA-PEG-GE11 (pre-GE11) NPs, by the process of nanoprecipitation (Figure 2.1a). The degree of peptide-polymer conjugation was carried out using ^{1}H NMR.

On the other hand, the post-conjugation strategy involved formulation of 30% PLGA-PEGmaleimide NPs by the process of nanoprecipitation. The GE11 peptide was then conjugated to these NPs using maleimide-thiol chemistry (Figure 2.1b). The efficiency of peptide-NP conjugation was carried out by measuring the concentration of unbound peptide in the supernatant using Nanodrop. In both cases, the GE11 peptide was first synthesized using solid phase peptide synthesis (SPPS) and purified by UPLC-MS (Appendix-1, Figure A1.1) and the formulated NPs were characterized for size surface charge using TEM and DLS.

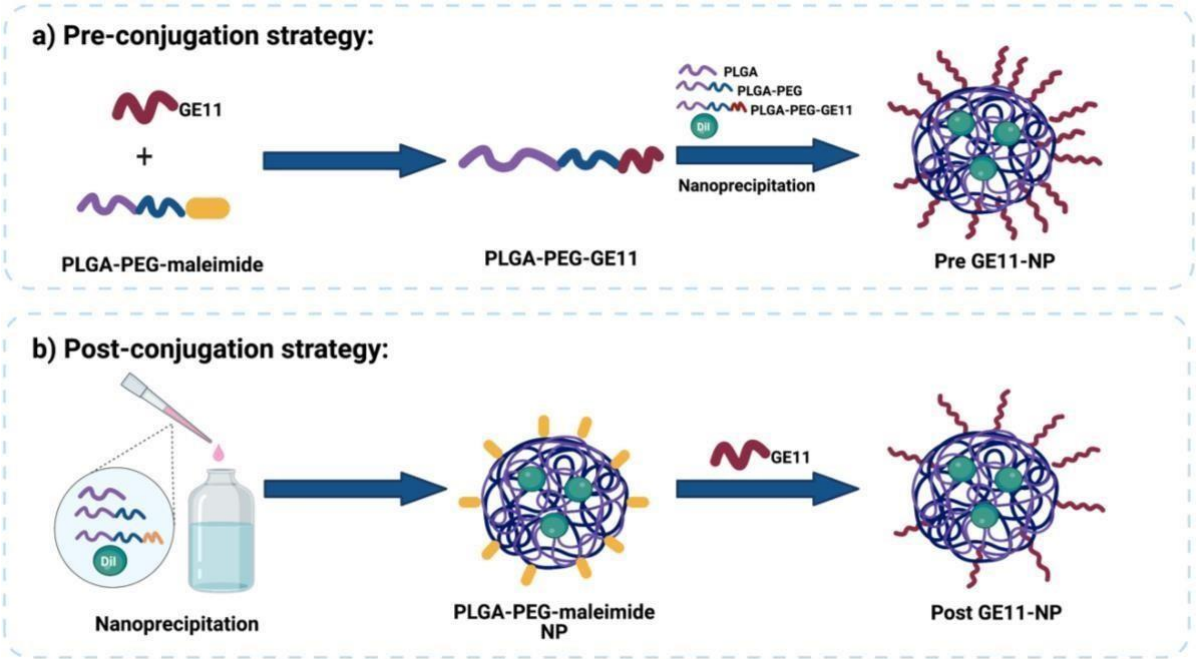

Figure 2.1 Schematic representation of pre- and post-GE11 conjugation strategies. *a) In the preconjugation strategy, GE11 peptide is conjugated to PLGA-PEG-maleimide polymer prior to PLGA-PEGWQP NPs formulation by nanoprecipitation, resulting in higher GE11 density on NP surface. b) In*

the post-conjugation strategy, PLGA-PEG-maleimide nanoparticles are first formulated by the process of nanoprecipitation and the GE11 peptide is then conjugated to the NPs, resulting in lower GE11 density on the NP surface.

2.2.2 Pre-GE11 conjugation, NP formulation and characterisation.

We pre-conjugated the GE11 peptide to PLGA-PEG-maleimide polymer in organic conditions and then purified it using precipitation and dialysis processes to finally obtain PLGA-PEG-GE11 conjugate. Next, we characterized the extent of this conjugation reaction using ^{1}H NMR, which allowed for obtaining the spectra for hydrogen nuclei specific for the polymer (PLGAPEG-Mal), the peptide (GE11), and the conjugate (PLGA-PEG-GE11) as shown overlapped in Figure 2.2a. The intense signals observed at d = 1.46, 4.9 and 5.2 ppm in the polymer and conjugate spectra correspond to the methyl (-CH_3), methylene (–CH_2) and methine (–CH) groups of PLGA. On the other hand, the signals observed in the conjugate and peptide spectra around d = 6.6 ppm, as shown in Figure A1.2 (Appendix 1), are attributed to the protons from the aromatic side chain of the amino acid Tyrosine (Y) in the peptide sequence, thereby confirming its successful conjugation to the polymer. After integrating the area under peaks corresponding to the protons of GE11 peptide with those from the polymer, the conjugation efficiency (CE) was calculated. We found that the pre-conjugation of WQP to the polymer allowed for a CE of 67,7%, as shown in Table A1.1 (Appendix 1).

We then formulated multivalent NPs having surface GE11 valency of 30% using the PLGA-PEGGE11 conjugate along with combinations of PLGA and PLGA-PEG co-polymers (x and y respectively) manually by the nanoprecipitation process[26,27]. For post-conjugation, we conjugated the GE11 peptide to formulated PLGA-PEG-Mal NPs using 1:3 molar ratio of NPs: GE11 peptide in 1X PBS under stirring conditions for 4h at room temperature. As a control, we used PLGA-PEG NPs lacking maleimide group to check for the efficiency of maleimide-thiol conjugation. We then collected the conjugated NPs by centrifugation using Amicon filters and

analyzed the supernatant for the presence of unbound GE11 using nanodrop, which was then used to indirectly calculate the CE. We found that the post-conjugation strategy gave a CE of 37.5%, shown in Table A1.2 (Appendix 1). Figure 2.2 b and c show the characterization of formulated pre- and post-NPs in terms of size and morphology using DLS and TEM and net surface charge (zeta [□] potential) using DLS. We found a very small increasing trend in the sizes between non-targeted PLGA-PEG-Mal NPs, 30% post-GE11 NPs and 30% pre-GE11, owing to a higher number of GE11 on their surface. However, given the small size of the peptide (13 amino acids), the increase in size is rather small (10-20nm). Furthermore, we do not see a big difference surface negative charge of PLGA-PEG NPs by addition of GE11 peptide, as it has a net neutral charge at physiological pH (7.0). In terms of NP morphology by TEM, we obtained spherical GE11-NPs with an average diameter of 105nm. The decrease in the diameter obtained by TEM can be attributed to the fact that DLS measures the hydrodynamic radius, while TEM measures naked particles (in dry conditions)[17].

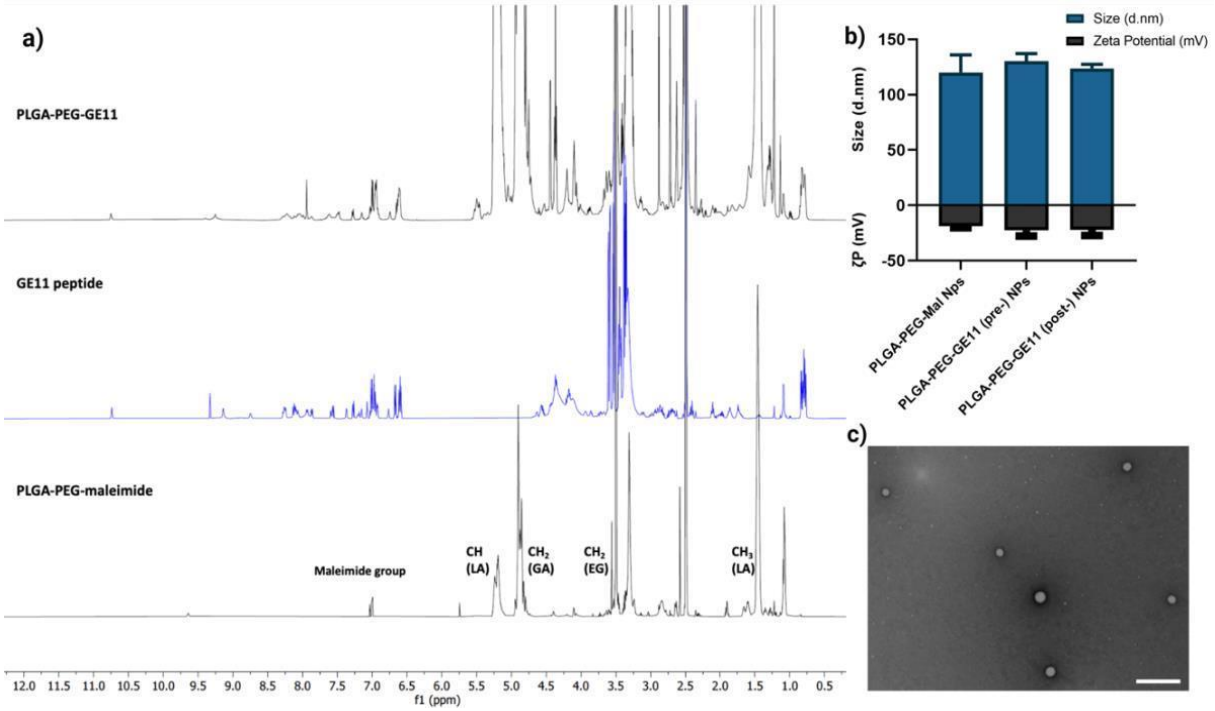

Figure 2.2 Pre- and post-GE11 conjugation, NP formulation and characterisation. *a) Pre-conjugation of PLGA-PEG-GE11 characterized by ^{1}H NMR. Overlapped spectra of the PLGAPEG-maleimide (polymer), GE11 (peptide) and PLGA-PEG-GE11 (conjugate) showing coinciding regions. b) 30%*

PLGAPEG NPs formulated by pre- and post-conjugation of GE11 peptide characterized for size (nm) and zeta (ζ) potential (mV) using DLS. c) Pre-GE11 conjugated NPs characterized for size (nm) and shape by TEM.

Scale bar 200nm.

2.2.3 Surface peptide quantification by specific enzymatic digestion.

As explained before, one of the main reasons behind inefficiency of targeted nanomedicines is the lack of robust characterization of surface ligands. Routinely employed techniques include some spectrometric or colorimetric tests[27], but these have limited utility in terms of the type of ligand used, in that, most of them are known to work predominantly for measuring larger molecules like proteins, antibodies, etc.[28] Furthermore, given the strengths and weaknesses of each technique, in most cases, a combinatorial approach must be employed[27], which is time-consuming and not always efficient. In this context, we developed the method of site-specific enzymatic digestion to quantify the number of surface peptides in a robust manner. Again, this method is routinely used for protein quantification[29], but we exploited its high sensitivity to show that it can also be easily used for quantification of small peptides.

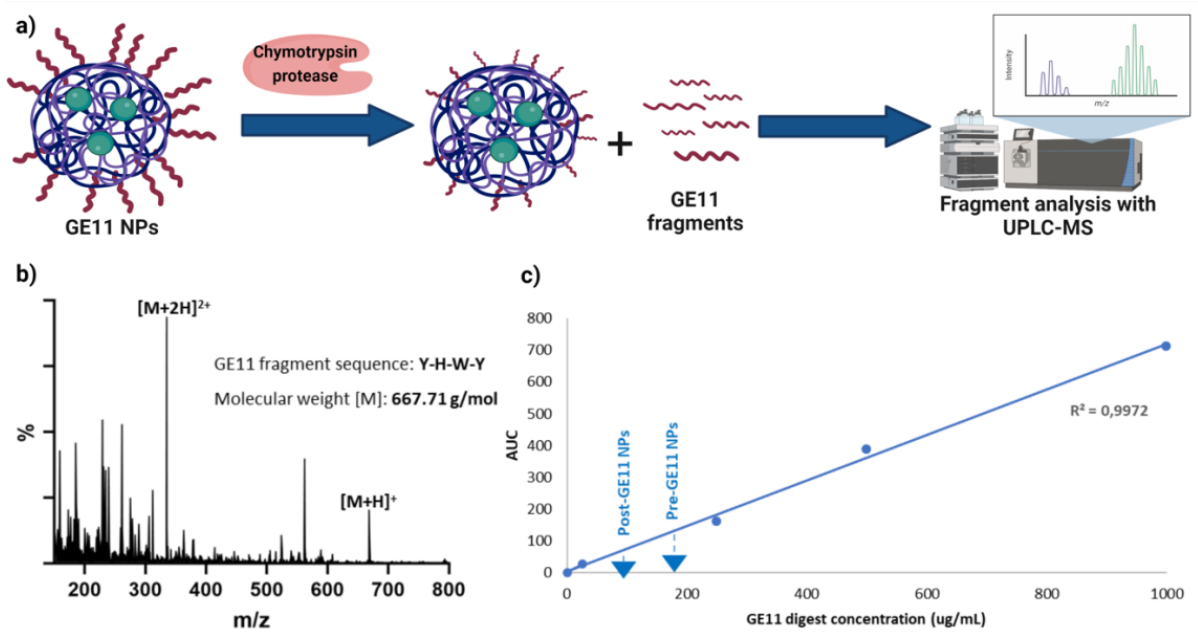

Figure 2.3 Chymotrypsin-mediated degradation of NP and quantification of surface GE11. *a) Schematic representation of enzymatic digestion process for GE11 quantification on NP surface. b) UPLC-MS spectra showing mass/charge (m/z) values of the chosen GE11 digested fragment and c) Calibration curve of GE11 digest used for calculation of number of surface GE11.*

Proteases are a type of enzyme that specifically cleave amino acid sequences in proteins[29]. Chymotrypsin protease is such an example, it is known to specifically cleave at the C-terminal of aromatic amino acids such as tryptophan (W), tyrosine (Y) and phenylalanine (F)[30]. In the sequence of GE11 peptide (Y-H-W-Y-G-Y-T-P-Q-N-V-I-C), we expected highly specific cleavages at the C-terminal ends of tyrosine (Y) at positions 4 and 6 (starting from N-terminal) and tryptophan (W) at position 3; while anticipating a less (likely) specific cleavages at the Cterminal ends of Y at position 1 and Isoleucine (I) at position 12. We confirmed the presence of the digested fragment of Y at position 4, having molecular weight of 667.71Da by analyzing the supernatant obtained after pelleting down the NPs by UPLC-MS as shown in the schematic in Figure 2.3a. The high sensitivity of UPLC-MS allowed us to detect the digested fragment as a distinct peak, which we integrated to obtain the corresponding area on the chromatogram at □= 280nm, as shown in Figure A1.3a (Appendix-1), which showed masses specific to the

fragment divided by charge of the protons (+1 and +2), in the corresponding spectra depicted in Figure 2.3b. We then prepared a calibration curve using a range of known concentrations of the digested peptide alone to calculate the number of GE11 from the concentration (µg/mL) of unknown samples as shown in Figure 2.3c. As demonstrated in Table 2.3, pre-GE11 NPs had a higher number and coverage of surface GE11 as compared to post-GE11 NPs, depicted in Figure A1.3b (Appendix-1). These results bring forth the underlining influence of different conjugation strategies on the number of ligands obtained on NP surface, an important parameter that needs to be accounted for in the design of efficient targeted nanosystems.

Samples	**Theoretical #GE11**	**Observed #GE11**	**Surface GE11 coverage (%)**
30% pre-GE11 NPs	1713	1620	94,32
30% post-GE11 NPs	1713	866	50,53

Table 2.3 Calculation of number (#) of GE11 on NP surface. *The availability (valency and coverage) of pre- and post-conjugated GE11 on NP surface is calculated by dividing the number of expected versus observed GE11 and getting a percentage of the formulated surface valency.*

2.2.4 EGFR expression and NP cytotoxicity analyses.

For cellular uptake assays, we employed a panel of PCa cell lines. These included the advanced stage prostatic carcinoma cell lines: LNCaP, PC3 and 22Rv1, while the prostate epithelial cell

line RWPE1 was used as a healthy control for selectivity analysis. Receptor immunostaining with anti-EGFR antibody was carried out and the EGFR expression across the cell lines was quantified by flow cytometry. Expectedly, PC3 cells showed highest expression of EGFR followed by 22Rv1 cells, while LNCaP and RWPE1 cells showed low/no expression, respectively (Figure 2.4a). These results provided a basis for further cell-based assays.

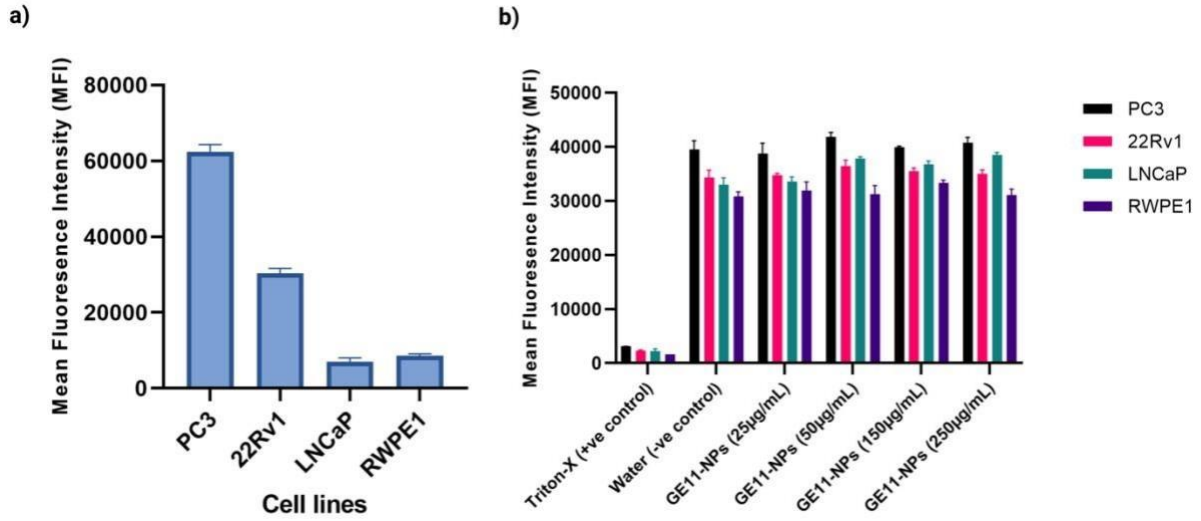

Figure 2.4 EGFR expression and cellular cytotoxicity analyses of pre-GE11 NPs. *a) EGFR expression across prostate (cancer and healthy) cell lines obtained as a mean fluorescence intensity of Alexa-647 tagged anti-EGFR antibody by flow cytometry. b) Cellular cytotoxicity of varying concentration ranges of 30% pre-GE11 Ps on all cell lines by PrestoBlue cell viability assay.*

For any nanoparticle targeting study, it is important to account for the cytotoxicity of the nanocarrier system to design optimal delivery systems with low/no side effects. Cytotoxicity analysis was carried out using PrestoBlue cell viability assay. PrestoBlue is a dye which is known to undergo modification under reducing environments of viable cells, thereby giving a measure of the cellular metabolism and activity. Pre-GE11 conjugated NPs, which showed higher number of surface GE11, were employed in increasing concentrations (25-250 □g/mL) for measuring cytotoxicity. Triton-X detergent was used as positive control, while Milli Q water was the negative control, both of which showed lower and higher fluorescence values as a

measure of cellular activity, respectively, as shown in Figure 2.4b. Further, higher fluorescence values were obtained for increasing concentrations of pre-GE11 NPs, which correlated to an increase in metabolic activity of the cells, thereby rendering minimal (if none) cytotoxicity for the entire range of concentrations.

2.2.5 Pre- versus post-GE11 NP mediated cellular uptake by CLSM and flow cytometry.

For testing the effect of pre- versus post-conjugated GE11 peptide NPs on the cellular uptake, we used four prostate (cancer- LNCaP, PC3 and 22Rv1; healthy- RWPE1) cell lines having varying levels of EGFR expression. The cells were incubated with 50µg/mL of control (PLGAPEG), pre- and post-GE11 NPs for 24h at 37ºC, 5% CO_2. We then imaged all the cell lines using CLSM for qualitatively assessing their cellular uptake.

As expected, we observed an increasing trend in the cellular uptake of pre-GE11 NPs over post-GE11 NPs and the control NPs (Figure 2.5). This increase in uptake can be attributed to a stronger multivalent effect obtained by a higher number of surface GE11 on the preconjugated NPs in comparison to the other two. Furthermore, we observed that this uptake increased with increasing expression levels of EGFR, in that the cells with higher EGFR expression (PC3 and 22Rv1) had the highest uptake over those with lower EGFR expression (LNCaP and RWPE1), thereby conferring selectivity for certain PCa cells.

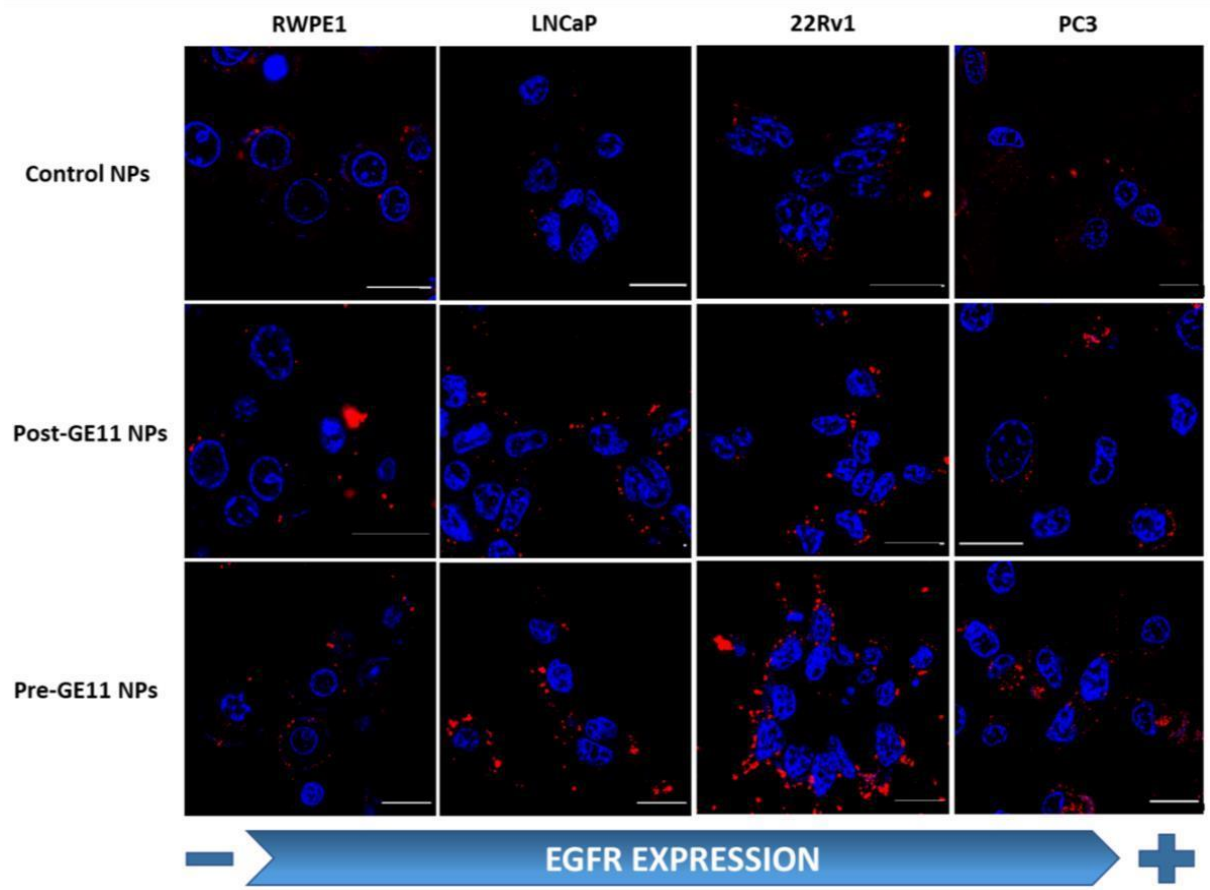

Figure 2.5. Qualitative assessment of cellular uptake of pre- vs. post-conjugated GE11 NPs by CLSM. *Cellular uptake of 30%NPs: PLGA-PEG (control), pre-GE11 and post-GE11 (encapsulated with Dil-red) in different prostate (healthy and cancerous) cell lines analyzed by CLSM. Cellular nuclei tagged with Hoechst33342 (blue). Scale bar 25um.*

Flow cytometry is a known robust technique that works on the principle of light scattering and fluorescence emission by the specific fluorescent probe-labelled cells as they pass through a laser beam. It offers several unique advantages as it allows fast, relatively quantitative, multiparametric analysis of cell populations at the single cell level [31]. We used flow cytometry to quantify and compare the uptake of pre- and post-GE11 over that of the non-targeted (control) NPs across different PCa cell lines.

Figure 2.6a shows a clear overall increase in cellular uptake of pre-GE11 NPs in comparison to post-GE11 NPs. This increase in uptake can be attributed to the increased affinity of GE11 peptide towards EGFR over-expressing cells, owing to an increased NP surface coverage in case of pre-conjugated NPs. Figure 2.6b shows the selectivity of pre- and post-conjugated GE11 NPs for uptake in PCa cell lines in comparison to the healthy RWPE1 cells. Interestingly, despite the uptake being highly selective in the case of PC3 and 22Rv1 cell lines having higher EGFR expression over the healthy RWPE-1 cells, the difference in selectivity between pre- and post-conjugated GE11 NPs is not very significant: 5-fold and 3-fold increase (PC3 cells) and 4-fold and 2.5-fold increase (22Rv1 cells), respectively. This can be attributed to strong binding affinity of the GE11 peptide towards EGFR, which somehow shadows the effect of multivalent targeting. In addition, a higher number of surface peptide could possibly result in non-specific binding to cells with lower EGFR expression, thus reducing the selectivity. Nonetheless, the choice of employing the right conjugation strategy plays an important role in selectivity, which is crucial for personalization of targeted nano therapies.

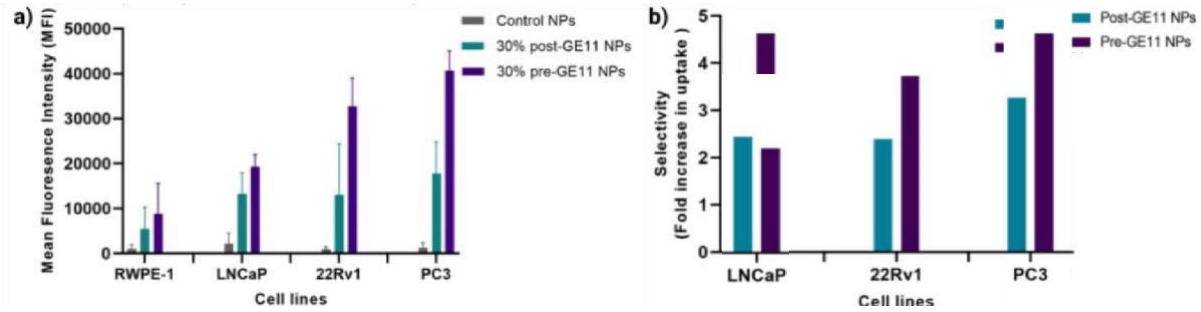

Figure 2.6. Quantitative assessment of cellular uptake of pre- vs. post-conjugated GE11 NPs by flow cytometry*. a) Cellular uptake of 30%NPs: control, pre- and post-GE11 NPs in different prostate (healthy and cancerous) cell lines as a measure of mean fluorescence intensity (MFI) analyzed by flow cytometry. b) Selective cellular uptake (fold increase) of pre- and post-GE11 NPs in comparison to healthy cells in PCa cell lines.*

2.3 Conclusions

In this work, we employed two commonly used conjugation strategies using GE11 peptide, a known targeting ligand for EGFR, and polymeric NPs, and compared their impact on their interaction with cells (uptake). We robustly characterized the conjugated NPs for surface peptide number using enzymatic digestion and found that pre-conjugation allowed for a higher surface coverage with GE11 peptide, a parameter that must be accounted for in the development of more effective active targeting nano-formulations. Having a higher number of surface peptides resulted not only in an increased cellular uptake, but it also led to selective targeting of cells overexpressing the target receptor. This property is extremely desirable for the development of personalized nanomedicines. We believe that these results have helped to improve our understanding of the importance of NP design parameters, leading to the development of highly efficient targeted nanosystems, paving the path for personalization of treatments.

2.4 Experimental section

Pre-GE11 conjugation, characterization, and NP formulation

For pre-conjugation, previously purified GE11 peptide was conjugated to $PLGA_{30k}PEG_{5k}$maleimide polymer using a previously described protocol[20]. The conjugation was allowed to take place in an organic solvent (ACN) and incubated under stirring conditions overnight. The conjugate was then purified from unreacted polymer by the process of precipitation using ice-cold diethyl ether/methanol (DEE/ MeOH) mixture. The precipitate was obtained by centrifugation at 4000xg for 15 minutes at 4ºC, after which it was washed twice with DEE/MeOH mixture and finally redissolved in ACN and dialyzed for a minimum of 24 hours against pure ACN to separate the unreacted GE11 from the conjugate. Next, the purified conjugate was lyophilized and a final yield of approximately 40% was obtained. Thereafter,

5mg of polymer (PLGA-PEG-maleimide), peptide (GE11) and the conjugate (PLGAPEG-GE11) were each dissolved in 0.7mL of deuterated dimethyl sulfoxide (d6-DMSO) and the degree of conjugation was characterized using Bruker 500Hz proton nuclear magnetic resonance (^{1}H NMR) and analyzed using the Mnova (v.14.0) software.

30% pre-GE11 NPs were formulated via the nanoprecipitation method according to literature[26]. Briefly, 3 mg of polymer mixture and 1.1 mM of DiI were dissolved in 300µL solvent phase (ACN) at room temperature. PLGA polymer was maintained at a ratio of 15% and mixed with $PLGA_{30k}$-PEG_{1k} and $PLGA_{30K}$-PEG_{5K}-GE11 conjugate at 30% of surface GE11 valency. For control PLGA-PEG formulations, PLGA-PEG-GE11-conjugate was substituted with PLGA-PEG-Mal, whilst the PLGA amount was maintained constant at 15%. The anti-solvent phase (MiliQ water) was stirred at 200-300 rpm whilst the solvent phase comprising the polymer solution (ACN) was pipetted at a 1:10 ratio (300µL polymer solution is pipetted into 3mL MiliQ water). Solvent extraction (evaporation) was continued for 5 h under magnetic stirring in a fume hood at room temperature. NPs were then collected by high-speed centrifugation (Avanti J-26 XPI, rotor JA-14) using Amicon Ultra-4 100kDa filters as per filter instructions (10 min at 5,000 x g at 20ºC) with filtered MiliQ water. NPs were stored in MiliQ water at a 10 mg/mL concentration in the dark at 4ºC until further use.

Post-GE11 conjugation and characterization

For post-conjugation, the GE11 peptide was conjugated to already formulated 30% PLGAPEGMal NPs, which were formulated similarly as described earlier, by the process of nanoprecipitation. The conjugation between the thiol-containing GE11 peptide and 30% PLGA-PEG-Mal NPs was carried out at a 2:1 molar ratio of GE11 peptide to maleimide polymer, to ensure optimal conjugation. For this, the GE11 peptide (x2 molar excess) was added from the stock to 1X PBS (pH=7.4) to which 300uL of 10mg/mL NPs were then added under stirring

conditions. The final volume of the reaction mixture was maintained at 1mL, and the solution was stirred for 4h at room temperature in dark conditions. Unconjugated GE11 was removed via centrifugation using Amicon Ultra-4 filters as per filter instructions for 10 min at 5,000 x g (rcf) at 20°C with filtered Milli Q water. Conjugated NPs were stored in Milli Q water at a concentration of 10mg/mL in the dark at 4°C.

Surface peptide quantification by enzymatic digestion

The quantification of conjugated GE11 on NP surface was carried out by site-specific digestion of the peptide using the enzyme Chymotrypsin protease by following the protocol provided by the manufacture (Pierce™, MAN0011638) with certain optimizations. As the protocol is usually used for large protein samples, the pre- and post-GE11 NPs were highly concentrated (25-50mg/mL), to have enough concentration of the digested peptide fragments to be detected by mass spectrometry. The digestion reaction was carried out at an enzyme: peptide sample ratio of 1:20, in the digestion buffer [500mM Tris HCl (pH 8.0) + 10mM $CaCl_2$]. The reaction vessel was incubated at 37ºC overnight and the digested fragments were collected from the supernatant obtained by brief (5 min) centrifugation of the samples to separate the NPs. The supernatant was then characterized by UPLC-MS at □=280 nm, where a peak corresponding to the mass of the chosen digested fragment was obtained, the integrated value of whose area along with a calibration curve of known concentrations of digested GE11 fragments was used to calculate the exact number of surface GE11. For calculation of theoretical (expected) number of GE11s, we used the formula as per Spherotech´s instructions as follows:

1. *Calculating the number of NPs in suspension*

= [6 x Polymer weight (g) / (3.14 x Polymer density (g/cm3) x NP diameter (um)^3] * 10^{12}.

2. *Calculating the number of GE11 molecules in suspension*

   = [Mass of GE11-conjugate (g) / Molecular weight of GE11-conjugate (g/mol)] * Avogadro´s number.

3. *Calculating the theoretical number of GE11 molecules per NP*

   = Number of GE11 molecules (2) / Number of NPs in suspension (1)

4. *Calculating moles of GE11-conjugate added*

   = Mass of GE11-conjugate added (g) / Molecular weight of GE11-conjugate (g/mol)

5. *Calculation of mass (□g/mL) of GE11 added*
   = moles of GE11-conjugate added * molecular weight of GE11.
6. *Calculation of moles of GE11 (observed) obtained on NP surface:*
   = Mass of GE11 (observed) / Molecular weight of GE11.

9. *Calculation of molecules of GE11 on NP surface*
   = Moles of GE11 (observed) * Avogadro´s number.

We divide this value by molecules of NPs in suspension obtained in (2) to get the number of GE11/ NP.

Nanoparticle cytotoxicity analysis.

For measuring the cytotoxicity of the formulated NPs, PrestoBlue cell viability assay was employed as per manufacturer´s instructions. Briefly, all cell lines were seeded in a 96-well

plate and incubated for 24h at 37ºC and 5% CO_2. They were then incubated with the formulated 30% pre-GE11 in varying concentrations (from 25 to 250µg/mL) for 24h at 37ºC and 5% CO_2. As a negative control, filtered MilliQ water of equal volume was used instead of culture medium. Next, the NP-containing medium was aspirated, and the cells were incubated with PrestoBlue (10%v/v of 5% PrestoBlue stock) and incubate for 1hr at 37ºC. Fluorescence was measured at 590nm. All measurements were carried out in triplicates and their mean□SD values were obtained.

Receptor expression analysis

For measuring the expression levels of EGFR, all the cell lines were stained with mouse monoclonal anti-EGFR antibody (MA5-13319- ThermoFisher Scientific) according to manufacturer´s protocol. Briefly 1µg/mL of 1º anti-EGFR antibody dissolved in 3% BSA was added to a monolayer of cells in LabTek on ice for 1hr. Next, the cells were washed thrice with 1X PBS and incubated with 1µg/mL (dilutions provided by manufacturer) of polyclonal goat: anti-mouse Alexa-647 secondary (2º) antibody for at least 1 hour in dark conditions. As a negative control, cells tagged with only 2º antibody were used to check for its non-specific binding. For flow cytometry, the cells were detached using 0.25% Trypsin-EDTA incubation for 10 mins at 37ºC, 5% CO_2 and obtained in suspension in 1X PBS. They were then stained with 10µg/mL of DAPI just before analysis with FACS Aria, with the 488nm laser. In total 10,000 cells (or events) were measured, and their mean fluorescence intensity values obtained. All the measurements were performed in triplicates and the mean□SD values were obtained.

Qualitative analysis of cellular uptake by confocal laser scanning microscopy (CLSM)

All cell lines (PC3, 22Rv1, LNCaP, and RWPE1) were cultured in an 8-well LabTek ($25x10^3$ cells/ well) for 24h at 37ºC and 5%CO_2, until they reached up to 70% confluence and then incubated

with a known concentration (50µg/mL) of 30% PLGA-PEG (Control) NPs, pre- and postconjugated 30% PLGA-PEG-GE11 NPs dissolved in culture medium without serum (RPMI 1640 for LNCaP, PC3 and 22Rv1; and KSFM for RWPE1) for 24h at 37ºC and 5% CO_2. Post incubation, the medium containing NPs was aspirated, and the cells were stained with the nuclear dye Hoechst33342 (1µg/mL) for 10 minutes at room temperature. The cells were then imaged live at 37ºC and 5% CO_2 using 63X oil immersion objective of the Zeiss LSM 800 confocal microscope. The cell nuclei and DiI encapsulated WQP-NPs were excited using 405nm and 561nm lasers at 3% power, respectively.

Quantitative analysis of cellular uptake by flow cytometry

For flow cytometry, all the cell lines were cultured in 6-well plates ($1x10^5$ cells/ well) for 24h until they reached up to 70% confluence and then incubated with a known concentration (50µg/mL) of 30% Control NPs, pre- and post-conjugated 30% PLGA-PEG-GE11 NPs for 24h at 37ºC and 5% CO_2. Post incubation with NPs, the adherent cells were detached using 0.25% Trypsin/EDTA, incubated for 10 minutes at 37ºC and 5% CO_2, and obtained in suspension by centrifugation at 3000rpm for 5 minutes at 4ºC. From this moment onwards, all the further steps like washing with 1X PBS and resuspension in 1X PBS, were carried out whilst maintaining the cells on ice. Finally, the cells were resuspended in 1X PBS solution with the live cell staining agent DAPI (10µg/mL) and analyzed using BD FACSAria™. The cells not stained with DAPI were excluded from the analysis. At least 10000 cells (or events) were analysed using two specific lasers for WQP-Cy5 (Red C-670nm) and multivalent WQP-NPs encapsulated with DiI (Green E-575nm). All measurements were carried out in triplicates and the standard deviation was obtained.

2.5 References.

1 M. J. Mitchell, M. M. Billingsley, R. M. Haley, M. E. Wechsler, N. A. Peppas and R. Langer, *Nat Rev Drug Discov*, 2021, **20**, 101–124.

2 Insights into Active Targeting of Nanoparticles in Drug Delivery: Advances in Clinical Studies and Design Considerations for Cancer Nanomedicine | Bioconjugate Chemistry, https://pubs-acsorg.sire.ub.edu/doi/full/10.1021/acs.bioconjchem.9b00456?casa_token=E8cGJfbLQf8AAAAA%3AkJwoJ7A08FJweU6eQaHYg43PE16yXp7YdXFXsKmTXIvkvxXtgAkJGsiI3rd6sbMN5D2Eny_ekbhw.

3 J. Yoo, C. Park, G. Yi, D. Lee and H. Koo, *Cancers*, 2019, **11**, 640.

4 H. Hossein-Nejad-Ariani, E. Althagafi and K. Kaur, *Sci Rep*, 2019, **9**, 2723.

5 A. Mousavizadeh, A. Jabbari, M. Akrami and H. Bardania, *Colloids Surf B Biointerfaces*, 2017, **158**, 507–517.

6 S. Wilhelm, A. J. Tavares, Q. Dai, S. Ohta, J. Audet, H. F. Dvorak and W. C. W. Chan, *Nat Rev Mater*, 2016, **1**, 16014.

7 L. Woythe, N. B. Tito and L. Albertazzi, *Advanced Drug Delivery Reviews*, 2021, **169**, 1–21.

8 K. Yu, Y. Zhou, Y. Li, X. Sun, F. Sun, X. Wang, H. Mu, J. Li, X. Liu, L. Teng and Y. Li, *Biomater. Sci.*, 2016, **4**, 1219–1232.

9 N. H. Abd Ellah and S. A. Abouelmagd, *Expert Opinion on Drug Delivery*, 2017, **14**, 201–214.

10 A. D. Friedman, S. E. Claypool and R. Liu, *Curr Pharm Des*, 2013, **19**, 6315–6329. 11 M. Brückner, J. Simon, K. Landfester and V. Mailänder, *Nanoscale*, 2021, **13**, 9816– 9824.

12 L. Martínez-Jothar, S. Doulkeridou, R. M. Schiffelers, J. Sastre Torano, S. Oliveira, C. F. van Nostrum and W. E. Hennink, *Journal of Controlled Release*, 2018, **282**, 101–109.

13 Y. Liu, K. Li, B. Liu and S.-S. Feng, *Biomaterials*, 2010, **31**, 9145–9155.

14 M. A. Gauthier and H.-A. Klok, *Chem. Commun.*, 2008, 2591.

15 J.-M. Rabanel, V. Adibnia, S. F. Tehrani, S. Sanche, P. Hildgen, X. Banquy and C. Ramassamy, *Nanoscale*, 2019, **11**, 383–406.

16 T. Nerreter, S. Letschert, R. Götz, S. Doose, S. Danhof, H. Einsele, M. Sauer and M. Hudecek, *Nat Commun*, 2019, **10**, 3137.

17 T. Andrian, P. Delcanale, S. Pujals and L. Albertazzi, *Nano Lett.*, 2021, **21**, 5360–5368. 18 D. G. Mullen and M. M. Banaszak Holl, *Acc. Chem. Res.*, 2011, **44**, 1135–1145. 19 I. Genta, E. Chiesa, B. Colzani, T. Modena, B. Conti and R. Dorati, *Pharmaceutics*, 2017, **10**, 2.

20 P. Ulivi, *Int J Biol Markers*, 2020, **35**, 16–19.

21 I. Belczacka, A. Latosinska, J. Metzger, D. Marx, A. Vlahou, H. Mischak and M. Frantzi, *Mass Spectrometry Reviews*, 2019, **38**, 49–78.

22 R. A. de Araújo, F. A. C. da Luz, E. da C. Marinho, C. P. Nascimento, L. de A. Marques, P. F. R. Delfino, R. M. Antonioli, B. J. Araújo, A. C. A. L. da Silva, M. L. G. dos R. Monteiro, M. B. Neto and M. J. B. Silva, Epidermal growth factor receptor (EGFR) expression in the serum of patients with triple-negative breast carcinoma, http://ecancer.org/en/journal/article/1431epidermal-growth-factor-receptor-egfrexpression-in-the-serum-of-patients-with-triplenegative-breast-carcinoma-prognosticvalue-of-this-biomarker.

23 B. Colzani, G. Speranza, R. Dorati, B. Conti, T. Modena, G. Bruni, E. Zagato, L. Vermeulen, G. R. Dakwar, K. Braeckmans and I. Genta, *Int J Pharm*, 2016, **511**, 1112–1123. 25 H. Sung, J. Ferlay, R. L. Siegel, M. Laversanne, I. Soerjomataram, A. Jemal and F. Bray, *CA: A Cancer Journal for Clinicians*, 2021, **71**, 209–249.

26 J. M. Barichello, M. Morishita, K. Takayama and T. Nagai, *Drug Development and Industrial Pharmacy*, 1999, **25**, 471–476.

27 A. G. Mares, G. Pacassoni, J. S. Marti, S. Pujals and L. Albertazzi, *PLOS ONE*, 2021, **16**, e0251821.

28 C. Chiva, M. Ortega and E. Sabidó, *J. Proteome Res.*, 2014, **13**, 3979–3986.

29 T. Klein, U. Eckhard, A. Dufour, N. Solis and C. M. Overall, *Chem. Rev.*, 2018, **118**, 1137–1168.

30 F. Uliana, M. Vizovišek, L. Acquasaliente, R. Ciuffa, A. Fossati, F. Frommelt, S. Goetze, B. Wollscheid, M. Gstaiger, V. De Filippis, U. auf dem Keller and R. Aebersold, *Nat Commun*, 2021, **12**, 1693.

31 S. M. Manohar, P. Shah and A. Nair, *Bioanalysis*, 2021, **13**, 181–198.

Chapter 3| Multivalent effect of WQP-peptide functionalized polymeric nanoparticles towards selective PSMA targeting

The concept of selective tumor targeting using nanomedicines has been around for decades, however, no targeted NP has yet reached the clinic. A key bottleneck is the non-selectivity of targeted nanomedicines in vivo, which is attributed to lack of specific characterization of its surface properties, especially the ligand number, thereby calling for robust techniques that allow quantifiable outcomes for an optimal design.

Multivalent interactions essentially comprise multiple copies of ligands attached to scaffolds, allowing simultaneous binding to receptors and play an important role in targeting. As such, ´multivalent´ NPs facilitate simultaneous interaction of weak surface ligands with multiple target receptors resulting in higher avidity and enhanced cell selectivity. Therefore, the study of weak binding ligands for membrane-exposed biomarkers is crucial for the successful development of targeted nanomedicines.

In this chapter, we evaluate the effect of WQP peptide mediated multivalent PSMA targeting over its monomeric form using polymeric NPs across a panel of prostate cancer cell lines. We believe that this kind of strategy can prove to be useful for improving the binding affinity of a weak ligand as a mean for selective tumor targeting.

Supportive information for this chapter can be found in **Appendix 2.*

3.1 Introduction

As stated in chapter 1 of this thesis, prostate cancer (PCa) is the most commonly diagnosed malignancy and the second prevalent cause of cancer deaths in males worldwide[1-5]. Prostate

specific membrane antigen (PSMA) is a 100 kDa type II transmembrane glycosylated protein with folate hydrolase activity and is overexpressed not only in nearly all prostate cancer cells[6] but also in tumor neovasculature in a variety of cancers[6–8]. On the contrary, it has minimal expression (100-1000 times lower) in normal prostate epithelium tissues and other normal tissues[7,9], making it an ideal biomarker for the design of various targeted therapies. Several different kinds of targeting ligands against PSMA have been discovered over the years[10–12], however, they have not yet had a successful clinical translation, owing to multiple factors, namely, high production cost, low shelf life and blood clearance rate, and immunogenicity[12,13].

Although antibodies and aptamers are the most commonly used ligands having high binding affinity to PSMA[10], small cancer CTPs offer a number of advantages, including small molecular weight, high permeability, improved stability, less immunogenicity, ease of synthesis and flexibility in chemical conjugation[4,14–16]. One such example is the WQP peptide, which is 12 amino acid long, having the sequence WQPDTAHHWATL, and is known to have a moderate/low binding affinity to the extracellular domain of PSMA, which can be further enhanced up to 10-fold, by its dimerization[17]. Even though multiple studies had previously shown that the peptide-binding affinity can be improved by increasing the binding avidity through use of multivalent binding strategies, such as dimeric or tetrameric peptides or streptavidin-biotinylated peptide tetramers[17–20], nanoparticle-mediated multivalent WQP targeting studies still remain scarce.

Surface properties such as the valency plays an important role in the determination of targeting potential of NPs and their subsequent cellular fate[31,32]. In the last few years, there has been a great deal of attention on the development of multivalent NPs for their improved biological performance[27,33]. The multivalency allows for simultaneous binding to multiple receptors, which varies sharply with receptor concentration, thus allowing for selective targeting of tumor cells [34], which is the preferred strategy moving towards personalized nanomedicine[33]. Furthermore, achieving super-selective targeting also revolves around the

use of weak-binding ligands[24], which allow binding only to a specific density of target receptors, thus providing a way to avoid the undesired off-site responses[35].

Within this framework, we designed a study to test the effect of multivalent targeting of the WQP peptide-functionalized polymeric NPs in comparison to its weak-binding monomeric counterpart on the cellular uptake across different PCa and healthy cell lines. We synthesized and characterized WQP-Cy5 monomer along with multivalent WQP-NPs having varying surface WQP valencies (5% and 30%). We employed the enzymatic digestion technique, which is routinely used in quantification of proteins, for the purpose of specifically quantifying surface WQP peptide in a robust manner, and further tested their impact on the cellular uptake of all formulations across a panel of cell lines with varied expression levels of PSMA.

3.2 Results and discussion

3.2.1 Mono- and multivalent WQP formulation.

A brief outline of the schemes employed for the synthesis of mono and multivalent WQP is demonstrated in Figure 3.1. The WQP peptide was synthesized using solid phase peptide synthesis (SPPS) and modified at the non-PSMA binding C-terminal using a cysteine amino acid having a free thiol group and then purified, as shown in Figure A2.1 (Appendix-2). For the monovalent form of the peptide (Figure 3.1a), the synthesized WQP was conjugated with a thiol-reactive fluorescent dye, sulfo-cy5-maleimide, using maleimide-thiol chemistry.

For multivalent NP formulations (Figure 3.1b), the peptide was first conjugated to PLGA-PEGmaleimide polymer using maleimide-thiol chemistry in an organic solvent overnight under stirring conditions. This was then followed by formulation of multivalent NPs having different WQP surface valencies (5 or 30%) by the manual process of nanoprecipitation.

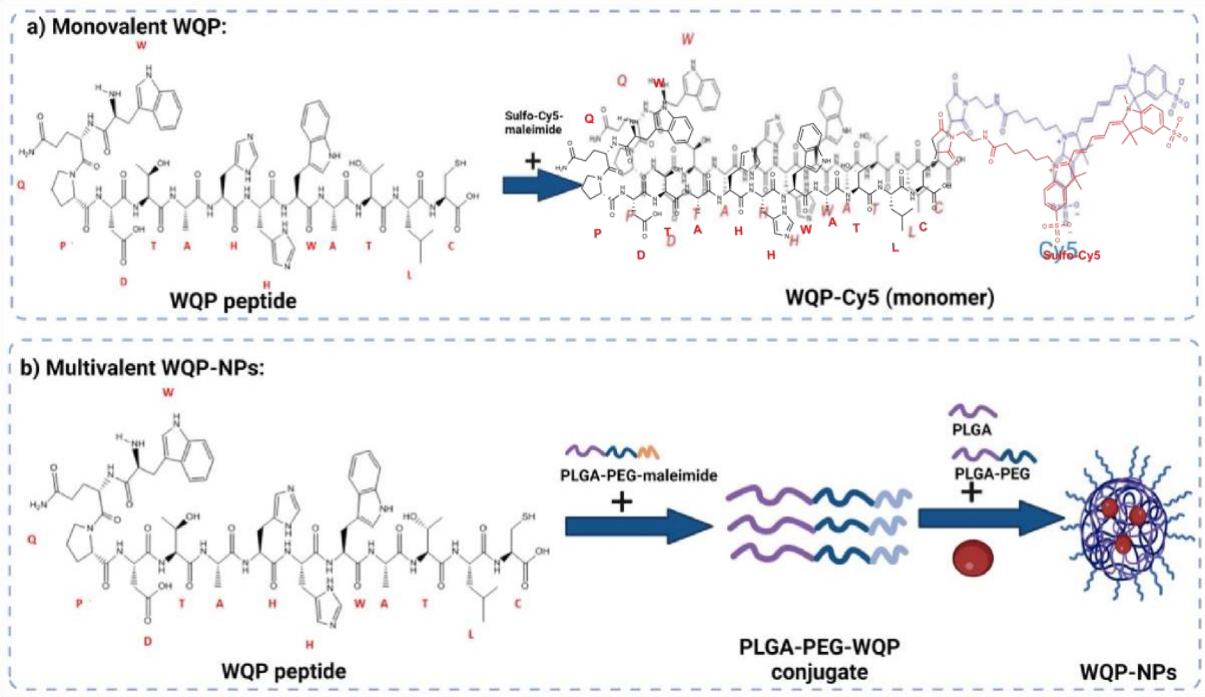

Figure 3.1 Scheme of mono and multivalent WQP synthesis. *a) WQP peptide is conjugated to sulfoCy5-maleimide dye by maleimide-thiol chemistry. b) WQP peptide is conjugated to PLGA-PEGmaleimide polymer and PLGA-PEG-WQP NPs are formulated by nanoprecipitation.*

3.2.2 WQP-Cy5 monomer synthesis, purification and characterization.

WQP peptide was synthesized using SPPS with the modification of thiol group containing cysteine (C) amino acid at the non-targeting C-terminal for downstream conjugation to maleimide containing Cy5 dye. It was then purified by semi-preparative HPLC-MS to yield 98% of pure WQP peptide and further analyzed by UPLC-MS giving a sharp peak in the chromatogram obtained at □=280nm with the corresponding m/z values with 2 and 3 protons obtained in the mass spectra (Figure 3.2a and b). Pure peptide was then conjugated to sulfocy5-maleimide dye using maleimide-thiol chemistry and the success of this conjugation was characterized using UPLC-MS, giving a distinct peak corresponding to WQP-Cy5 conjugate in the chromatogram obtained at □=280nm with its corresponding m/z values obtained in the mass spectra as shown in Figure 3.2c and d, respectively.

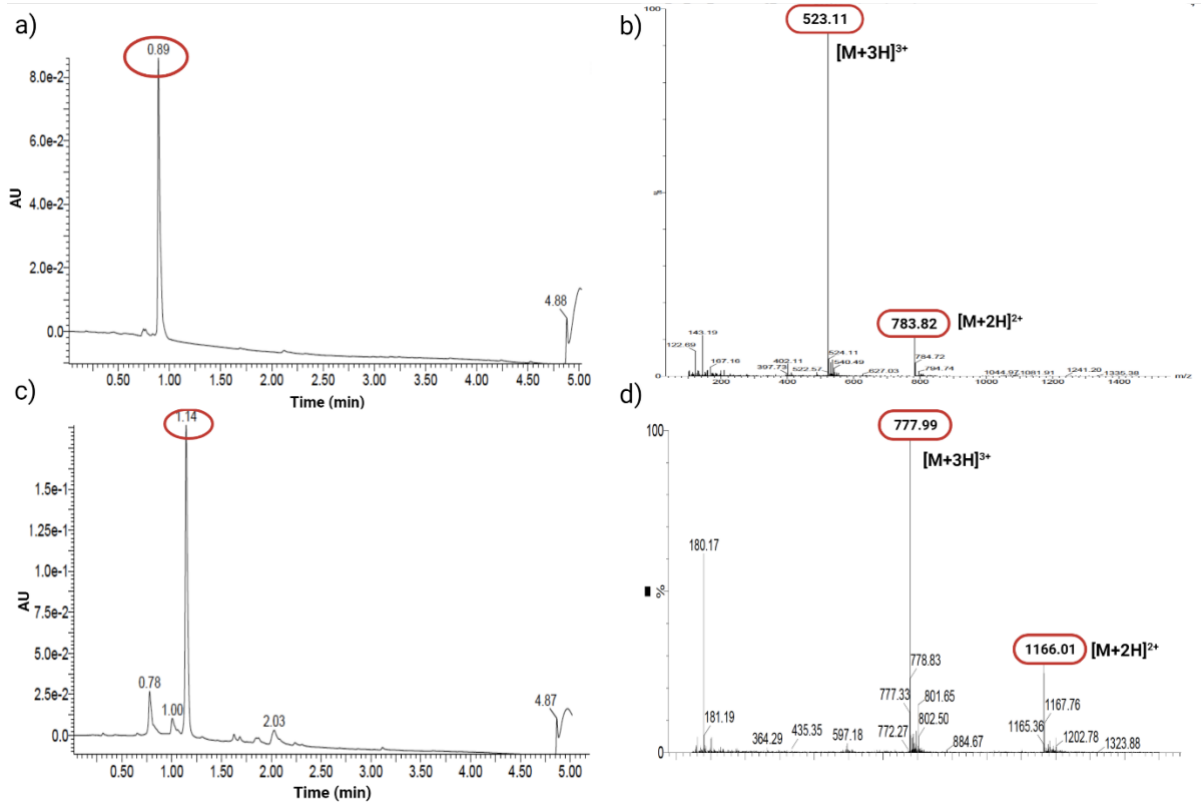

Figure 3.2 Synthesis and purification of WQP and WQP-Cy5. *a) UPLC-MS chromatogram at λ=280nm of purified WQP. b) Mass spectra of purified WQP showing corresponding m/z values. c) UPLC-MS chromatogram at λ=280nm of purified WQP-Cy5 and d) mass spectra of purified WQP-Cy5 showing corresponding m/z values.*

3.2.3 Polymer-peptide conjugation, multivalent NP formulation and characterization.

We employed the pre-conjugation strategy developed in the previous chapter. Briefly, we pre-conjugated WQP peptide to PLGA-PEG-maleimide polymer in organic conditions and then purified it using precipitation and dialysis processes to finally obtain PLGA-PEG-WQP conjugate. Next, we characterized the extent of this conjugation reaction using ^{1}H NMR, which allowed for obtaining the spectra for hydrogen nuclei specific for the polymer (PLGAPEG-Mal), the peptide (WQP), and the conjugate (PLGA-PEG-WQP) as shown overlapped in Figure 3.3a. The intense signals observed at d = 1.46, 4.9 and 5.2 ppm in the PLGA-PEG-Mal and PLGA-

PEG-WQP spectra correspond to the methyl (-CH_3), methylene (– CH_2) and methine (–CH) groups of PLGA. On the other hand, the signals observed in the PLGAPEG-WQP and pure WQP spectra around d = 7.31 and 7.53 ppm, as shown in the zoom-in spectra in Figure A2.1 (Appendix-2), are attributed to the protons from amide group (-NH_2) present in the amino acid Tryptophan (W) of the peptide, thereby confirming its successful conjugation to the polymer. After integrating the area under peaks corresponding to the protons of WQP peptide with those from the polymer shown in Figure A2.1 (Appendix-2), the conjugation efficiency (CE) was calculated. We found that the pre-conjugation of WQP to the polymer allowed for a CE of 77%, shown in Table A2.1 (Appendix-2).

We then formulated multivalent NPs with varying surface WQP valencies (5% and 30%) using the PLGA-PEG-WQP conjugate along with combinations of PLGA and PLGA-PEG co-polymers manually by the nanoprecipitation process[36]. Figure 3.3b and c shows the characterization of formulated multivalent NPs in terms of size and morphology using DLS and TEM and net surface charge using □-potential. We found a small increasing trend in the sizes of nontargeted PLGA-PEG NPs, 5% and 30% PLGA-PEG-WQP NPs, owing to increasing number of WQP on NP surface (90-120nm). However, given the small size of the peptide (1566kDa), the increase in size is rather small (10-20nm). Similarly, we see a small increase of surface negative charge of PLGA-PEG NPs by addition of WQP peptide (18-20mV) which has a net charge of (-0.9) at physiological pH (7.0). In terms of NP morphology by TEM, we obtained spherical multivalent WQP-NPs with an average diameter of 95nm.

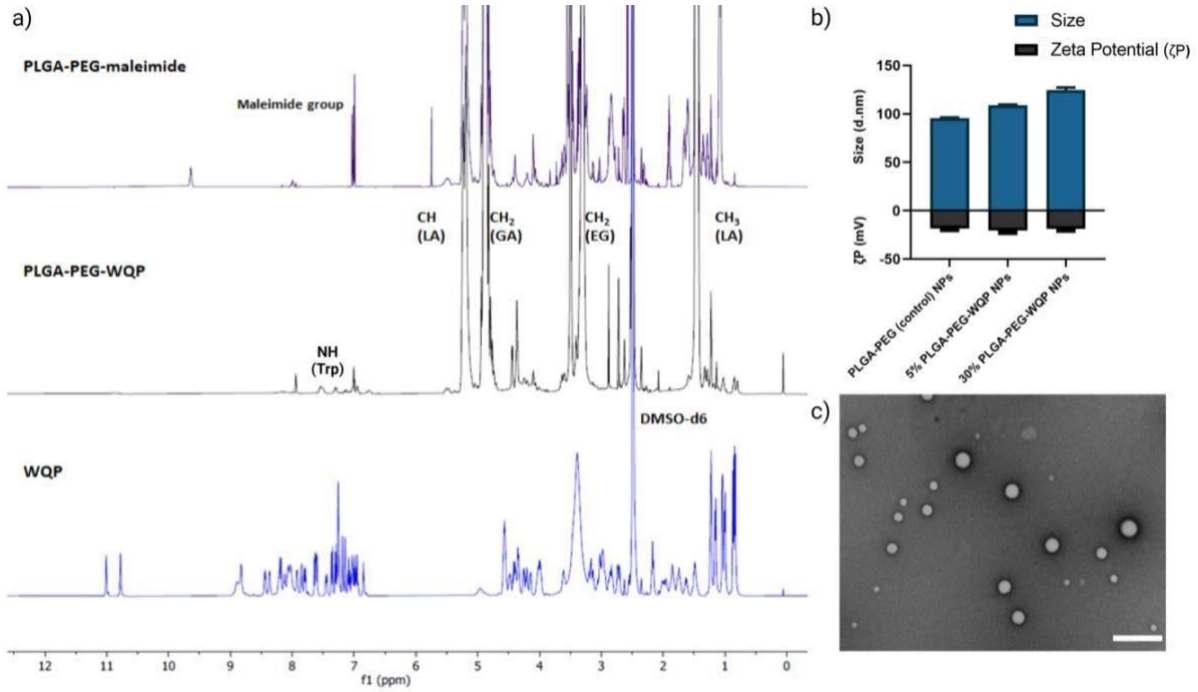

Figure 3.3 Multivalent WQP-NPs pre-conjugation, formulation, and characterization. *a) Characterization of PLGA-PEG-WQP conjugation by ^{1}H NMR: Overlapped spectra with coinciding regions shown. b) Multivalent WQP-NPs formulated from WQP conjugate characterized for size (nm) and □-potential (mV) using DLS and c) TEM image of 30% WQPNPs at scale bar 200nm.*

3.2.4 Quantification of WQP on NP surface by specific enzymatic degradation.

Here, we employed the method of site-specific enzymatic digestion developed earlier using chymotrypsin protease, a highly sensitive method routinely used for protein quantification[39], adapted it to quantify the number of WQP on multivalent NP surface. As described earlier, chymotrypsin protease is known to be highly specific for aromatic amino acid sequences. In the sequence of WQP peptide (WQPDTAHHWATLC), we expected a highly specific cleavage at the C-terminal end of tryptophan (W) at position 9 (starting from N-terminal).

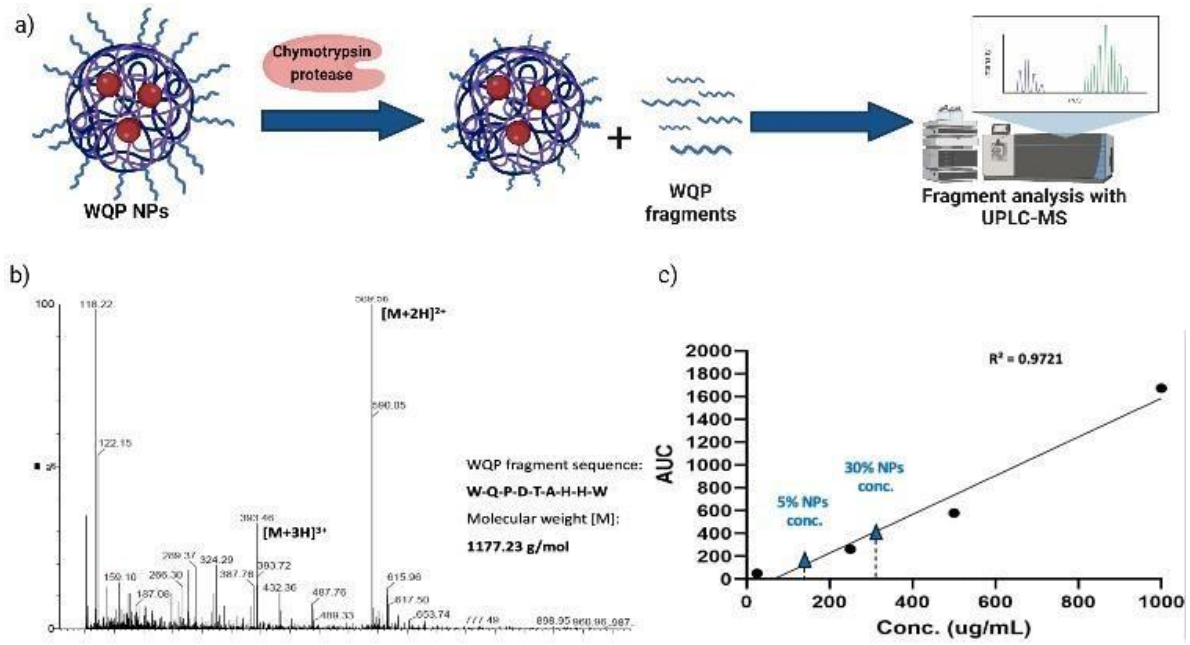

Figure 3.4 Enzymatic degradation of WQP-NPs and quantification of surface WQP. *a) Chymotrypsin protease specifically cleaves at the C-terminal of aromatic amino acids (tryptophan-W), resulting in digested fragments of surface WQP peptide, one of which is then chosen for analysis using UPLC-MS. b) UPLC-MS spectrum of the chosen digested WQP fragment and c) Calibration curve of digested WQP fragment with varying concentrations used for calculation of number of WQP on NP surface.*

We confirmed the presence of the digested fragment having molecular weight of 1177.23Da by analyzing the supernatant obtained after pelleting down the NPs and using UPLC-MS as shown in the schematic in Figure 3.4a. The high sensitivity of UPLC-MS allowed us to detect the digested fragment as a distinct peak, which we integrated to obtain the corresponding area on the chromatogram at □= 280nm as shown in Figure A2.2 (Appendix-2), which showed masses specific to the fragment divided by charge of the protons (+2 and +3), in the corresponding spectra shown in Figure 3.4b. We then prepared a calibration curve using a range of concentrations of the digested peptide alone to calculate the number of WQP from the concentration (µg/mL) of unknown samples as shown in Figure 3.4c. As demonstrated in table 3.1, quite expectedly, 5% NPs had lower number of WQP on the surface in comparison to 30% NPs, owing to increase in surface valency. However, somewhat counterintuitively, 5%

NPs showed a better surface coverage, in that, 91% of WQP were found on NP surface in comparison to 53% of WQP on the surface of 30% NPs. These changes in surface coverage of WQP could be attributed to the stearic hindrance caused by overcrowding of the surface with ligands in NPs with higher ligand density (30%), which could possibly result in embedding of WQP in the NP core, subsequently causing a decreased number of WQP peptide on the NP surface for reaction with the enzyme.

Multivalent NP samples	**Expected #WQP**	**Observed #WQP**	**Surface WQP coverage (%)**
5% WQP-NPs	286	259	91
30% WQP-NPs	1716	908	53

Table 3.1 Calculation of number (#) of WQP on NP surface. *The availability (valency and coverage) (%) of WQP on NP surface is calculated by dividing the number of expected versus observed WQP and getting a percentage of the formulated surface valency.*

Thus, we see that the expected surface WQP number and its coverage are not linearly correlated. And in order to determine the ideal surface valency to observe a multivalent effect, both these properties need to be accounted for, pushing forth the parameters for rational design of effective targeted NPs.

3.2.5 Receptor expression and multivalent NP cytotoxicity analyses

PSMA expression analysis was carried out by immunostaining of a panel of PCa cell lines with anti-PSMA antibody. They were then analyzed by flow cytometry for quantification of PSMA

levels. As expected, LNCaP cells showed highest expression of PSMA followed by 22Rv1 cells having moderate expression and PC3 and RWPE1 cells having low expression (Figure 3.5a).

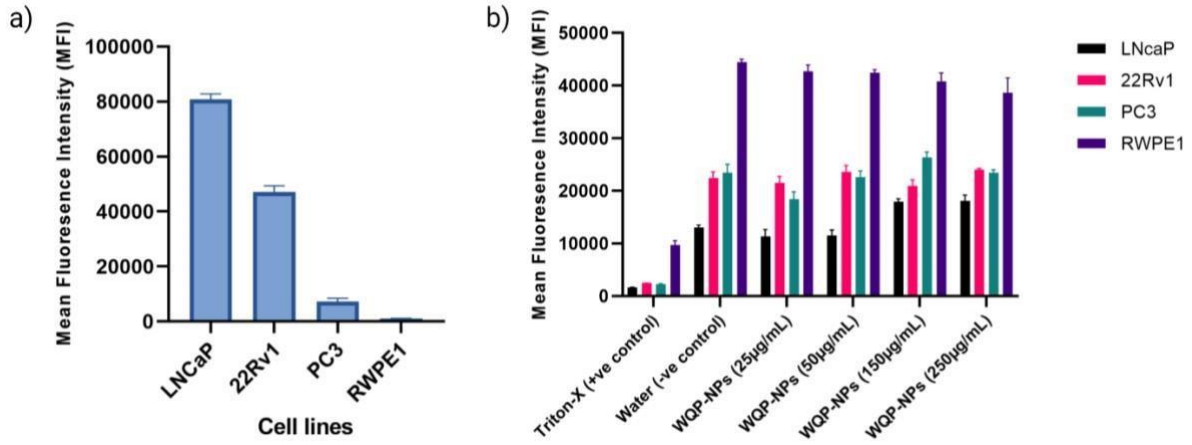

Figure 3.5 PSMA expression and cellular cytotoxicity of multivalent WQP-NPs. *a) PSMA expression across prostate cancer and healthy cell lines obtained by immunostaining as a mean fluorescence intensity of Alexa-488 tagged anti-PSMA antibody using flow cytometry. b) Cellular cytotoxicity of varying concentration ranges of multivalent 30% WQP-NPs on all cell lines by PrestoBlue cell viability assay.*

The cytotoxicity of the targeted nanosystem governs it´s biological performance and is a crucial parameter for regulatory approvals. Here, we employed the PrestoBlue cell viability assay to assess the cytotoxicity of increasing concentrations (25-250□g/mL) of multivalent-30% WQP NPs. PrestoBlue is a dye which is known to undergo modification under reducing environments of viable cells, thereby giving a measure of the cellular metabolism and activity. As shown in Figure 3.5b, higher fluorescence values were obtained for all concentrations of 30% WQP-NPs, which correlated to increase in metabolic activity of the cells, thereby rendering minimal (if none) cytotoxicity for the entire range of concentrations.

3.2.6 Effect of mono- versus multivalent WQP-mediated uptake in PCa cell lines by CLSM and flow cytometry.

For testing the multivalent effect of WQP peptide on cellular uptake, we used four prostate (cancer- LNCaP, PC3 and 22Rv1; healthy- RWPE1) cell lines having varying levels of PSMA expression. The cells were incubated with 50µg/mL of both WQP-Cy5 monomer and (5% and 30%) WQP-NPs for 24h at 37ºC, 5% CO_2. Next, we imaged all the cell lines using CLSM for qualitatively analyzing the cellular uptake of WQP-tagged fluorophores (Cy5 from the monomer and DiI encapsulated within the NPs).

As expected, we observed an increased cellular uptake in case of multivalent WQP-NPs, with higher uptake by NPs with higher surface WQP valency (30% WQP-NPs), in comparison to the WQP-Cy5 monomer (Figure 3.6). This increase in uptake can be attributed to the multivalent targeting by WQP-tagged NPs. Furthermore, we observed a higher uptake in cells with higher PSMA expression (LNCaP and 22Rv1) over those with lower PSMA expression (PC3 and RWPE1), thereby allowing for selective targeting of PCa cells, a desirable property in nanomedicine targeting strategies.

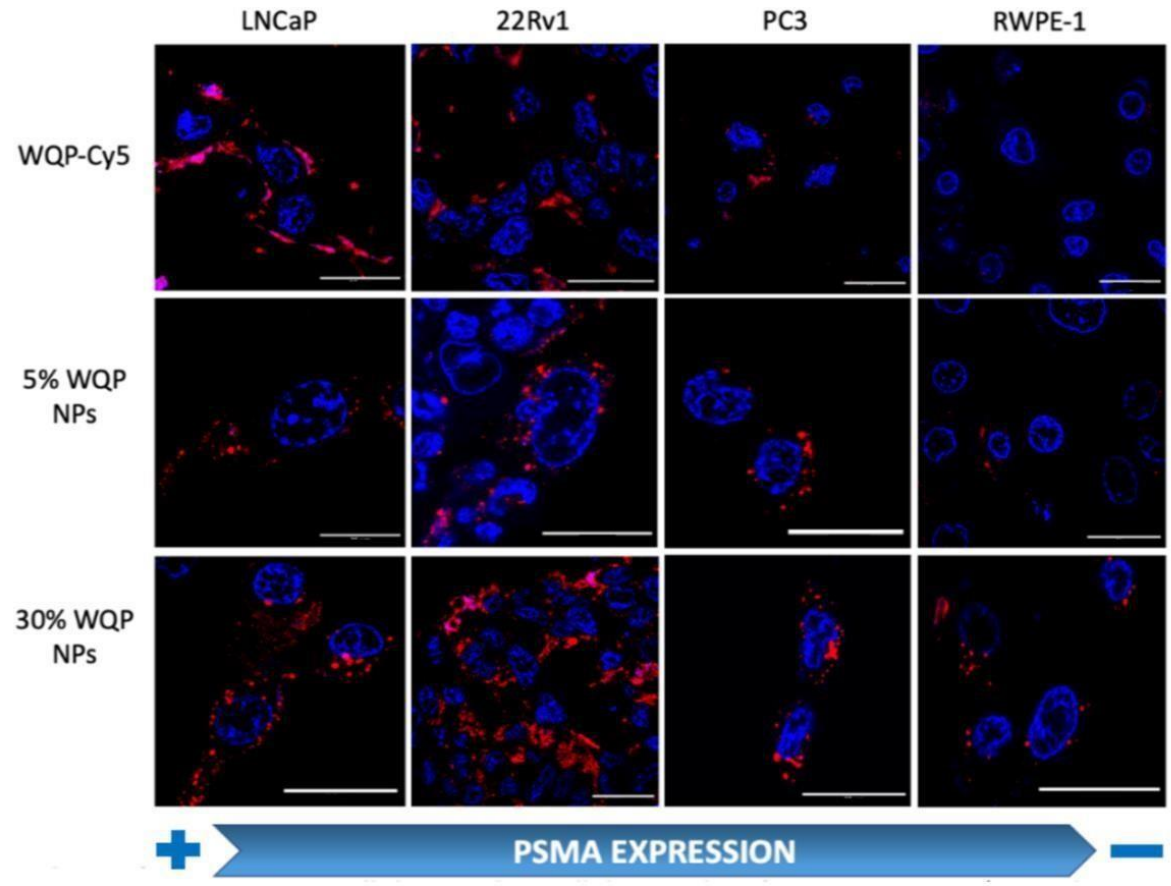

Figure 3.6 Multivalency effect of WQP-NPs on cellular uptake by confocal imaging. *Cellular uptake of WQP-monomer (tagged with Cy5-red) and multivalent WQP-NPs (encapsulated with DiI-red) having different surface WQP densities (5 and 30%) across different prostate (healthy and cancerous) cell lines post 24h of incubation analyzed by confocal laser scanning microscopy. Cellular nuclei tagged with Hoechst33342 (blue). Scale bar is 25□m.*

Further, for quantitative analysis of the cellular uptake, we employed flow cytometry. Figure 3.7a shows a clear overall increase in cellular uptake of multivalent WQP-NPs with varying surface valencies in comparison to WQP monomer. As expected, an increasing trend with regards to increasing surface valencies is observed. This increase in uptake can be attributed to the avidity or the combined strength of higher number of WQP peptide towards PSMA over-expressing cells. Additionally, the uptake is higher for multivalent NPs with higher surface valency (30% over 5%), thus highlighting the importance of a robust method for

quantification of surface WQPs. Figure 3.7b shows the selective uptake of multivalent WQPNPs (having 5% and 30% surface valencies) and the WQP monomer in comparison to the healthy RWPE1 cells. What is interesting to note, is that the uptake was highly selective in the case of LNCaP and 22Rv1 cell lines, which have higher expression levels of PSMA (Figure S4), in comparison to the healthy RWPE-1 cells: 6 and 10-fold increase (LNCaP cells) and 4 and 9fold increase (22Rv1 cells) from 5% and 30%WQP-NPs respectively, over a 2.5 and 1.5-fold increase from the WQP-Cy5 monomer, thus conferring selectivity through combined strength of the ligand (avidity). This is an important concept in personalization of targeted therapies, with the goal of reducing undesirable effects off-site.

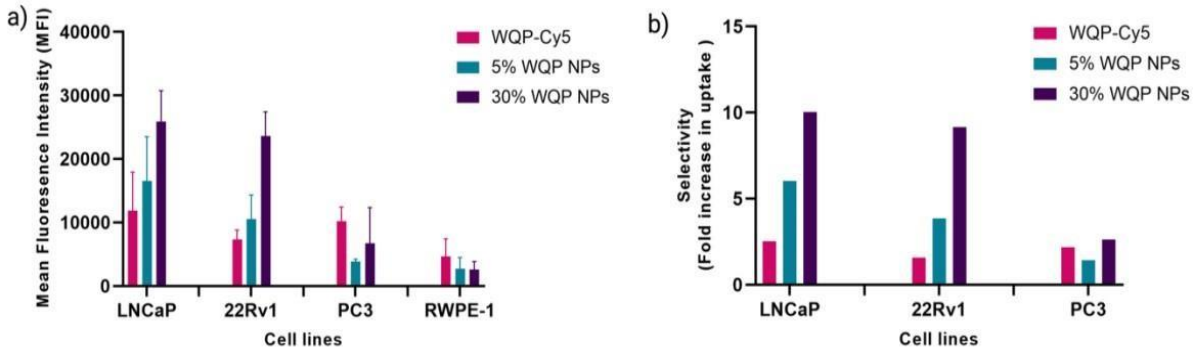

Figure 3.7 WQP-NPs mediated selective cellular uptake. *a) Cellular uptake of monomeric WQP-Cy5 and multivalent WQP-NPs (5 and 30%) quantified by flow cytometry. b) Selective cellular uptake (fold increase) of multivalent WQP-NPs and WQP-Cy5 monomer in comparison to healthy prostate cells in PCa cell lines.*

3.3 Conclusions

We formulated stable and monodisperse multivalent WQP-tagged NPs with varying surface valencies and compared their interaction with cells (uptake) to that of the monomeric peptide. We characterized conjugated NPs for surface peptide number using enzymatic digestion and found that, while the formulations with lower WQP density have lower number of surface WQP than the higher density formulations, they tend to have a higher surface

coverage, a property that must be considered for development of more effective active targeting nano-formulations. Having a lower affinity to target receptor may be disadvantageous for the monomer, but we successfully demonstrate that this affinity can be improved by multivalent targeting using polymeric NPs. Furthermore, we show that this multivalency allows for selective targeting, a property that is desirable and extremely sought after for the development of more efficient nanomedicines. We believe that these studies help to improve our understanding and would lead to the development of more complex, but effective multi-ligand targeting strategies, paving the way towards personalization of treatments.

3.4 Experimental section.

Synthesis of WQP-Cy5 monomer

The WQP peptide was synthesized by solid phase peptide synthesis (SPPS) using the 9fluorenylmethoxycarbonyl/tertbutyl (Fmoc/tBu) strategy[43,44] 2-Chlorotrityl resin, L-Fmoc protected amino acids (2 equivalents), coupling agent TBTU (2 equivalents), and DIEA (6 equivalents) were used. The Fmoc protecting group was cleaved by treatment with a solution of 20% piperidine in DMF (2 x 10 min). Peptides were cleaved from the resin by treatment with Reagent B (88% TFA, 2% TIPS, 5% water and 5% phenol) for 4h. The crude peptide obtained was then purified at a wavelength of 280nm by semipreparative RP-HPLC-MS [Waters 2487 Dual Absorbance Detector equipped with a Waters 2700 Sample Manager, a Waters 600 Controller, a Waters Fraction Collector, a Symmetry column (C18, 5 mm, 30 x 100 mm)] using the MassLynx software. HPLC conditions: Flow=6 mL/min. Gradient=30–60% B in 5 min; A=0.1% TFA in H_2O, B=0.05% TFA in ACN. A total of 40% yield of pure WQP was obtained.

Part of the purified peptide was then conjugated to sulfo-Cy5 maleimide using maleimidethiol reaction using the protocol provided by the manufacturer (ThermoFisher Molecular Probes

(B7884)). Briefly, 5mg of pure WQP peptide in 1mL of 1X PBS (pH 7.4) was first treated with x10 molar excess of TCEP solution for 20 minutes at R.T. under stirring conditions (to reduce thiol groups). Next, 5mg of sulfo-Cy5-maleimide was dissolved in 500 L of DMSO to have a final molar ratio of 1:2 of thiol: maleimide and added dropwise to the peptide solution. The reaction was allowed to take place for 2 hours at room temperature with constant stirring. Unconjugated dye was removed in the form of supernatant via centrifugation using Amicon Ultra-4 (3kDa) filters as per filter instructions for 10 min at 5,000 x g (rcf) at 20ºC with filtered miliQ water. Conjugated WQP-Cy5 was then purified using semi-preparative HPLC-MS (similar conditions as WQP purification), and the obtained sample was stored in MiliQ water in the dark at 4ºC until further use.

Polymer-peptide pre-conjugation

Previously purified WQP peptide was pre-conjugated to $PLGA_{30k}$-PEG_{5k}-maleimide polymer using an organic solvent (ACN) and incubated under stirring conditions overnight. Next, the conjugate was purified from unreacted polymer by precipitation using ice-cold diethyl ether/methanol (DEE/ MeOH) mixture. The precipitate obtained was washed twice with DEE/MeOH mixture and finally redissolved in ACN and dialyzed for a minimum of 24 hours against pure ACN to separate the unreacted WQP from the conjugate. Next, the purified conjugate was lyophilized and a final yield of approximately 35% was obtained. Thereafter, 5mg of polymer, WQP peptide and the conjugate each were dissolved in 0.7mL of deuterated dimethyl sulfoxide (d6-DMSO) and characterized using Bruker 500Hz proton nuclear magnetic resonance (^{1}H NMR) and analyzed using the Mnova (v.14.0) software.

Multivalent nanoparticle formulation

Multivalent PLGA-PEG-WQP NPs were formulated via the nanoprecipitation method according to literature[45]. Briefly, 3 mg of polymer mixture and 1.1 mM of

1,1'dioctadecyl3,3,3'3'-tetramethylindocarbocyanine perchlorate (DiI) were dissolved in 300µL solvent phase (ACN) at room temperature. PLGA polymer was maintained at a ratio of 15% and mixed with $PLGA_{30k}$-PEG_{1k} and $PLGA_{30K}$-PEG_{5K}-WQP conjugate at 5% or 30% of surface WQP valencies. For control PLGA-PEG formulations, PLGA-PEG-WQP-conjugate was substituted with PLGA-PEG-Mal, whilst the PLGA amount was maintained constant at 15%. The anti-solvent phase (MiliQ water) was stirred at 200-300 rpm whilst the solvent phase comprising the polymer solution (ACN) was pipetted at a 1:10 ratio (300µL polymer solution is pipetted into 3mL MiliQ water). Solvent extraction (evaporation) continued for 5 h under magnetic stirring in a fume hood at room temperature. NPs were then collected by high-speed centrifugation (Avanti J-26 XPI, rotor JA-14) using Amicon Ultra-4 100kDa filters as per filter instructions (10 min at 5,000 x g at 20ºC) with filtered MiliQ water. NPs were stored in MiliQ water at a 10 mg/mL concentration in the dark at 4ºC until further use.

Surface peptide quantification by enzymatic digestion

The quantification of surface WQP was carried out using Chymotrypsin protease by following the protocol provided by the manufacture (Pierce™, MAN0011638) with certain optimizations. Since the protocol is usually used for protein samples, the WQP-NP samples were were concentrated up to 25-50mg/mL so as to have enough concentration of the digested peptide fragments to be detected by mass spectrometry. The digestion reaction was carried out using an enzyme: peptide sample ratio of 1:20, in the digestion buffer [500mM Tris HCl (pH 8.0) + 10mM $CaCl_2$]. The reaction vessel was incubated at 37ºC overnight and the digested fragments were collected from the supernatant obtained by briefly (5 min) centrifuging the samples to separate the NPs and characterized by UPLC-MS at □=280 nm as a peak corresponding to the mass of the chosen digested fragment. Calculation of number of WQP of NP surface was carried out using the same method described earlier in Chapter 2, (details provided in Appendix-2).

Multivalent NP cytotoxicity analysis

For measuring the cytotoxicity of the formulated NPs, PrestoBlue cell viability assay was employed as per manufacturer´s instructions. Briefly, all cell lines were seeded in a 96-well plate and incubated for 24h at 37ºC and 5% CO_2. They were then incubated with the formulated multivalent 30%WQP-NPs in varying concentrations (from 25 to 250µg/mL) for 24h at 37ºC and 5% CO_2. As a negative control, filtered MilliQ water of equal volume was used instead of culture medium. Next, the NP-containing medium was aspirated, and the cells were incubated with PrestoBlue (10%v/v of 5% PrestoBlue stock) and incubate for 1hr at 37ºC. Fluorescence was measured at 590nm. All measurements were carried out in triplicates and their mean ± SD values were obtained.

Receptor expression analysis by flow cytometry

For measuring the expression levels of PSMA receptor, all the cell lines were stained with rabbit monoclonal anti-PSMA antibody (ab133579- Abcam Netherlands B.V.) according to manufacturer´s protocol. Briefly 1µg/mL of 1º anti-PSMA antibody dissolved in 3% BSA was added to a monolayer of cells in LabTek on ice for 1hr. Next, the cells were washed thrice with 1X PBS and incubated with 1µg/mL (dilutions provided by manufacturer) of polyclonal goat: anti-rabbit Alexa-488 secondary (2º) antibody for at least 1 hour in dark conditions. For flow cytometry, the cells were detached using 0.25% Trypsin-EDTA incubation for 10 mins at 37ºC, 5% CO_2 and obtained in suspension in 1X PBS. They were then stained with 10ug/mL of DAPI just before analysis with FACS Aria, with the 488nm laser. In total 10,000 cells (or events) were measured, and their mean fluorescence intensity values obtained. All measurements were carried out in triplicates and their mean ± SD values were obtained.

Qualitative analysis of cellular uptake by confocal laser scanning microscopy (CLSM)

All cell lines (LNCaP, PC3, 22Rv1 and RWPE1) were cultured in an 8-well LabTek ($25x10^3$ cells/ well) for 24h at 37ºC and 5%CO_2, until they reached up to 70% confluence and then incubated with a known concentration (50µg/mL) of WQP-Cy5 monomer, and 5% and 30% multivalent WQP-NPs dissolved in culture medium without serum (RPMI 1640 for LNCaP, PC3 and 22Rv1; and KSFM for RWPE1) for 24h at 37ºC and 5% CO_2. Post incubation, the medium containing WQP-monomer and multivalent NPs was aspirated, and the cells were stained with the nuclear dye Hoechst33342 (1□g/mL) for 10 minutes at room temperature. The cells were then imaged live at 37ºC and 5% CO_2 using 63X oil immersion objective of the Zeiss LSM 800 confocal microscope. The cell nuclei, WQP-Cy5 monomer and DiI encapsulated WQP-NPs were excited using 405nm, 640nm and 561nm lasers, respectively at 3% laser power.

Quantitative analysis of cellular uptake by flow cytometry

For flow cytometry, all the cell lines were cultured in 6-well plates ($1x10^5$ cells/ well) for 24h until they reached up to 70% confluence and then incubated with a known concentration (50µg/mL) of WQP-Cy5 monomer, and 5% and 30% multivalent WQP-NPs for 24h at 37ºC and 5% CO_2. Post incubation with NPs, the adherent cells were detached using 0.25% Trypsin/EDTA, incubated for 10 minutes at 37ºC and 5% CO_2, and obtained in suspension by centrifugation at 3000rpm for 5 minutes at 4ºC. From this moment onwards, all the further steps like washing with 1X PBS and resuspension in 1X PBS, were carried out whilst maintaining the cells on ice. Finally, the cells were resuspended in 1X PBS solution with the live cell staining agent DAPI (10 g/□mL) and analysed using BD FACSAria™. The cells not stained with DAPI were excluded from the analysis. At least 10000 cells (or events) were analysed using two specific lasers for WQP-Cy5 (Red C-670nm) and multivalent WQP-NPs encapsulated with DiI (Green E-575nm). All measurements were carried out in triplicates and the standard deviation was obtained.

3.5 References.

1 H. Sung, J. Ferlay, R. L. Siegel, M. Laversanne, I. Soerjomataram, A. Jemal and F. Bray, *CA: A Cancer Journal for Clinicians*, 2021, **71**, 209–249.

2 P. Cornford, R. C. N. van den Bergh, E. Briers, T. Van den Broeck, M. G. Cumberbatch, M. De Santis, S. Fanti, N. Fossati, G. Gandaglia, S. Gillessen, N. Grivas, J. Grummet, A. M. Henry, T. H. van der Kwast, T. B. Lam, M. Lardas, M. Liew, M. D. Mason, L. Moris, D. E. Oprea-Lager, H. G. van der Poel, O. Rouvière, I. G. Schoots, D. Tilki, T. Wiegel, P.-P. M. Willemse and N. Mottet, *European Urology*, 2021, **79**, 263–282.

3 S. Sumanasuriya and J. De Bono, *Cold Spring Harb Perspect Med*, 2018, **8**, a030635. 4 W. Jin, B. Qin, Z. Chen, H. Liu, A. Barve and K. Cheng, *International Journal of Pharmaceutics*, 2016, **513**, 138–147.

5 A. Adjiri, *Oncol Ther*, 2016, **4**, 17–33.

6 T. M. Gorges, S. Riethdorf, O. von Ahsen, P. Nastały, K. Röck, M. Boede, S. Peine, A. Kuske, E. Schmid, C. Kneip, F. König, M. Rudolph and K. Pantel, *Oncotarget*, 2016, **7**, 34930– 34941.

7 A. Ghosh and W. D. W. Heston, *Journal of Cellular Biochemistry*, 2004, **91**, 528–539.

8 S. Bravaccini, M. Puccetti, M. Bocchini, S. Ravaioli, M. Celli, E. Scarpi, U. De Giorgi, M. M. Tumedei, G. Raulli, L. Cardinale and G. Paganelli, *Sci Rep*, 2018, **8**, 4254.

9 H. Wang, T. Amiel, C. Würnschimmel, T. Langbein, K. Steiger, I. Rauscher, T. Horn, T. Maurer, W. Weber, H.-J. Wester, K. Knorr and M. Eiber, *EJNMMI Research*, 2021, **11**, 76. 10 K. Rahbar, A. Afshar-Oromieh, H. Jadvar and H. Ahmadzadehfar, *Mol Imaging*, 2018, **17**, 1536012118776068.

11 A. Afshar-Oromieh, J. W. Babich, C. Kratochwil, F. L. Giesel, M. Eisenhut, K. Kopka and U. Haberkorn, *Journal of Nuclear Medicine*, 2016, **57**, 79S-89S.

12 S. Sengupta, M. Asha Krishnan, S. Chattopadhyay and V. Chelvam, *Cancer Rep (Hoboken)*, 2019, **2**, e1169.

13 D. Rosenblum, N. Joshi, W. Tao, J. M. Karp and D. Peer, *Nat Commun*, 2018, **9**, 1410.

14 A. David, *Advanced Drug Delivery Reviews*, 2017, **119**, 120–142.

15 S. Marqus, E. Pirogova and T. J. Piva, *Journal of Biomedical Science*, 2017, **24**, 21.

16 H. Kulhari, D. Pooja, S. Shrivastava, N. V.G.M and R. Sistla, *Colloids and Surfaces B: Biointerfaces*, 2014, **117**, 166–173.

17 S. Aggarwal, P. V. Singh, O. Topaloglu, J. T. Isaacs and S. R. Denmeade, *Cancer research*, 2006, **66**, 9171–9177.

18 S. Aggarwal, S. Janssen, R. M. Wadkins, J. L. Harden and S. R. Denmeade, *Biomaterials*, 2005, **26**, 6077–6086.

19 S. E. Cwirla, P. Balasubramanian, D. J. Duffin, C. R. Wagstrom, C. M. Gates, S. C. Singer, A. M. Davis, R. L. Tansik, L. C. Mattheakis, C. M. Boytos, P. J. Schatz, D. P. Baccanari, N. C.

Wrighton, R. W. Barrett and W. J. Dower, *Science*, 1997, **276**, 1696–1699.

20 N. C. Wrighton, P. Balasubramanian, F. P. Barbone, A. K. Kashyap, F. X. Farrell, L. K. Jolliffe, R. W. Barrett and W. J. Dower, *Nat Biotechnol*, 1997, **15**, 1261–1265.

21 M. Wang and M. Thanou, *Pharmacological Research*, 2010, **62**, 90–99.

22 M. J. Y. Ang, S. Y. Chan, Y.-Y. Goh, Z. Luo, J. W. Lau and X. Liu, *Advanced Drug Delivery Reviews*, 2021, **178**, 113907.

23 O. K. Nag and J. B. Delehanty, *Pharmaceutics*, 2019, **11**, 543.

24 F. J. Martinez-Veracoechea and D. Frenkel, *PNAS*, , DOI:10.1073/pnas.1105351108.

25 S. Wang and E. E. Dormidontova, *Soft Matter*, 2011, **7**, 4435.

26 S. Wilhelm, A. J. Tavares, Q. Dai, S. Ohta, J. Audet, H. F. Dvorak and W. C. W. Chan, *Nat Rev Mater*, 2016, **1**, 16014.

27 J. Cao, Y. Zhang, Y. Wu, J. Wu, W. Wang, Q. Wu and Z. Yuan, *Colloids and Surfaces B: Biointerfaces*, 2018, **161**, 508–518.

28 L. Woythe, N. B. Tito and L. Albertazzi, *Advanced Drug Delivery Reviews*, 2021, **169**, 1–21.

29 T. Andrian, P. Delcanale, S. Pujals and L. Albertazzi, *Nano Lett.*, 2021, **21**, 5360–5368.

30 D. G. Mullen and M. M. Banaszak Holl, *Acc. Chem. Res.*, 2011, **44**, 1135–1145.

31 A. Albanese, P. S. Tang and W. C. W. Chan, *Annual Review of Biomedical Engineering*, 2012, **14**, 1–16.

32 M. Gulumian, C. Andraos, A. Afantitis, T. Puzyn and N. J. Coville, *Int J Mol Sci*, 2021, **22**, 8347.

33 Y. Zhang, M. Cheng, J. Cao, Y. Zhang, Z. Yuan, Q. Wu and W. Wang, *Nanoscale*, 2019, **11**, 5005–5013.

34 J. F. Stefanick, D. T. Omstead, T. Kiziltepe and B. Bilgicer, *Nanoscale*, 2019, **11**, 4414–4427.

35 G. V. Dubacheva, T. Curk, R. Auzély-Velty, D. Frenkel and R. P. Richter, *PNAS*, 2015, **112**, 5579–5584.

36 A. G. Mares, G. Pacassoni, J. S. Marti, S. Pujals and L. Albertazzi, *PLOS ONE*, 2021, **16**, e0251821.

37 S. Mourdikoudis, R. M. Pallares and N. T. K. Thanh, *Nanoscale*, 2018, **10**, 12871–12934.

38 S. Muro, *Journal of Controlled Release*, 2012, **164**, 125–137.

39 C. Chiva, M. Ortega and E. Sabidó, *J. Proteome Res.*, 2014, **13**, 3979–3986.

40 T. Klein, U. Eckhard, A. Dufour, N. Solis and C. M. Overall, *Chem. Rev.*, 2018, **118**, 1137–1168.

41 F. Uliana, M. Vizovišek, L. Acquasaliente, R. Ciuffa, A. Fossati, F. Frommelt, S. Goetze, B. Wollscheid, M. Gstaiger, V. De Filippis, U. auf dem Keller and R. Aebersold, *Nat Commun*, 2021, **12**, 1693.

42 S. M. Manohar, P. Shah and A. Nair, *Bioanalysis*, 2021, **13**, 181–198.

43 D. A. Wellings and E. Atherton, in *Methods in Enzymology*, Academic Press, 1997, vol. 289, pp. 44–67.

44 R. B. Merrifield, Solid Phase Peptide Synthesis. I. The Synthesis of a Tetrapeptide, http://pubs.acs.org/doi/pdf/10.1021/ja00897a025, (accessed February 21, 2022). 45 J. M. Barichello, M. Morishita, K. Takayama and T. Nagai, *Drug Development and Industrial Pharmacy*, 1999, **25**, 471–476.

Chapter 4| Co-operative dual peptide-mediated strategy for selective targeting of prostate cancer.

A key bottleneck of current cancer treatments is the lack of selective targeting of cancer cells to reduce undesirable side-effects. Nanoparticles (NPs) allow for the design of ligand-coated materials that can fulfil this function but have not yet shown consistent clinical results to make the 'magic bullet' theory a paradigm. To further improve the efficacy of targeted nanosystems, multi-ligand targeting strategies have been proposed, however, they remain challenging as they involve an intricate interplay between a multitude of factors like choice of ligands, their receptor binding affinities, and NP surface properties like valency and stoichiometric ratios, thereby calling for studies involving the impact of each of these properties on their targeting potential.

In this chapter, we report a synthetic strategy for dual peptide-NPs mediated targeting using WQP and GE11 peptides, explored in previous chapters, having varying binding affinities for PSMA and EGFR respectively. By systematically varying their surface properties, specifically valency and stoichiometric ratios, we establish their impact on uptake across a panel of prostate cancer (PCa) cell lines. We explore the impact of different peptide valencies on NP surface of dual NPs in comparison to single peptide-NPs on the uptake in different PCa cell lines caused by cooperation between the dual peptides. Next, we check the effect of different surface peptide ratios on tumor uptake and determine an optimal ratio for improved targeting

of only those cells expressing both receptors, by the virtue of improved selectivity. Our findings demonstrate that through refined design and well-characterized NP formulations, dualpeptide targeted nanosystems hold potential to provide selective cancer treatments.

Supportive information for this chapter can be found in **Appendix 3.*

4.1 Introduction

Selective targeting of cancer in order to minimize off-site effects has been a crucial aspect in the field of nanomedicine[1,2]. To this end, the most common practice includes active NP targeting by conjugating different targeting ligands to the NP surface to improve their interaction with the target biomarker, which is usually overexpressed by the tumor cells[3,4]. While this strategy might be useful for highly specific tumor biomarkers, in most cases, it is limited by the ubiquitous expression of tumor biomarkers in healthy tissues, albeit in variable amounts, resulting in systemic toxicity[5–7]. As a consequence, there are no targeted NPs in the clinic so far[7,8], calling for the development of improved NP design strategies to circumvent the side effects of non-selective targeting for their successful clinical translation.

Multiple targeting ligand types and schemes have been employed to direct nanoparticles to tumors[3,4,9,10]. However, conventional targeting systems involving single-ligand conjugation often consider cancer as a one-dimensional disease, often failing to factor in tumor heterogeneity[10,11]. To address this issue, multi-ligand targeted NPs strategy has been proposed in the past decade with a view to increase targeting selectivity and intracellular delivery to a tumor site that overexpresses more than one targetable biomarkers[12–14]. There have been numerous studies employing multiple ligands not only for differential targeting[14–16], but also for theranostic applications[17–19]. In particular, the use of small peptides has been predominant for studies with multi-ligand targeting because they offer some distinct advantages over other types of ligands[20–22]. However, these studies still remain controversial

as they have to account for an interplay of parameters relating to not just the ligands themselves, but also the control of NP properties, which is very challenging[12,23–25].

Within this framework, we designed a study for dual receptor targeting by employing two known PCa biomarkers- PSMA which is specifically overexpressed in castration resistant metastatic PCa whilst having significantly low expression in healthy prostate cells[26–30]; and EGFR, which is a commonly studied biomarker having ubiquitous expression in healthy tissues as well[31–34]. Further, we employed two CTPs, namely WQP and GE11 having different binding affinities as explored in previous chapters, in that, WQP is a weak-binding ligand for PSMA[35,36], while GE11 is well known for having strong binding affinity for EGFR[37–39]. We aimed at exploiting the difference in chemical specificities of these CTPs for improving NP targeting selectivity using polymeric NPs by the virtue of cooperativity between dual peptides. First, we explored the effect of different NP surface peptide valencies on their uptake across a panel of PCa cell lines to determine the optimal surface valency for dual peptide targeting. Subsequently, we checked the impact of different peptide stoichiometric ratios on tumor uptake to establish an optimal one for enhanced targeting of only those cells expressing both receptors, by the virtue of improved selectivity.

4.2 Results and discussion

4.2.1 Design of dual-peptide NPs for selective targeting of prostate cancer.

A summary of the workflow employed in the design of dual-peptide NPs for selective PCa targeting is shown in Figure 4.1.

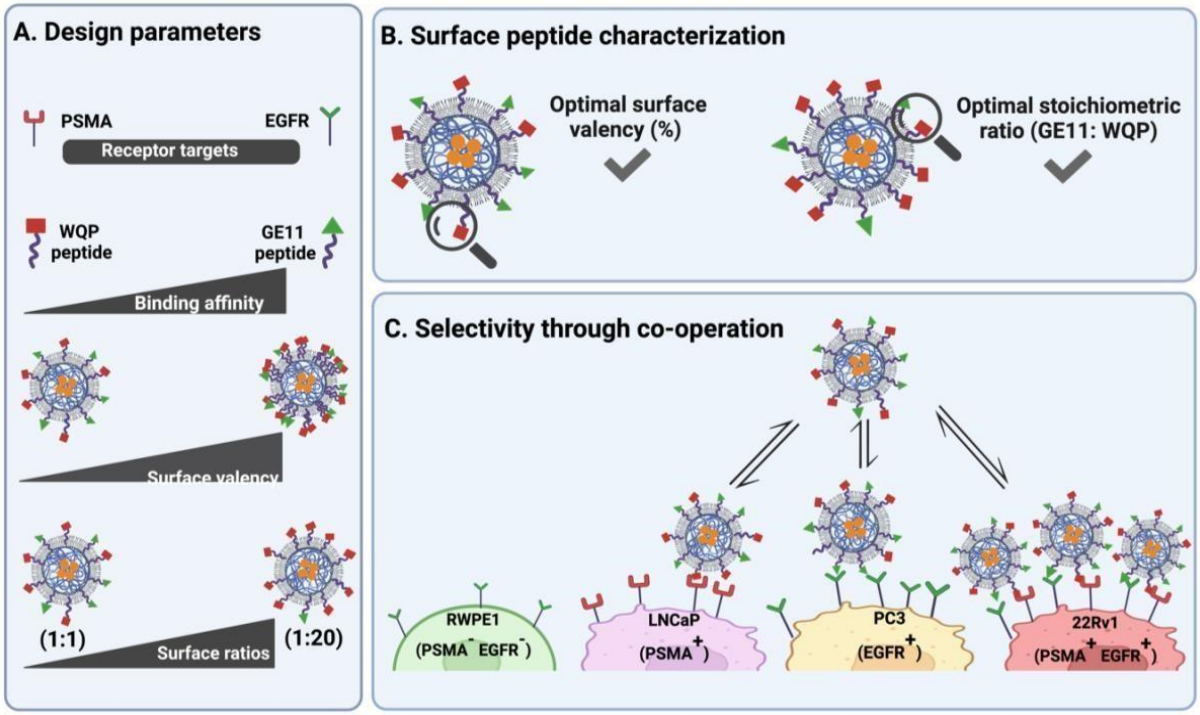

Figure 4.1 Schematic representation of design of dual-peptide NPs for selective targeting of prostate cancer cells. *Through systematic control of peptide valency on NP surface and stoichiometric ratios of both peptides, each having strong affinity and avidity respectively, efficient dual-peptide NPs are designed to selectively target cancer cells overexpressing both the receptors.*

NP surface valency and peptide stoichiometric ratios are the essential features investigated in the dual-NP design to optimize cell selectivity. In addition, factors such as the choice of target receptors and the varying levels of binding affinities of each of the peptides towards them are also taken into account (Figure 4.1A). The characterization of NP surface in terms of the

number of peptides incorporated is crucial for establishing cell selectivity, and for this purpose, robust characterization was carried out to establish the optimal values (Figure 4.1B) using specific enzymatic digestion. Finally, the impact of these parameters was evaluated in a panel of PCa cell lines having varying expression levels of the target receptors- PSMA and EGFR (Figure 4.1C) to establish the formulations with maximum selectivity for cells overexpressing both target receptors.

4.2.2 Evaluation of PSMA and EGFR expression across prostate cell lines.

As described in previous chapters, we evaluated the expression levels of PSMA and EGFR for dual targeting studies across a panel of prostate (cancer and healthy) cell lines including PCa (LNCaP, PC3 and 22RV1), and prostate epithelial (RWPE1) cell lines via flow cytometry by using fluorescently labeled PSMA and EGFR specific antibodies (Fig. 4.2A and B). PSMA positive (P^+) and EGFR-positive (E^+) cell line was found to be 22Rv1 (P^+/E^+). While PSMA-positive and EGFRnegative cell line was LNCaP (P^+/E^-); PSMA-negative and EGFR-positive cell line was PC3 (P/E^+); and finally, PSMA-negative and EGFR-negative cell line was found to be RWPE1 (P^-/E^-) (Figure 4.2C). These cell lines provided an effective panel to design a dual-receptor targeted approach.

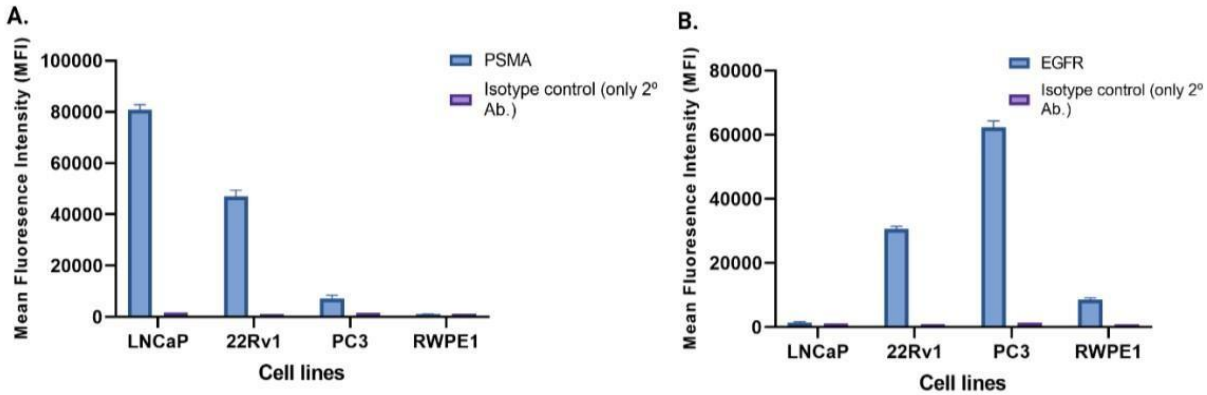

C.

Cell lines	PSMA (P)	EGFR (E)
LNCaP	+	-
22Rv1	+	+
PC3	-	+
RWPE1	-	-

Figure 4.2 Dual target receptor expression analysis by flow cytometry. A) *Expression levels of PSMA across prostate (cancer and healthy) cells obtained as mean fluorescence intensity (MFI) of Alexa-488 tagged Anti-PSMA antibodies by flow cytometry.* ***B)*** *Expression levels of EGFR across prostate (cancer and healthy) cells obtained as MFI of Alexa-647 tagged Anti-EGFR antibodies by flow cytometry. Blue columns are primary antibodies and purple columns are isotype controls (only 2º antibodies). All experiments were performed in triplicates and data represents mean (±SD)* ***C)*** *Summary of PSMA and EGFR expression across the panel of PCa cell lines.*

4.2.3 Characterization and optimization of dual-peptide NP surface valency for cooperative cellular uptake.

For an optimal design of dual-peptide NPs for selective targeting, we first explored the impact of NP surface valency as it plays a crucial role in enhancing the targeting potential of the nanosystem. This, however, also depends on the binding affinity of the ligand for the target receptor, in that, weak-binding ligands provide enhanced selectivity by the virtue of avidity provided my multivalent targeting with NPs having higher surface valency[40]. On the contrary, ligands with strong target binding affinity often lead to non-specific binding resulting in off-

cancer toxicities[25]. In this context, we wanted to establish the cooperativity of the dual peptides for selectively targeting cells overexpressing both receptors, with the most optimal surface valency. So, we kept the ratio of the two peptides constant (1:1) and evaluated its impact on cellular uptake in comparison to their single-peptide counterparts administered individually and together across a panel of PCa cell lines having varying expression levels of target receptors, to then determine the optimal surface valency.

For single and dual-peptide NP formulation, we pre-conjugated the peptides to PLGA-PEGmaleimide polymer as described in previous chapters and characterized the extent of this conjugation using ^{1}HNMR. We then formulated NPs with different surface valencies (5 and 30%) by the manual process of nanoprecipitation. For dual-peptide NP formulation, we used the CTPs in a unimolar (1:1) ratio and characterized them for size and surface charge (□potential) using DLS. We observed a slight increase in the sizes of peptide-functionalized NPs (both single and dual) in comparison to non-functionalized (control) NPs. The small increase is attributed to the small sizes (1.5-1.6kDa) of the CTPs. Additionally, the zeta potential also increased slightly, thereby confirming the incorporation of CTPs having slightly negative charges at pH 7.0 (Figure 4.3A). The quantification of number of peptides on NP surface was carried out using site-specific enzymatic digestion by chymotrypsin protease. The characterization of this digestion was carried out using UPLC-MS, and chromatograms obtained at □=280nm for both single- and dual-peptide NPs having 5% and 30% surface valency were obtained as shown in Figures A3.1, A3.2 and A3.3, along with their corresponding mass spectra shown in Figure A 3.4A (Appendix-3). The calibration curve shown in Figure A3.4B (Appendix-3) was used to calculate the number of surface peptides and their coverage on NP surface as shown in Table A3.1 (Appendix-3). Further, as depicted in Figure 4.3B, both single- and dual-peptide NPs having 5% surface valency showed maximum surface coverage. While in the case of 30% single- and dual-peptide NPs, the surface coverage was found to decrease, particularly for dual-peptide NPs, possibly owing to the overcrowding of

NP surface and also the possible embedding of the peptides within the hydrophobic core, rendering them unavailable for surface interactions.

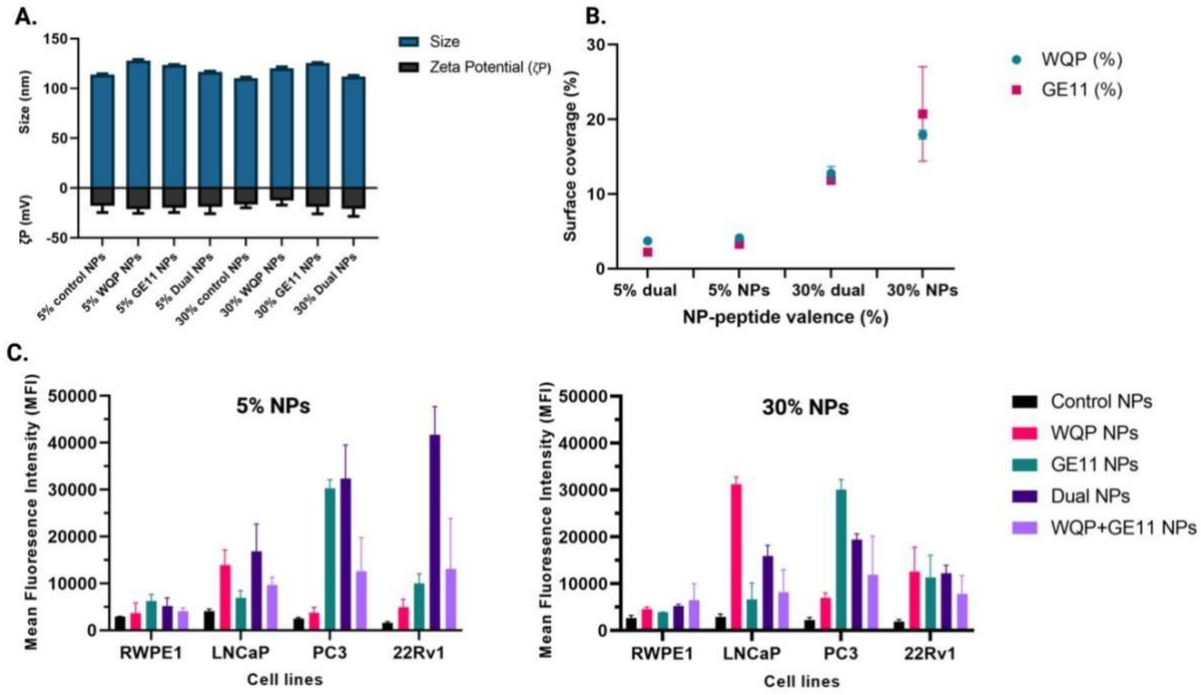

Figure 4.3 Characterization of dual-peptide NP having different valencies and optimization of their co-operative cellular uptake. *A) DLS characterization of size (hydrodynamic diameter) and zeta potential of formulated dual-peptide NPs having different surface valencies. B) Quantification of surface content of dual-peptide NP and their coverage obtained by integrating the area under peaks corresponding to peptide fragments. C) Overall cellular uptake of dual-peptide NP having different surface valencies in comparison to their single- peptide NP counterparts administered individually and together, to establish their cooperativity by flow cytometry. All measurements were performed in triplicates, and the mean (±SD) values are plotted.*

For establishing the cooperativity of dual peptides over their individual impact on cellular uptake, we quantified the cellular uptake of dual peptide NPs having different surface valencies in comparison to their single-peptide counterparts (administered individually and together), using flow cytometry, a known robust technique for quantification of cellular uptake (Figure 4.3C). We found that for lower surface valency (5%) NPs, dual-peptide NPs

showed the highest cellular uptake in 22Rv1 cells expressing both receptors. This can be clearly attributed to the surface coverage (distribution) of the CTPs available for interaction with their target receptors, which is, somewhat counterintuitively, provided by maintaining a lower valency on the NP surface. On the other hand, in case of higher surface valency (30%) NPs, the single-peptide NPs showed highest uptake in cell lines overexpressing their respective target receptor, as a result of multivalent targeting from individual ligands with higher densities of target receptor. Therefore, 5% surface valency was determined to be the most optimal for our design. Our results demonstrate the impact of NP surface valency to improve targeting potential of the nanosystems, thereby bringing us a step closer to a rational design of efficient nanomedicines.

4.2.4 Characterization and optimization of dual-peptide NPs having different surface ratios: Impact on cellular uptake.

After optimizing the surface valency, we explored the impact of different stoichiometric ratios of dual peptides on NP surface on the overall cellular uptake across a panel of PCa cell lines. As GE11 peptide is known to have a strong binding affinity (K_d = 22nM) for its target EGFR[37], we kept it at a fixed ratio, thus allowing it to drive the selective targeting. In contrast, the WQP peptide has weak binding affinity to its target PSMA, and so, we used it in increasing ratios in order to explore its optimal concentration for showing a multivalent effect on account of a strong avidity. We tested a total of 5 formulations of dual-peptide (D) NPs having different stoichiometric ratios of (GE11: WQP) as D-1 (1:1), D-2 (1:3), D-3 (1:5), D-4 (1:10) and D-5 (1:20) for their impact on cellular uptake using flow cytometry.

Figure 4.4A shows the characterization of formulated dual-peptide NPs for size and surface charge (□-potential) using DLS. We found no significant changes in both size (range between 110-130nm) and zeta potential (-18 to -25mV). This can be again attributed to the small sizes of the CTPs. Figure 4.4B shows the quantification of surface content (%) obtained by calculating the number of individual peptides, detailed in Table A3.2 (Appendix-3) by specific

enzymatic digestion of the peptides as explained in the earlier section. We found the observed ratios of peptides on NP surface to be in accordance with the expected ratios for all formulations except for D4 and D-5, as demonstrated in Table A3.3 (Appendix-3), in which case, the extremely low concentration of GE11 was below the limit of detection of the UPLCMS equipment. Nonetheless, we were able to robustly quantify the peptides using this technique, which was crucial to further study its biological impact.

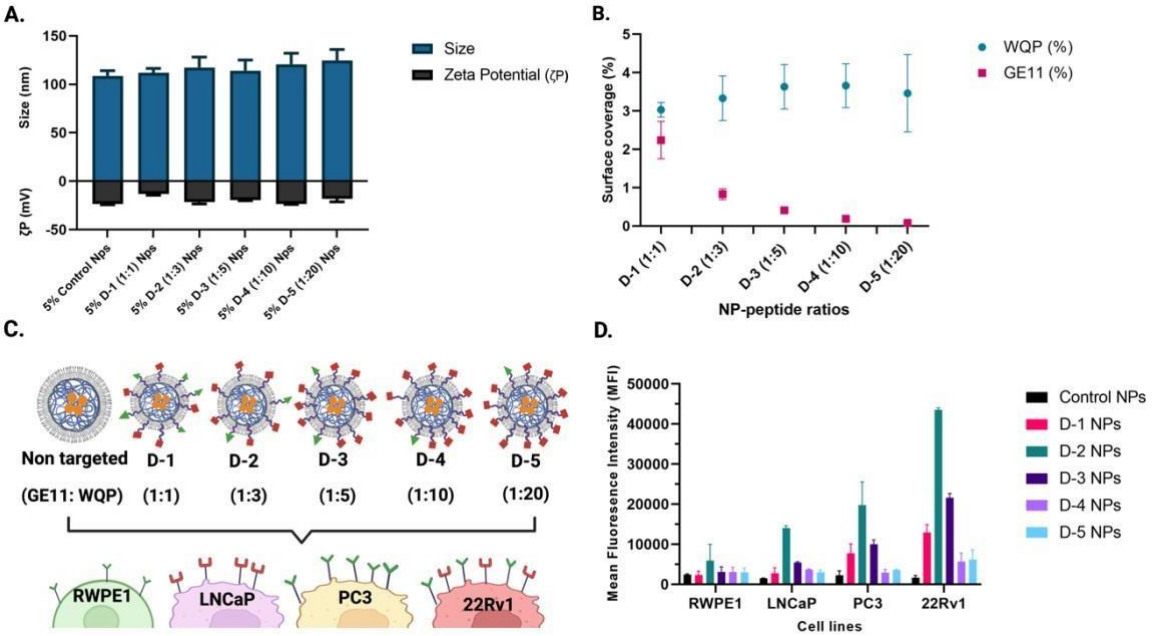

Figure 4.4 Characterization of dual-peptide NP having different ratios and their impact on cellular uptake. A) *DLS characterization of size (hydrodynamic diameter) and zeta potential of formulated dual-peptide NPs having different surface peptide ratios.* ***B)*** *Quantification of surface content of dualpeptide Ps and their coverage obtained by integrating the area under peaks corresponding to specific peptide fragments.* ***C)*** *Schematic representation of optimization of cellular uptake of dual-peptide NP with different surface ratios across different Ca cell lines.* ***D)*** *Overall cellular uptake of dual-peptide NPs having different surface peptide ratios across different PCa cell lines obtained by flow cytometry. All measurements were performed in triplicates and the mean (+SD) values are plotted.*

A schematic representation of the design of assay for cellular uptake of dual-peptide NPs having different surface ratios is provided in Figure 4.4C. Briefly, all dual-NP formulations (D1 to D-5) are administered to a panel of PCa cell lines at a defined concentration (50ug/mL) along with non-targeted (control) NPs and incubated for 24h after which the uptake is quantified by flow cytometry. Figure 4.4D shows the overall uptake of different formulations of dual-peptide NPs having varying surface peptide ratios. We found that D-2 NPs showed an overall highest cellular uptake in 22Rv1 cells followed by D-3 and D-1 NP formulations. As expected, D-4 and D-5 NP formulations had a negligible uptake, almost equivalent to nontargeted NPs, possibly due to insufficient levels of the driver GE11 peptide. For PC3 and LNCaP cells which express only EGFR and PSMA respectively, the overall uptake was lower, thereby highlighting the specificity and selectivity of dual-peptide NPs towards cells expressing both target receptors.

4.2.5 Establishing the targeting specificity and selectivity of dual-peptide NPs having different surface ratios by flow cytometry.

To evaluate if the observed uptake of dual-peptide NP formulations is specific, we studied the uptake of a non-targeted (control) NP for comparison. As the chemical surface environment of NPs dictates the potential non-specific targeting with cells, it is important to compare dualpeptide targeted NPs to a control particle having similar surface chemistry and ligand valency. As a measure for specificity, the ratio between dual-peptide NPs having different surface peptide ratios compared to the control NPs was calculated and expressed as a difference in fold increase (Figure 4.5A). We found that D-2 NPs showed maximum specificity (□25-fold increase) for 22Rv1 cells expressing both receptors. Their specificity is however, significantly reduced in case of PC3 and LNCaP cells that express only one target receptor (EGFR and PSMA, respectively) (Figure 4.5B). This could possibly attribute to the ratio of CTPs which allowed for a rather less specific reaction in either of the cell lines by the virtue of either strong affinity or avidity of GE11 and WQP peptides, respectively. Furthermore, a specificity

ratio of 1 indicates no difference in uptake between dual peptide targeted and non-targeted NPs as obtained in the case of RWPE1 cells, implying a non-specific uptake of all the formulations, thus highlighting the interplay between the dual peptides and the minimal expression levels of receptors required for targeting.

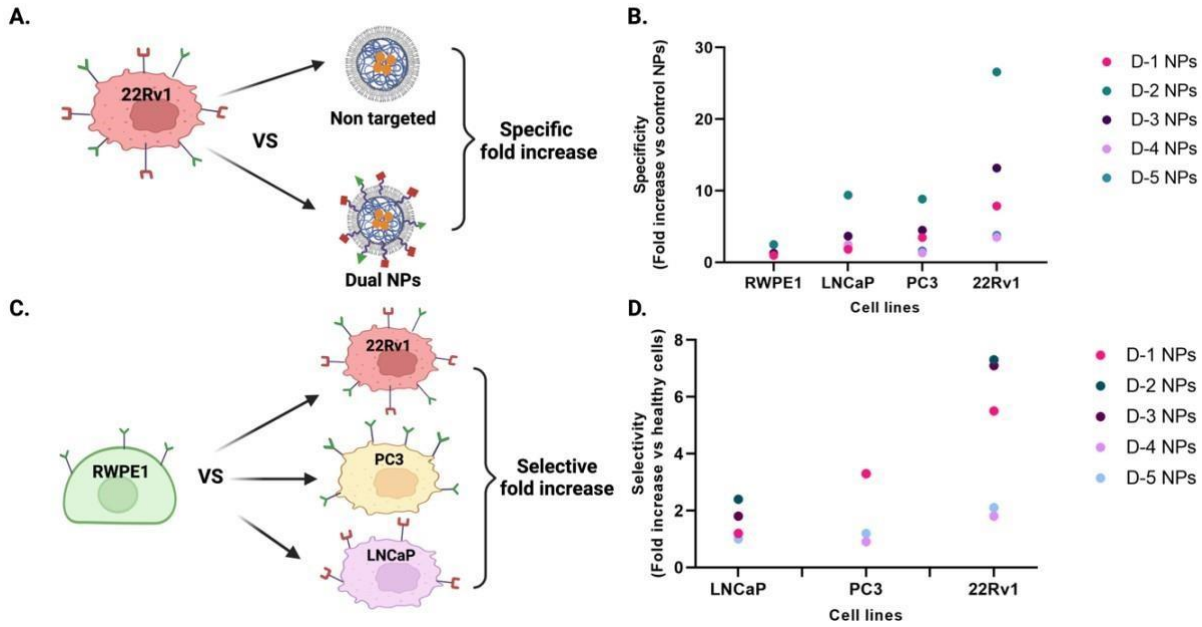

Figure 4.5 Targeting specificity and selectivity of dual-peptide NPs having different surface ratios. A) *Schematic representation of specific cellular uptake of 5% dual-peptide NP having different surface ratios in comparison to non-targeted (control) PLGA-PEG NPs. The difference in fold increase is measured to establish the specificity of each of the formulations.* ***B)*** *Specificity of dual-peptide NP having different ratios for PCa cells expressing both target receptors in comparison to non-targeted NPs* ***C)*** *Schematic representation of selective cellular uptake of 5% dual-peptide NPs having different surface ratios in prostate cancer cell lines in comparison to healthy (RWPE-1) cells. The difference in fold increase is measured to establish the selectivity of each of the formulations.* ***D)*** *Selectivity of dualpeptide NP having different surface ratios for prostate cancer cells overexpressing both target receptors over healthy cells.*

Selective NPs are those that can distinguish between cells having varying expression levels of target receptors, in that, they target only those cells that overexpress the target receptors, thereby reducing off-target effects which are often undesirable. To study the selectivity of our dual-peptide formulations, we determined the ratio of uptake between cells having higher expression levels of either or both receptors compared to those having low/no expression of target receptors as shown in the represented schematically in Figure 4.5C. We observed maximum selectivity (□8-fold increase in uptake) of D-2 NPs closely followed by D3 and D-1 NPs (□7-fold and □6-fold increase in uptake, respectively) in 22Rv1 cells. This suggests that these formulations would be effective in selectively targeting the cells that show dual receptor expression, thus highlighting the importance of the optimizing the stoichiometric ratios and the role played by each of the peptides in achieving selective targeting. As with the cell lines expressing only one receptor, we found that the D-1 and D-2 NPs were selective, albeit to a lesser extent, to PC3 and LNCaP cells, respectively (Figure 4.5D). This can once again be attributed to the ratio of peptides providing the necessary binding affinity and avidity for selectively targeting each of the receptors. Thus, these results successfully shed light on the importance of exploring the impact of different stoichiometric ratios of surface ligands to achieve selective targeting of cells expressing one or more target receptors, driving us towards personalization of nanomedicine targeting strategies.

4.3 Conclusions

Active NP targeting of cancer cells has been around for decades without any successful clinical translation yet. One of the key bottlenecks is the expression of target receptor in the healthy tissue in variable amounts, consequently resulting in non-selective targeting and systematic toxicity. This can be addressed by targeting more than one receptor simultaneously to improve selectivity. To this point, multivalent cooperative interactions between multiple ligands can be explored to achieve increased selectivity of NP targeting towards target cells. In this work, we chose two target receptors having specific (PSMA) and systemic (EGFR)

expression levels in prostate cancer, with a view to design nanosystems with enhanced selectivity for aggressive cancers involving the overexpression of both receptors. As targeting ligands, we chose two CTPs each having a strong affinity (GE11 for EGFR) and avidity (WQP for PSMA) for respective target receptors. We then explored the impact of two of the most important NP surface parameters- Valency and stoichiometric ratios on the overall uptake and specificity and selectivity of NP targeting. We showed that having lower surface valency (5%) allowed for better surface coverage of dual peptides consequently resulting in increased uptake in 22Rv1 cells expressing both receptors in comparison to those with a higher surface valency (30%). Furthermore, we formulated dual peptide- NP formulations having different stoichiometric ratios and established the most optimal ones having improved selectivity not only for 22Rv1 cells expressing both receptors, but also for PC3 and LNCaP cells, that express only one target receptor (EGFR and PSMA, respectively).

Our results demonstrated that through a systematic design, a dual-peptide mediated NP targeting strategy can significantly improve the selectivity and efficiency of active targeting approaches to achieve results otherwise unattainable with traditional strategies implementing a single ligand- receptor targeting. We believe that the application of this dualpeptide mediated targeting strategy may ultimately allow for the customization of peptidefunctionalized nanosystems to fit individual patient needs, providing a personalized approach in anti-cancer treatments for improved patient outcome.

4.4 Experimental section

Peptide-polymer pre-conjugation and characterization.

For pre-conjugation, the synthetic peptides (WQP and GE11) were conjugated to $PLGA_{30k}PEG_{5k}$-maleimide polymer using a previously described protocol[38]. The conjugation was allowed to take place in an organic solvent (ACN) and incubated under stirring conditions overnight. The conjugates were then purified from unreacted polymers by the process of

precipitation using ice-cold diethyl ether/methanol (DEE/ MeOH) mixture. The precipitate was obtained by centrifugation at 4000xg for 15 minutes at 4ºC, after which it was washed twice with DEE/MeOH mixture and finally redissolved in ACN and dialyzed for a minimum of 24 hours against pure ACN to separate the unreacted peptides from the conjugates. Next, the purified conjugates were lyophilized and a final yield of approximately 35-40% was obtained. Thereafter, 5mg of polymer (PLGA-PEG-maleimide), peptides (WQP and GE11) and the conjugates (PLGA-PEG-WQP and PLGA-PEG-GE11) were each dissolved in 0.7mL of deuterated dimethyl sulfoxide (d6-DMSO) and the degree of conjugation was characterized using Bruker 500Hz proton nuclear magnetic resonance (^{1}H NMR) and analyzed using the Mnova (v.14.0) software.

Formulation of dual-peptide NPs having different surface valencies and stoichiometric ratios

Single- and Dual-peptide NPs having different surface valencies (5% and 30%) were formulated via the nanoprecipitation method according to literature[42]. Briefly, 3 mg of polymer mixture and 1.1 mM of DiI were dissolved in 300µL solvent phase (ACN) at room temperature. PLGA polymer was maintained at a ratio of 15% and mixed with $PLGA_{30k}$-PEG_{1k} and $PLGA_{30K}$-PEG_{5K}GE11 and $PLGA_{30K}$-PEG_{5K}-WQP at 5% and 30% surface valency. For formulation of dual-peptide NPs, along with PLGA and $PLGA_{30k}$-PEG_{1k} co-polymers, the $PLGA_{30K}$-PEG_{5K}-GE11 and $PLGA_{30K}$-PEG_{5K}-WQP conjugates were maintained in a unimolar ratio (1:1) for both 5% and 30% surface valencies.

For 5% dual-peptide NPs having different stoichiometric ratios, the GE11 peptide (strong binding affinity- driver) was maintained at a fixed ratio (1) while increasing ratios of WQP peptide (strong avidity- supporter) were explored. In total 5 different formulations having varied (GE11: WQP) ratios were tested- D-1 (1:1) NPs, D-2 (1:3) NPs, D-3 (1:5) NPs, D-4 (1:10) NPs and D-5 (1:20) NPs. For control PLGA-PEG formulations, the polymer-peptide conjugates

were substituted with PLGA-PEG-Mal, whilst maintaining the PLGA amount constant at 15%. The anti-solvent phase (MiliQ water) was stirred at 200-300 rpm whilst the solvent phase comprising the polymer solution (ACN) was pipetted at a 1:10 ratio (300µL polymer solution is pipetted into 3mL MiliQ water). Solvent extraction (evaporation) was continued for 5h under magnetic stirring in a fume hood at room temperature. NPs were then collected by high-speed centrifugation (Avanti J-26 XPI, rotor JA-14) using Amicon Ultra-4 100kDa filters as per filter instructions (10 min at 5,000 x g at 20ºC) with filtered MiliQ water. NPs were stored in MiliQ water at a 10 mg/mL concentration in the dark at 4ºC until further use.

NPs characterization.

Particle size and surface charge (□-potential) was measured using DLS analysis via Malvern Zetasizer Nano—ZS equipped with 633 nm laser and 173˚ detection optics. The following SOP settings were used Refractive index (RI): 1.460, Absorption: 0.0, Dispersant: water, viscosity: 0.887 cP, RI: 1.33, Temperature: 25˚C, equilibration time: 30 seconds, Cell: Quartz cuvettes ZEN2112. 50 µL of NPs suspension was added into the cuvette and the size measured in triplicate. Three independent batches were measured for each condition and the mean particle size value with standard deviation are reported. The cuvette was flushed 3x with purified water before each sample.

Surface peptide quantification by enzymatic digestion

The quantification of conjugated WQP and GE11 peptides on NP surface was carried out by site-specific digestion of the peptides using the enzyme Chymotrypsin protease by following the protocol provided by the manufacture (Pierce™, MAN0011638) with certain optimizations. As the protocol is usually used for large protein samples, the NP samples were highly concentrated (25-50mg/mL), to have enough concentration of the digested peptide fragments to be detected by mass spectrometry. The digestion reaction was carried out at an

enzyme: peptide sample ratio of 1:20, in the digestion buffer [500mM Tris HCl (pH 8.0) + 10mM $CaCl_2$]. The reaction vessel was incubated at 37ºC overnight and the digested fragments were collected from the supernatant obtained by brief (5 min) centrifugation of the samples to separate the NPs. The supernatant was then characterized by UPLC-MS at 280 nm, where a peak corresponding to the mass of the chosen digested fragment was obtained, the integrated value of whose area along with a calibration curve of known concentrations of digested WQP and GE11 fragments was used to calculate the exact number of surface peptides.

Dual receptor expression analysis by flow cytometry

For measuring the expression levels of PSMA and EGFR receptors, all the cell lines were stained with rabbit monoclonal anti-PSMA antibody (ab133579- Abcam Netherlands B.V.) and mouse monoclonal anti-EGFR antibody (MA5-13319- ThermoFisher Scientific) according to manufacturer´s protocol. Briefly 1 g/mL of 1º antibodies dissolved in 3% BSA were added to a monolayer of cells one after the other in LabTek on ice for 30 minutes each. Next, the cells were washed thrice with 1X PBS and incubated with 1 g/mL (dilutions provided by manufacturer) of polyclonal goat: anti-rabbit Alexa-488 secondary and goat: anti-mouse Alexa-647 2º antibodies, respectively for anti-PSMA and anti-EGFR 1º antibodies, for at least 1 hour in dark conditions. For flow cytometry, the cells were detached using 0.25% Trypsin-EDTA incubation for 10 mins at 37ºC, 5% CO_2 and obtained in suspension in 1X PBS. They were then stained with 10ug/mL of DAPI just before analysis with FACS Aria, with the 488nm laser. In total 10,000 cells (or events) were measured, and their mean fluorescence intensity values obtained. All measurements were carried out in triplicates and their mean SD values were obtained.

Quantitative analysis of cellular uptake by flow cytometry

For flow cytometry, all the cell lines were cultured in 6-well plates ($1x10^5$ cells/ well) for 24h until they reached up to 70% confluence and then incubated with a known concentrations (50µg/mL) of control, single and dual-peptide NP formulations having different surface valencies and 5% dual-peptides NPs having different surface stoichiometric ratios for 24h at 37ºC and 5% CO_2. Post incubation with NPs, the adherent cells were detached using 0.25% Trypsin/EDTA, incubated for 10 minutes at 37ºC and 5% CO_2, and obtained in suspension by centrifugation at 3000rpm for 5 minutes at 4ºC. From this moment onwards, all the further steps like washing with 1X PBS and resuspension in 1X PBS, were carried out whilst maintaining the cells on ice. Finally, the cells were resuspended in 1X PBS solution with the live cell staining agent DAPI (10 g/mL) and analysed using BD FACSAria™. The cells not stained with DAPI were excluded from the analysis. At least 10000 cells (or events) were analysed using two specific lasers for WQP-Cy5 (Red C-670nm) and multivalent WQP-NPs encapsulated with DiI (Green E-575nm). All measurements were carried out in triplicates and the standard deviation was obtained.

4.5 References.

1 M. J. Mitchell, M. M. Billingsley, R. M. Haley, M. E. Wechsler, N. A. Peppas and R. Langer, *Nat Rev Drug Discov*, 2021, **20**, 101–124.

2 L. Woythe, N. B. Tito and L. Albertazzi, *Advanced Drug Delivery Reviews*, 2021, **169**, 1–21.

3 Insights into Active Targeting of Nanoparticles in Drug Delivery: Advances in Clinical Studies and Design Considerations for Cancer Nanomedicine | Bioconjugate Chemistry 4 J. Yoo, C. Park, G. Yi, D. Lee and H. Koo, *Cancers*, 2019, **11**, 640.

5 D. Fukumura and R. K. Jain, *Journal of Cellular Biochemistry*, 2007, **101**, 937–949.

6 A. Schroeder, D. A. Heller, M. M. Winslow, J. E. Dahlman, G. W. Pratt, R. Langer, T. Jacks and D. G. Anderson, *Nat Rev Cancer*, 2012, **12**, 39–50.

7 H. Chen, W. Zhang, G. Zhu, J. Xie and X. Chen, *Nature Reviews Materials*, 2017, **2**, 17024.

8 S. Wilhelm, A. J. Tavares, Q. Dai, S. Ohta, J. Audet, H. F. Dvorak and W. C. W. Chan, *Nat Rev Mater*, 2016, **1**, 16014.

9 O. K. Nag and J. B. Delehanty, *Pharmaceutics*, 2019, **11**, 543.

10 N. Khan, Ruchika, R. K. Dhritlahre and A. Saneja, *Drug Discovery Today*, 2022, **27**, 2288–2299.

11 P. N. Navya, A. Kaphle, S. P. Srinivas, S. K. Bhargava, V. M. Rotello and H. K. Daima, *Nano Convergence*, 2019, **6**, 23.

12 J. H. Yoon, D. K. Kim, M. Na and S. Y. Lee, *Biophysical Chemistry*, 2016, **213**, 25–31.

13 X. Feng, J. Yao, X. Gao, Y. Jing, T. Kang, D. Jiang, T. Jiang, J. Feng, Q. Zhu, X. Jiang and J. Chen, *ACS Appl. Mater. Interfaces*, 2015, **7**, 27885–27899.

14 P. M. Peiris, F. He, G. Covarrubias, S. Raghunathan, O. Turan, M. Lorkowski, B. Gnanasambandam, C. Wu, W. P. Schiemann and E. Karathanasis, *Nanoscale*, 2018, **10**, 6861– 6871.

15 H. Xu, S. Kona, L.-C. Su, Y.-T. Tsai, J.-F. Dong, E. S. Brilakis, L. Tang, S. Banerjee and K. T. Nguyen, *J. of Cardiovasc. Trans. Res.*, 2013, **6**, 570–578.

16 J. Vanderburgh, J. L. Hill, M. K. Gupta, K. A. Kwakwa, S. K. Wang, K. Moyer, S. K. Bedingfield, A. R. Merkel, R. d'Arcy, S. A. Guelcher, J. A. Rhoades and C. L. Duvall, *ACS Nano*, 2020, **14**, 311–327.

17 V. J. Yao, S. D'Angelo, K. S. Butler, C. Theron, T. L. Smith, S. Marchiò, J. G. Gelovani, R. L. Sidman, A. S. Dobroff, C. J. Brinker, A. R. M. Bradbury, W. Arap and R. Pasqualini, *Journal of Controlled Release*, 2016, **240**, 267–286.

18 T. Anani, S. Rahmati, N. Sultana and A. E. David, *Theranostics*, 2021, **11**, 579–601. 19 A. Costagliola di Polidoro, G. Zambito, J. Haeck, L. Mezzanotte, M. Lamfers, P. A. Netti and E. Torino, *Cancers*, 2021, **13**, 503.

20 S. Marqus, E. Pirogova and T. J. Piva, *Journal of Biomedical Science*, 2017, **24**, 21.

21 C. J. Cheng and W. M. Saltzman, *Biomaterials*, 2011, **32**, 6194–6203.

22 E. S. Olson, T. Jiang, T. A. Aguilera, Q. T. Nguyen, L. G. Ellies, M. Scadeng and R. Y. Tsien, *Proc. Natl. Acad. Sci. U.S.A.*, 2010, **107**, 4311–4316.

23 L. Belfiore, D. N. Saunders, M. Ranson, K. J. Thurecht, G. Storm and K. L. Vine, *Journal of Controlled Release*, 2018, **277**, 1–13.

24 S. Muro, *Journal of Controlled Release*, 2012, **164**, 125–137.

25 D. Rosenblum, N. Joshi, W. Tao, J. M. Karp and D. Peer, *Nat Commun*, 2018, **9**, 1410. 26 D. G. Bostwick, A. Pacelli, M. Blute, P. Roche and G. P. Murphy, *Cancer*, 1998, **82**, 2256– 2261.

27 T. Maria, A. Panagiotis, C. Marina, K. Eleni, V. Ioanna, M. Georgia and P. Ioannis, *J Cancer Res Ther*, 2014, **10**, 133–141.

28 A. Ghosh and W. D. W. Heston, *Journal of Cellular Biochemistry*, 2004, **91**, 528–539.

29 T. M. Gorges, S. Riethdorf, O. von Ahsen, P. Nastały, K. Röck, M. Boede, S. Peine, A. Kuske, E. Schmid, C. Kneip, F. König, M. Rudolph and K. Pantel, *Oncotarget*, 2016, **7**, 34930– 34941.

30 S. Bravaccini, M. Puccetti, M. Bocchini, S. Ravaioli, M. Celli, E. Scarpi, U. De Giorgi, M. M. Tumedei, G. Raulli, L. Cardinale and G. Paganelli, *Sci Rep*, 2018, **8**, 4254.

R. A. de Araújo, F. A. C. da Luz, E. da C. Marinho, C. P. Nascimento, L. de A. Marques, P. F. R. Delfino, R. M. Antonioli, B. J. Araújo, A. C. A. L. da Silva, M. L. G. dos R. Monteiro, M. B. Neto and M. J. B. Silva, Epidermal growth factor receptor (EGFR) expression in the serum of patients with triple-negative breast carcinoma, http://ecancer.org/en/journal/article/1431epidermal-growth-factor-receptor-egfrexpression-in-the-serum-of-patients-with-triplenegative-breast-carcinoma-

prognosticvalue-of-this-biomarker, (accessed August 3, 2022). 31 Z. Cheng, A. A. Zaki, J. Z. Hui, V. R. Muzykantov and A. Tsourkas, *Science*, 2012, **338**, 903– 910.

32 R. I. Nicholson, J. M. W. Gee and M. E. Harper, *European Journal of Cancer*, 2001, **37**, 9– 15.

33 M. Westphal, C. L. Maire and K. Lamszus, *CNS Drugs*, 2017, **31**, 723–735.

34 S. Aggarwal, P. V. Singh, O. Topaloglu, J. T. Isaacs and S. R. Denmeade, *Cancer research*, 2006, **66**, 9171–9177.

35 W. Jin, B. Qin, Z. Chen, H. Liu, A. Barve and K. Cheng, *International Journal of Pharmaceutics*, 2016, **513**, 138–147.

36 I. Genta, E. Chiesa, B. Colzani, T. Modena, B. Conti and R. Dorati, *Pharmaceutics*, 2017 37 B. Colzani, G. Speranza, R. Dorati, B. Conti, T. Modena, G. Bruni, E. Zagato, L. Vermeulen, G. R. Dakwar, K. Braeckmans and I. Genta, *Int J Pharm*, 2016, **511**, 1112–1123. 38 K. Li, L. Pang, X. Pan, S. Fan, X. Wang, Q. Wang, P. Dai, W. Gao and J. Gao, *Technol Cancer Res Treat*, 2021, **20**, 15330338211004954.

39 M. R. W. Scheepers, L. J. van IJzendoorn and M. W. J. Prins, *Proc Natl Acad Sci USA*, 2020, **117**, 22690–22697.

40 F. Uliana, M. Vizovišek, L. Acquasaliente, R. Ciuffa, A. Fossati, F. Frommelt, S. Goetze, B. Wollscheid, M. Gstaiger, V. De Filippis, U. auf dem Keller and R. Aebersold, *Nat Commun*, 2021, **12**, 1693.

41 J. M. Barichello, M. Morishita, K. Takayama and T. Nagai, *Drug Development and Industrial Pharmacy*, 1999, **25**, 471–476.

Chapter 5| Discussion

This chapter provides an overall summary and a comprehensive discussion of the work presented in the previous chapters. It focuses on different surface peptide parameters regulating the selectivity of targeting of polymeric nanocarriers towards prostate cancer cells using each of the targeting peptides. The use of dual peptide-based targeting strategy is then proposed for selectivity towards prostate cancer cells that simultaneously express both target receptors, and the impact of surface peptide properties is assessed to obtain optimal surface valency and stoichiometric ratio values, as a mean for future applications in the development of precision nanotherapeutics against prostate cancer.

Cancer nanomedicine holds the promise of providing selective drug delivery at the specific tumor site, consequently enhancing its efficacy, while reducing toxicity. However, the socalled ´magic bullet´ theory postulated by Paul Ehrlich centuries ago, is yet to become a paradigm. Despite the extensive arsenal of targeting nanocarriers developed using various ligands, the active targeting field is still in dearth of favorable regulatory authorizations and any successful clinical translation till date. This certainly calls for a deeper and more quantitative understanding of the factors governing targeting of cancer nanomedicines. Being a highly interdisciplinary field, nanomedicine can benefit greatly by combining expertise from its varied branches of nanoscience, nanotechnology, and biomedical engineering, to offer rational designs of targeted nanomedicines. The aim of this thesis was to create a platform for dual peptide-based selective nanoparticle targeting by using cell-targeting peptides having varying levels of binding affinity for their respective target prostate cancer receptors. It involved unveiling the effects of various surface peptide properties such as multivalency, surface peptide number and stoichiometric ratios on the downstream targeting applications using either and/or both peptides. Taken together, these new insights provide a platform for the development of smart nanocarriers for selective prostate cancer targeting, bringing us a step closer towards the long-lasting goal of precision nanomedicines.

The conjugation of a targeting ligand to NP surface and it´s downstream biological application is often governed by the type of conjugation method used. In that, accounting for the targeting ligand properties like ligand type, size, charge, hydrophilicity/ hydrophobicity, etc. along with inherent heterogeneities of polymeric NPs, would result in a higher number of surface ligands. In **Chapter 2**, the strong binding affinity of GE11 peptide to EGFR, overexpressed on prostate cancer cells, was utilized with polymeric (PLGA-PEG) NPs to carry out a comparative analysis of the role played by two commonly employed (pre- and post-) conjugation methods on surface peptide properties. Further, their impact on selective

targeting of cells over-expressing EGFR was investigated across a panel of cell lines (PCa-LNCaP, PC3 and 22Rv1; and healthy- RWPE1) having varying EGFR expression levels. The preconjugation method involved conjugating the GE11 peptide to PLGA-PEG polymer synthesized with a maleimide group for attachment of the peptide through thiol (-SH) group of cysteine added at the C-terminal of the peptide under organic conditions. The degree of conjugation was obtained using ^{1}H-NMR, which gave a conjugation efficiency of ~70%, which was quite high. This was then followed by the formulation of 30% GE11 NPs using PLGA and PLGA-PEG copolymers by the manual process of nanoprecipitation. On the other hand, the postconjugation method involved conjugating the GE11 peptide to already formulated 30% PLGAPEG NPs having maleimide group on the surface for attachment of the thiol containing GE11 peptide. The degree of this conjugation was obtained indirectly by quantifying the amount of unbound GE11 peptide in the supernatant of 30% GE11 NPs using Nanodrop, which gave a conjugation efficiency of 37,5%. Furthermore, a method for robust quantification of the number of GE11 on the surface of pre- and post-conjugated NPs was developed using sitespecific digestion by chymotrypsin protease. This allowed for quantifying the number of surface GE11 in the supernatant of digested (pre- and post-) GE11 NPs, obtained by analysis using UPLC-MS having very high sensitivity. Next, the cellular uptake of non-targeted (30% PLGA-PEG), and pre- and post-conjugated 30% GE11 NPs was quantified using flow cytometry. The localization of targeted NPs was carried out using confocal microscopy, which allowed for visualization of non-targeted and GE11-NPs within or on the cells.

It was demonstrated that pre-conjugation of GE11 to PLGA-PEG polymer prior to NP formulation allowed for a higher and more controlled number of GE11 on NP surface, making it the preferred choice for further experiments. The use of long-chain (5K) PLGA-PEG linker having maleimide group for peptide attachment, along with short-chain (1K) PLGA-PEG copolymer formulating the PEG layer of the NPs imparting stealth properties, allowed for a better distribution and therefore, exposure of GE11 on NP surface, increasing its availability

for cellular targeting. In comparison, post-conjugation of GE11 to formulated 30% PLGA-PEGmaleimide NPs failed to offer much control, especially over the availability of maleimide group on the NP surface. This, in turn, could possibly lead to a highly heterogenous distribution of maleimide on NP surface within the same batch. Consequently, it resulted in only about half the surface coverage of the post-conjugated GE11 NPs. The increased availability of surface GE11 in pre-GE11 NPs resulted not only in an overall increased cellular uptake but also led to selective targeting of EGFR over-expressing prostate cancer cells. However, even though the difference in overall uptake of pre-GE11 NPs was significantly higher than post-GE11 NPs, it did not seem to affect much the selectivity, possibly owing to the strong affinity of GE11 for EGFR. These findings shine light on the importance of the influence of conjugation strategies and the interplay between ligand binding affinity and surface valency on the rational design of nanosystems for selective tumor targeting.

Multivalency is a property that involves the binding of multiple targeting ligands to many different targets at the same time. This is widely explored for active NP targeting especially using weak-binding ligands. In **Chapter 3**, the avidity of WQP, a small peptide having weak/moderate binding affinity to PSMA overexpressed on prostate cancer cells, was explored for its selective targeting potential. In particular, the targeting ability of WQP monomer for PSMA was compared to that of multivalent WQP-functionalized NPs having varying surface valency (5% and 30% WQP) using polymeric PLGA-PEG NPs across a panel of prostate cancer cell lines with varying levels of PSMA expression. It was already established that the monomeric form of WQP binds weakly to the cytoplasmic domain of PSMA, however, in its dimeric configuration, this binding could be increased up to 10-fold. The idea was to evaluate whether functionalization of WQP to NP surface would allow for simultaneous binding of multiple peptides to multiple receptor sites, and by the virtue of its avidity, enhance its cellular uptake. The purpose of testing different surface valencies (low and high) was to evaluate if there is a direct correlation between the number of surface peptides on the

selectivity of targeting. A panel of different prostate cells having different expression levels of PSMA was employed to investigate the targeting selectivity of multivalent WQP NPs. For formulating multivalent WQP-NPs having varied surface valencies, pre-conjugation of WQP peptide to PLGA-PEG polymer was employed, followed by NPs formulation by nanoprecipitation. The quantification of number of WQPs on the NP surface was carried out by site-specific digestion using chymotrypsin protease. This method allowed for a robust quantification of surface WQPs, a step which is often overlooked in the development of targeted NPs, consequently impacting their biological performance. For quantification of cellular uptake, flow cytometry was employed, while the localization of targeted NPs was carried out using confocal microscopy.

Indeed, it was observed that multivalent WQP-NPs showed higher cellular uptake in comparison to WQP monomer. Furthermore, this uptake was found to be linearly correlated to the surface WQP valency, in that, there was an increase from 5% to 30% WQP NPs. However, given that cellular receptor expression changes over time, we believe that there would be a surface valency which causes saturation of the surface receptors, however, as that would further pose issues of particle aggregation, we chose the maximum surface valency to be 30%. Additionally, WQP-NPs were found to have a higher overall uptake in PSMA overexpressing LNCaP cells, followed by 22Rv1 cells having moderate PSMA expression and lowest in PC3 and RWPE1 cells having low/no PSMA expression, thus imparting targeting selectivity. This was attributed to a stronger avidity of multivalent WQP-NPs for selective PSMA targeting. We believe that this kind of strategy can be useful for improving the binding affinity of a weak ligands as a mean for selective tumor targeting.

Lastly, having established the contributions of affinity and avidity for achieving targeting selectivity regimes for each of the peptides, **Chapter 4** involved the reporting of a synthetic strategy employing both peptides functionalized to PLGA-PEG NPs with systematically varied

surface properties. Further, their impact on selective targeting was investigated across a panel of prostate cancer cell lines having varying levels of both target receptors. The main rationale behind the design of this strategy was to combine the affinity of one peptide and the avidity of the other to act synergistically for achieving targeting selectivity. In addition, the impact of different surface properties of dual-peptide NPs like valency and stoichiometric ratios was investigated. The quantification of surface coverage by both peptides was carried out using the optimized method of site-specific digestion using chymotrypsin protease and analyzed with high sensitivity by UPLC-MS. Further, the impact of different surface peptide valency (5% and 30% NPs) on the overall cellular uptake of dual-peptide NPs having unimolar (1:1) ratio of peptides was evaluated by comparing to that of single peptide-NPs, to determine whether there was co-operativity at play between the two peptides, or it were a mere additive effect. The insights obtained from this study further allowed to establish the optimal surface valency for exploring the impact of different stoichiometric ratios of peptides on the targeting selectivity. In particular, the ratio of GE11 peptide having stronger affinity was maintained constant, while that of the weak binding WQP peptide was used in increasing proportions. A total of 5 different stoichiometric ratios (GE11: WQP) were tested, namely D1 to D-5 (1:1, 1:3, 1:5, 1:10 and 1:20). For quantification of the cellular uptake in both studies, flow cytometric analyses was carried out.

The results obtained for different surface valency for dual-peptide NPs corroborated with those obtained using single-peptide NPs earlier, showing an increasing trend in the number of surface peptides with increasing surface valency. However, their surface coverage (%) was not found to be linearly correlated with this. For the lower surface valency (5%) NPs, a higher surface coverage was obtained in comparison to NPs with higher surface valency (30%). This could possibly be attributed to the overcrowding of the NP surface in case of the latter, resulting in the embedding of the peptides in the NP core, thus causing a decrease in the number of surface peptides. Therefore, somewhat counterintuitively, 5% dual-peptide NPs

showed higher cellular uptake than the 30% dual NPs in 22Rv1 cells expressing both target receptors. For cell lines overexpressing only one target receptor (i.e., LNCaP cells for PSMA and PC3 cells for EGFR), the single-peptide NPs having 30% surface valency showed the highest uptake respectively. In addition, the uptake of single-peptide NPs added together was tested in comparison to dual-peptide NPs and demonstrated a higher uptake of dual-peptide NPs in 22Rv1 cells, thereby confirming the role of co-operativity of the two peptides for synergistic targeting. Thus, 5% was established to be the optimal surface valency for further studies.

For 5% dual-peptide formulations having different surface stoichiometric ratios, the sizes and zeta potential values by DLS were found to be almost like one another, owing to the small size and close to neutral charges of the peptides, respectively. The surface quantification of each of the number of surface peptides yielded values close to those expected for D-1, D-2 and D3 NP formulations. However, for the D-4 and D-5 NPs, the amount of GE11 was lower than the limit of detection of the equipment and could thus, not be detected well. D-2 NPs having the surface peptide ratio (GE11: WQP) of 1:3 showed an overall highest cellular uptake in 22Rv1 cells followed by D-3 (1:5) and D-1 (1:1) NP formulations. Expectedly, D-4 and D-5 NP formulations were found to have a negligible uptake, almost equivalent to non-targeted NPs, possibly due to insufficient levels of the driver GE11 peptide. For PC3 and LNCaP cells which express only one of the target receptors (EGFR and PSMA, respectively), the overall uptake was found to be low, thus emphasizing the underlying specificity and selectivity of dualpeptide NPs for cells expressing dual target receptors. For measuring the specificity, the ratio of cellular uptake between dual-peptide NPs was compared to the non-targeted (control) NPs, expressed as a difference in fold increase. D-2 NPs proved to be highly specific, having a □25-fold increase for 22Rv1 cells. However, this was found to be decreased in case of PC3 and LNCaP cells, expressing only one target receptor. This could be accredited to the ratio of CTPs employed, which allowed for a rather specific interaction with the dual target receptors, rendering the non-specific interactions with other cells rather insignificant. For determining

the selectivity of uptake of individual formulations, a ratio of uptake between cancer cells with healthy (RWPE-1) cells was carried out. D-2 and D-3 NPs showed 8-fold and 7-fold increase in selective uptake for 22Rv1 cells; while D-1 and D-2 NPs were found to be 2-fold and 3-fold selective for LNCaP and PC3 cells, respectively. These findings were extremely crucial is determining the optimal surface peptide ratios for selective targeting of cells expressing either or both target receptors, and successfully demonstrated that through a refined design and well-characterized NP formulations, dual peptide-based nanosystems hold promise of providing precision tumor targeting.

Conclusions

This section summarizes the research findings obtained in each of the chapters presented in this thesis.

The past two years have witnessed the fruits of tremendous efforts from the nanomedicine community for providing effective solutions to tackle a global pandemic, thus ascertaining their relevance for our society. Indeed, the utility of nanocarriers for encapsulation of mRNA therapeutic for the successful development of SARS-CoV-2 vaccines has highlighted the importance of collaborative efforts from different scientific disciplines. Besides vaccinology, nanoparticle drug delivery also entered clinical trials for diagnostics and anti-cancer applications, the latter being the primary focus of this thesis. However, the cancer nanomedicine field is yet to unlock its full potential, owing to the issues pertaining to poor bench-to-bedside translations. This calls for the development of multidisciplinary approaches for the design of smart targeting systems able to offer improvement over existing treatments by making them more selective. In this work, we aimed to employ small targeting peptides for active targeting of prostate cancer cells in a selective manner using polymeric nanoparticles. It involved characterization of the interplay various surface ligand properties like binding affinity, avidity, multivalency and co-operativity, explored for selective prostate cancer targeting using each of the peptides. It resulted in the development of a dual peptidebased targeting strategy for selective recognition of cancer cells showing presence of both target receptors. Taking this general outcome into account, the main conclusions retrieved from this thesis are as follows:

In **chapter 2**, we employed the strong binding affinity of GE11 peptide for EGFR overexpressed on PCa cells to explore the role of two commonly used conjugation strategies using polymeric NPs and compared their impact on cellular uptake. We developed a method of site-specific enzymatic digestion for the robust characterization of GE11 peptide obtained on the surface of NPs conjugated by both techniques. We found that pre-conjugation allowed for a higher number and surface coverage of NPs with the GE11 peptide, an essential parameter for the development of more effective active targeting nano-formulations. Having a higher number of surface GE11 peptides resulted not only in an increased cellular uptake, but it also led to

selective targeting of cells overexpressing EGFR, thus establishing pre-conjugation as the preferred strategy for further studies.

Next, we used the WQP peptide having weak-binding affinity for PSMA, another important PCa biomarker, and explored its avidity in **chapter 3** for selective targeting of PSMA using multivalent NPs. We formulated stable and monodisperse multivalent WQP-NPs with varying surface valencies and compared their interaction with cells (uptake) to that of the peptide monomer. We characterized conjugated NPs for surface peptide number using enzymatic digestion and found that, while the formulations with lower WQP density have lower number of surface WQP than the higher density formulations, they tend to have a higher surface coverage, a property that must be considered for development of more effective active targeting nano-formulations. Having a lower binding affinity to target receptor was disadvantageous for the monomer, but we successfully demonstrated that this affinity could be improved by multivalent targeting using polymeric NPs. Furthermore, we show that this multivalency allows for selective targeting, a property that is desirable and extremely sought after for the development of more efficient nanomedicines.

Finally, based on the insights obtained from studies with individual peptides, in **chapter 4**, we developed a dual peptide-based targeting strategy for selective targeting of cells showing expression of dual receptors, by the virtue of co-operativity between the two peptides. To this end, we explored the impact of two of the most important NP surface parameters- Valency and stoichiometric ratios on the overall uptake and specificity and selectivity of NP targeting. We showed that having lower surface valency (5%) allowed for better surface coverage of dual peptides consequently resulting in an increased uptake in 22Rv1 cells expressing both receptors in comparison to those with a higher surface valency (30%), which showed higher uptake in cells expressing only one target receptor. Next, we formulated dual peptide- NPs having different stoichiometric ratios and established the most optimal one having improved selectivity for 22Rv1 cells expressing both receptors.

Our results conclusively show that through a systematic design, dual-peptide mediated NP targeting strategy can significantly improve the selectivity and efficiency of active targeting approaches, which is not possible with traditional single ligand- receptor targeting strategies. We believe that the application of this dual-peptide mediated targeting strategy may ultimately allow for the customization of peptide-targeted nanosystems tailored for individual cases, providing a personalized approach in anti-cancer treatments for improved patient outcome.

Outlook

This section provides possible future perspectives for the research conducted in the chapters presented in this thesis.

Prostate cancer is the second leading cause of deaths in males globally. Given the dynamic nature of the disease and a high rate of tumor relapses, current treatment efforts are moving towards selective delivery of therapeutics. In that regard, nanoparticulate systems are widely explored, but there is still a long road to go. It is clear, that there is a need for more comprehensive studies unveiling the impact of NP surface properties on their selective targeting ability, whilst accounting for the numerous heterogeneities occurring at both NP and cellular levels. Furthermore, targeting using single type of ligand may not always provide the required efficacy, resulting in development of dual-ligand strategies to achieve this goal. However, the more complex the strategy, the more parameters are involved which need to be thoroughly understood and accounted for. The work carried out in this thesis explored the impact of several surface ligand properties of small peptides on their selective targeting potential. Based on the insights obtained, the development of a dual peptide-based strategy for selective targeting of prostate cancer cells was reported. We believe that this work laid foundation for future experiments involving higher levels of complexity, further directing towards smart platforms for development of precision targeting nanosystems. However, the occurrence of global COVID-19 pandemic amidst the span of this work added its own set of challenges. Yet, it also provided an opportunity to think, reflect and change gears, which is crucial for effective scientific research. In the following sections, the future perspectives for each of the chapters presented in this thesis are provided.

Chapters 2 and 3 involved studies exploring the impact of different NP surface ligand properties including surface ligand number, overall ligand distribution on particle surface, affinity of ligands to bind with target receptors and multivalency, on their selectivity of targeting using each of the peptides. These studies not only offered insights in the design of smart and efficient nanosystems for selective PCa targeting, but also have multiple applications and possible parameters that still remain to be explored. Foremost, it could be interesting to employ other types of CTPs or targeting ligands in general to enhance their

targeting potential by a specific conjugation method or by multivalent binding for other types of solid tumors. The conjugation methods tested could be expanded beyond covalent conjugation and include physical adsorption and further branch out to test the impact of different conjugation chemistries, for example, EDC/NHS instead of maleimide-thiol coupling. The multivalent binding could be tested for enhancing the targeting potential of multiple different weak-binding ligands. To make the formulation process more high-throughput, the use of microfluidics-assisted platforms could provide a possible direction. Taken together, these can be used for a multiparametric analysis of various NP surface ligand properties, useful for generation of a library of targeted nanocarriers, for personalizing NP targeting schemes based on individual tumor samples. At the biological level, these studies could be expanded for testing *in-vivo*, requiring further optimizations for the same.

Chapter 4 reported an important synthetic strategy involving dual peptide-based NP targeting of PCa cells showing expression of dual target receptors in a super-selective manner. It provided a platform which could be utilized to further explore various combinations of same or different types of ligands, depending on the properties of target receptors. For example, it could be of interest to expand the applicability of this strategy for selective targeting of the tumor microenvironment (comprising endothelial cells, components of ECM, and cancer stem cells) in addition to tumor cells. We carried out a pilot study adding a layer of complexity by testing selective targeting of tumor spheroids as described in Appendix-4, although the results were not entirely conclusive just yet. We believe, however, that with further optimizations, these studies would indeed offer valuable insights about the behavior of targeted NPs in a complex environment, with an intermediate three-dimensional model, allowing for the selection of optimal candidates for further carrying out animal studies. Another interesting outlook would be employing the microfluidics platform for carrying out cellular uptake studies under flow conditions, which would be invaluable for simulating the behavior of NPs under

complex *in vivo*-like conditions, allowing the selection of best possible candidates for precision targeting, bringing us a step closer to the clinic.

Appendix 1

*This Appendix provides supportive information to the results presented in the **Chapter 2** of this thesis. It includes the chromatograms and mass-spectrometry information obtained for synthesis and purification of GE11 peptide as well as for the characterization of NP surface coverage by pre- and post-conjugated GE11. The ^{1}H-NMR spectra for calculation of conjugation efficiency of pre-GE11 is provided and the efficiencies for both pre- and postconjugation methods are obtained. It also depicts the chromatograms obtained for surface quantification of number of GE11 peptides along with the quantification of their surface coverage.*

GE11 synthesis and purification:

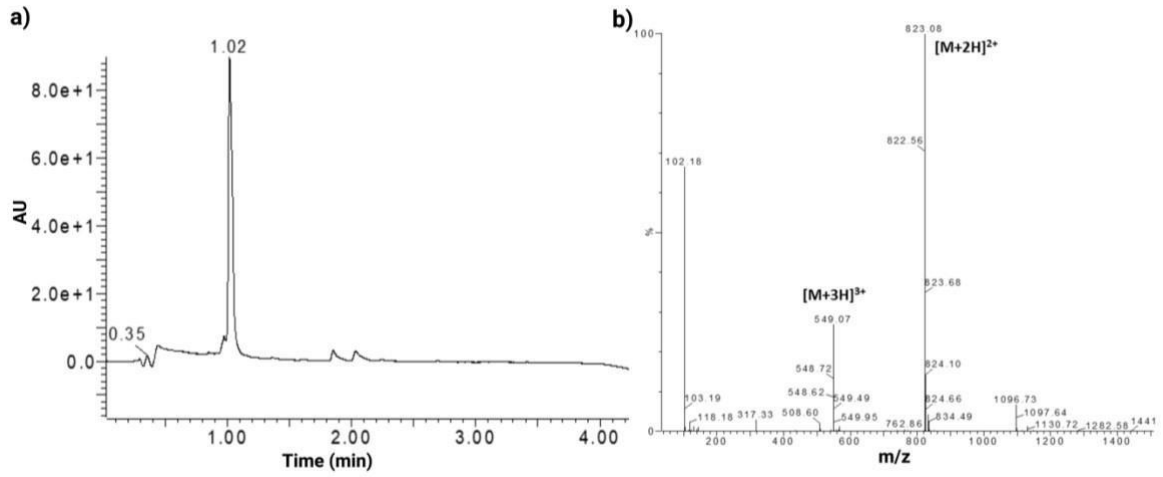

Figure A1.1 Synthesis and purification of GE11 peptide. *a) UPLC-MS chromatogram at l=280nm of peak corresponding to purified GE11. b) Mass spectra of purified GE11 showing corresponding m/z values.*

The GE11 peptide was synthesized using solid phase peptide synthesis and modified at the Cterminal using a cysteine amino acid having a free thiol group for future conjugation with maleimide polymer/ NPs. For SPPS, the 9-fluorenylmethoxycarbonyl/tertbutyl (Fmoc/tBu) strategy[1,2]. 2-Chlorotrityl resin, L-Fmoc-protected amino acids (2 equivalents), coupling agent TBTU (2 equivalents), and DIEA (6 equivalents) were used. The Fmoc protecting group was cleaved by treatment with a solution of 20% piperidine in DMF (2 x 10 min). Peptides were cleaved from the resin by treatment with Reagent B (88% TFA, 2% TIPS, 5% water and 5% phenol) for 4h. The crude peptide obtained was then purified at a wavelength ( ) of 280nm by semipreparative RPHPLC-MS [Waters 2487 Dual Absorbance Detector equipped with a Waters 2700 Sample Manager, a Waters 600 Controller, a Waters Fraction Collector, a Symmetry column (C18, 5 mm, 30 x 100 mm)] using the MassLynx software.

It was then characterized using UPLC-MS where a sharp peak corresponding to pure GE11 was obtained (figure A1.1), giving a purity of 98%. HPLC conditions: Flow=6 mL/min. Gradient=30–60% B in 5 min; A=0.1% TFA in H_2O, B=0.05% TFA in ACN. A total of 50% yield of pure GE11 was obtained.

GE11 conjugation and characterisation:

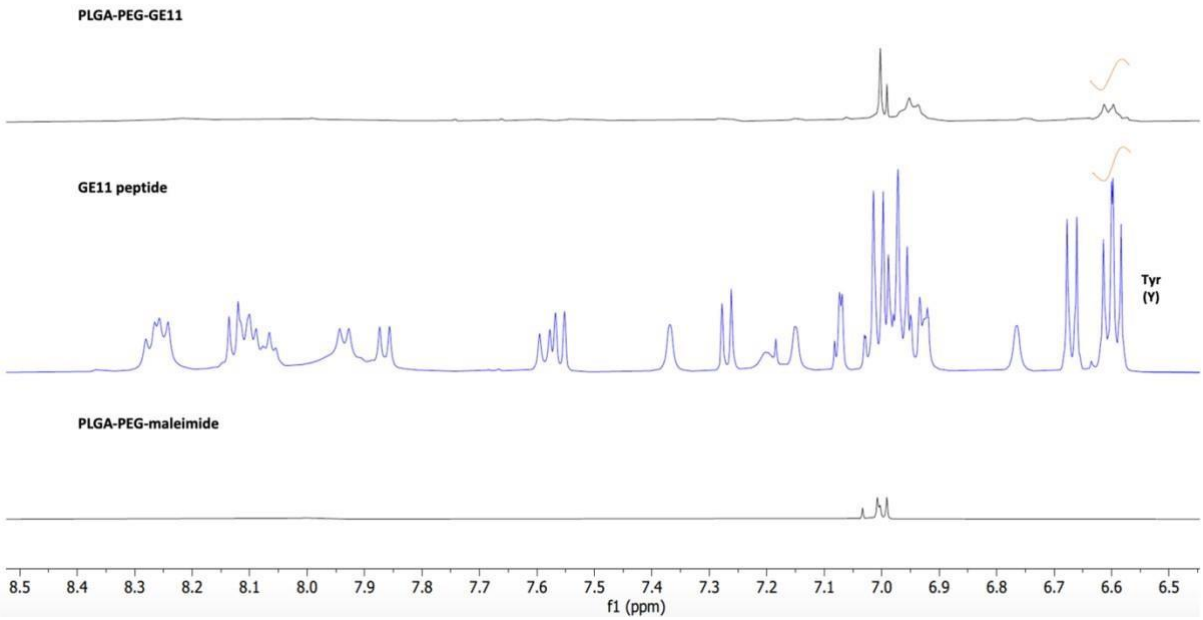

Figure A1.2 Characterisation of pre-GE11 conjugation by ^{1}H NMR. *Overlapped spectra of zoomed-in aromatic regions (6.5 to 9ppm) of polymer, peptide, and conjugate.*

The integrated area value of the coinciding triplet peak obtained at 6.6 ppm corresponding to the protons from aromatic side chain of tyrosine (Y) is used for calculation of CE.

Peak	ppm	Integrated area (a_i)	Number of protons (m_i)	Number of repeating units (n_i)	WQP/ PLGA (CE) (%)
Tyrosine (Y) protons	6,61	37,76	6	3	67,7
CH (LA)	1,459	3000	3	333,33	

Table A1.1 *Calculation of CE by ^1H NMR.*

The conjugation degree of PLGA-PEG copolymer with GE11 was calculated by the ratio between the integrated area of the triplet observed at d = 6.61 corresponding to protons corresponding to the aromatic side chain of tyrosine in the peptide sequence, and that of the integrated peak observed at d = 1.5 (Figure 2.2 a), corresponding to the protons of the methyl groups ($–CH_3$) of PLGA.

The CE is calculated as a ratio between GE11/PLGA obtained using the following equation[3]

$$\underline{\text{GE11}} = \frac{a_{GE11} / m_{GE11}}{(a_{GE11} / m_{GE11}) + (a_{CH3} / (m_{CH3} \times n_{CH3}))} = \frac{37,76/6}{(37,76/6) + (3000/ (3 \times 333,33))} = 0,677$$

where a_i corresponds to the integrated area under the signals of the ^1H-NMR spectrum for the respective fractions, m_i corresponds to the number of protons corresponding to each signal, and n_i is the number of repetition units of the fraction i. The calculation indicates that for every PLGA there is 0,77 units of GE11. Thus, the value of CE is 67,7%.

Sample	Unbound GE11 by Nanodrop (A_{280})	Molar equivalents added	CE (%)
Only GE11	0,056	3	37,50
Post-GE11 NPs	0,049		

Table A1.2 *Calculation of CE by absorbance of unbound GE11.*

The conjugation degree of post-conjugated GE11 to PLGA-PEG NPs was calculated by measuring the difference between absorbance of only GE11 added and the unbound GE11 from conjugated NPs and dividing by the absorbance of total GE11 added for the reaction, presented as a percentage. The CE for this reaction obtained is 37,50%.

GE11 surface quantification by specific enzymatic digestion:

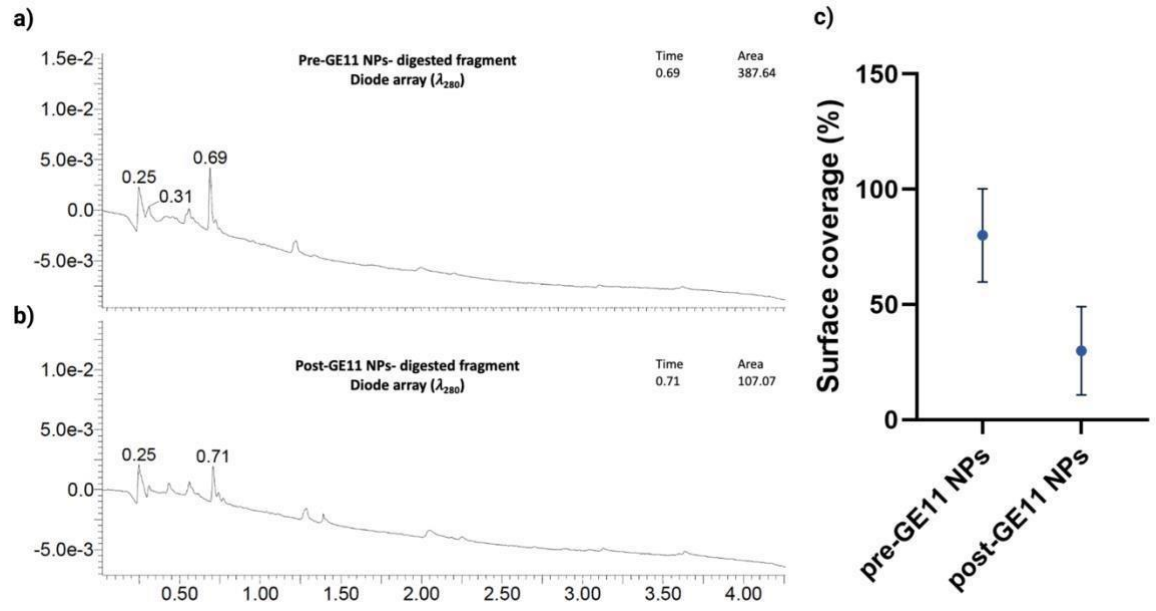

Figure A1.3 Quantification of GE11 on NP surface by enzymatic digestion. *Integrated chromatograms (area under curve values shown) of the chosen digested fragments of* ***a)*** *preGE11 NPs and* ***b)*** *post-GE11 NPs having 30% surface valency obtained at ≥280nm.* ***c)*** *Calculation of surface coverage (%) of GE11 NPs for both pre- and post-conjugated formulations.*

References

1 D. A. Wellings and E. Atherton, in *Methods in Enzymology*, Academic Press, 1997, vol. 289, pp. 44–67.

2 R. B. Merrifield, Solid Phase Peptide Synthesis. I. The Synthesis of a Tetrapeptide, http://pubs.acs.org/doi/pdf/10.1021/ja00897a025, (accessed February 21, 2022).

3 G. P. Hoyos-Ceballos, B. Ruozi, I. Ottonelli, F. Da Ros, M. A. Vandelli, F. Forni, E. Daini, A. Vilella, M. Zoli, G. Tosi, J. T. Duskey and B. L. López-Osorio, *Pharmaceutics*, 2020, **12**, 72.

4 Technical Page - Characteristics of Polystyrene Particles-Spherotech, https://www.spherotech.com/particle.html, (accessed February 22, 2022).

5 Application Verification Testing for Immunofluorescence (Adherent and Suspension) - ES, https://www.thermofisher.com/es/es/home/life-science/antibodies/antibodieslearningcenter/antibodies-resource-library/antibody-application-testingprotocols/immunofluorescence-protocol-adherent-suspension-applicationtesting.html, (accessed August 3, 2022).

Appendix 2

*This Appendix provides supportive information to the results presented in the **Chapter 3** of this thesis. It includes the chromatograms and mass-spectrometry information obtained for the characterization of NP surface coverage by peptides. It also details the method used to calculate the exact number of surface peptides.*

Pre-WQP conjugation and characterisation:

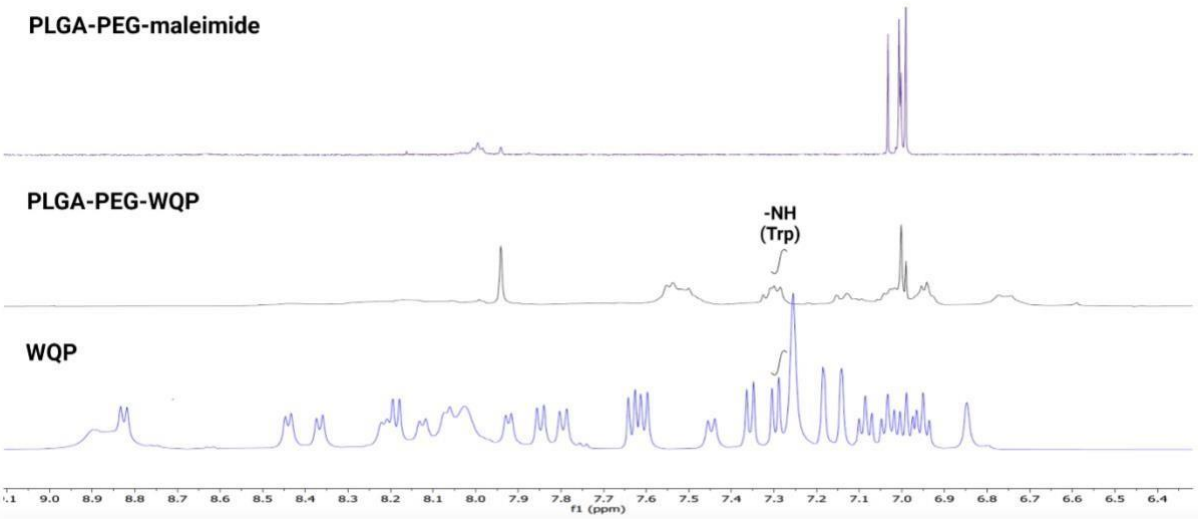

Figure A2.1 Characterization of peptide-polymer conjugation by ^{1}H NMR. *Overlapped zoomed-in spectra of the aromatic region (6.5 to 9ppm) of PLGA-PEG-maleimide polymer, WQP peptide and the PLGA-PEG-WQP conjugate. Integrated areas of coinciding peaks (7.31ppm) corresponding to protons from -NH group of the indole ring of tryptophan (Trp) are used for calculation of CE.*

The CE Is calculated as a ratio between WQP/PLGA obtained using the following equation[1]

$$\frac{WQP}{PLGA} = \frac{a_{WQP} / m_{WQP}}{(a_{WQP} / m_{WQP}) + (a_{CH3} / (m_{CH3} \times n_{CH3})} = \frac{1,01/1}{(1,01/1) + (300/ (3 \times 333,33))} = 0,77 \quad (1)$$

where a_i corresponds to the integrated area under the signals of the 1H-NMR spectrum for the respective fractions, m_i corresponds to the number of protons corresponding to each signal, and n_i is the number of repetition units of the fraction i. The calculation indicates that for every PLGA there is 0,77 units of WQP. Thus, the value of CE is 77%.

Peak	ppm	Integrated area (a_i)	Number of protons (m_i)	Number of repeating units (n_i)	WQP/ PLGA (CE) (%)
-NH (W)	7,31	1,01	1	1	77,1
CH_3 (PLGA)	1,46	300	3	333,33	

***Table A2.1 Calculation of CE by ^{1}H NMR**. The conjugation degree of PLGA-PEG copolymer with WQP was calculated by the ratio between the integrated area of the doublet observed at d = 7.31 corresponding to amide protons of tryptophan in the peptide sequence, and that of the integrated peak observed at d = 1.5 (Figure 3.3), corresponding to the protons of the methyl groups (–CH3) of PLGA.*

Surface WQP characterisation by specific enzymatic digestion:

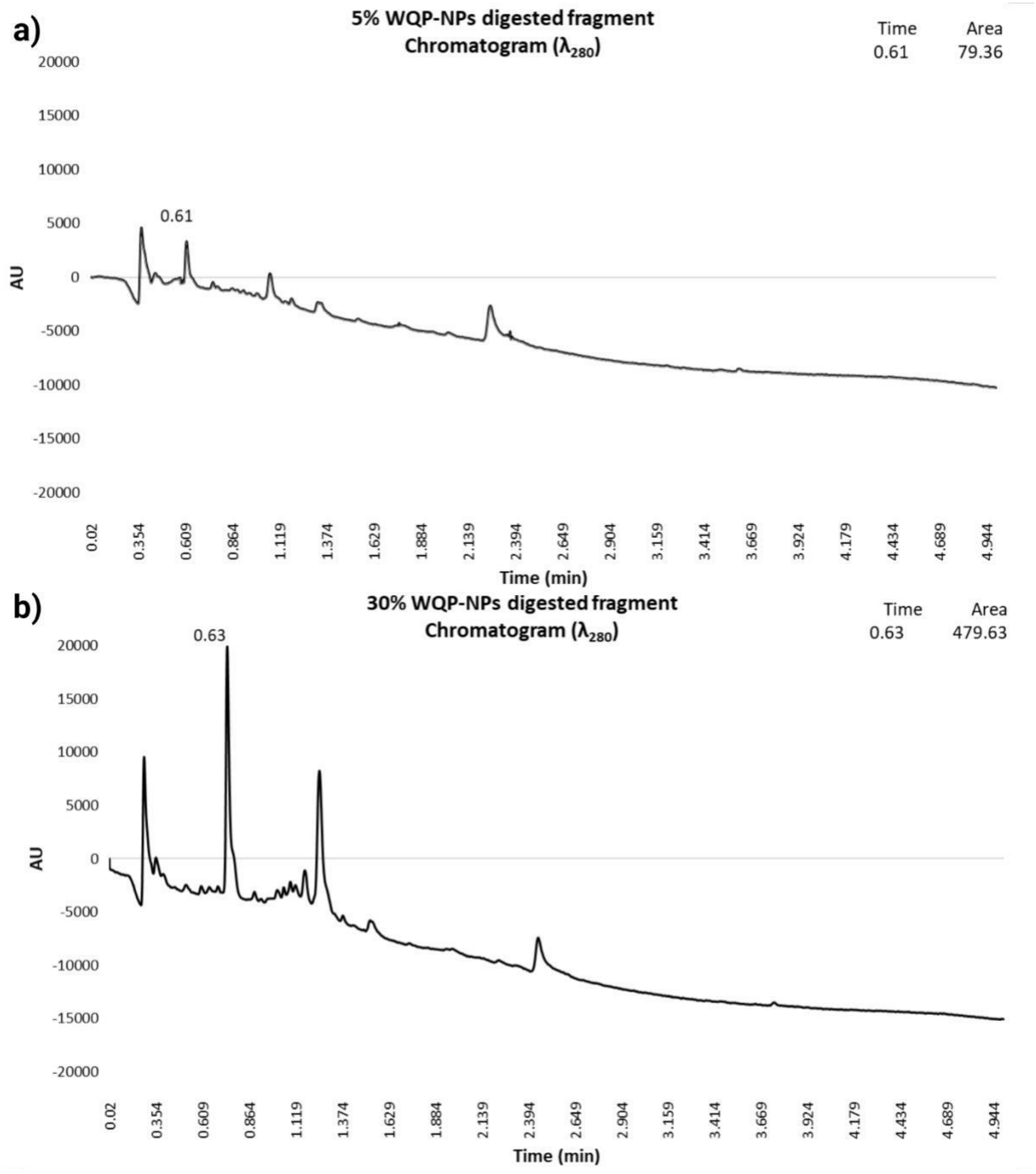

Figure A2.3 UPLC-MS analysis of surface WQP on multivalent NPs. *Integrated chromatograms of digested fragments of multivalent WQP-NPs having different surface valencies a) 5% and b) 30% obtained at λ=280nm.*

Calculation of number of WQP on NP surface by enzymatic digestion:

For calculation of theoretical (expected) number of WQPs, we used the formula as per Spherotech´s instructions[2] as follows:

1. Calculating the number of NPs in suspension:

   $$\frac{(6 \times \text{Polymer weight (g)})}{(3.14 \times \text{Polymer density (g/cm3)} \times \text{NP diameter (um)}^3)} \times 10^{12} \quad (2)$$

2. Calculating the number of WQP molecules in suspension:

   $$\left(\frac{\text{Mass of WQP-conjugate (g)}}{\text{Molecular weight of WQP-conjugate (g/mol)}}\right) \times \text{Avogadro´s number} \quad (3)$$

3. Calculating the theoretical number of WQP molecules per NP:

   $$\frac{\text{Number of WQP molecules}}{\text{Number of NPs in suspension}} \quad (4)$$

4. Calculating moles of WQP-conjugate added:

   $$\frac{\text{Mass of WQP-conjugate added (g)}}{\text{Molecular weight of WQP-conjugate (g/mol)}} \quad (5)$$

5. Calculation of mass (□g/mL) of WQP added:

   moles of WQP-conjugate added X molecular weight of WQP (6)

6. Calculation of moles of WQP obtained on NP surface:

   $$\frac{\text{Mass of WQP (observed)}}{\text{Molecular weight of WQP}} \quad (7)$$

7. Calculation of molecules of WQP on NP surface:

   Moles of WQP (observed) X Avogadro´s number. (8)

This value is divided by the molecules of NPs in suspension obtained in (2) to get the number of WQP/ NP as demonstrated in Table 3.1.

References

(1) Hoyos-Ceballos, G. P.; Ruozi, B.; Ottonelli, I.; Da Ros, F.; Vandelli, M. A.; Forni, F.; Daini, E.; Vilella, A.; Zoli, M.; Tosi, G.; Duskey, J. T.; López-Osorio, B. L. PLGA-PEG-ANG-2 Nanoparticles for Blood–Brain Barrier Crossing: Proof-of-Concept Study. *Pharmaceutics* **2020**, *12* (1), 72. https://doi.org/10.3390/pharmaceutics12010072.

(2) Technical Page - Characteristics of Polystyrene Particles - Spherotech. https://www.spherotech.com/particle.html (accessed 2022-02-22).

(3) *Indirect flow cytometry (FACS) protocol | Abcam*. https://www.abcam.com/protocols/indirect-flow-cytometry-protocol (accessed 202202-22). (4) Lall, N.; Henley-Smith, C. J.; De Canha, M. N.; Oosthuizen, C. B.; Berrington, D. Viability Reagent, PrestoBlue, in Comparison with Other Available Reagents, Utilized in Cytotoxicity and Antimicrobial Assays. *Int J Microbiol* **2013**, *2013*, 420601. https://doi.org/10.1155/2013/420601.

(5) *PrestoBlue Assays for Cell Viability - ES*. https://www.thermofisher.com/es/es/home/lifescience/cell-analysis/fluorescencemicroplate-assays/microplate-assays-cellviability/prestoblue-cell-viability-reagent.html (accessed 2022-07-27).

Appendix 3

*This Appendix provides supportive information to the results presented in the **Chapter 4** of this thesis. It includes the chromatograms and mass-spectrometry information obtained for characterization of NP surface coverage by peptides. It also details the method used to calculate the exact number of surface peptides and highlights this information in tabular forms.*

UPLC-MS data obtained for characterization of NP surface peptides by specific enzymatic digestion:

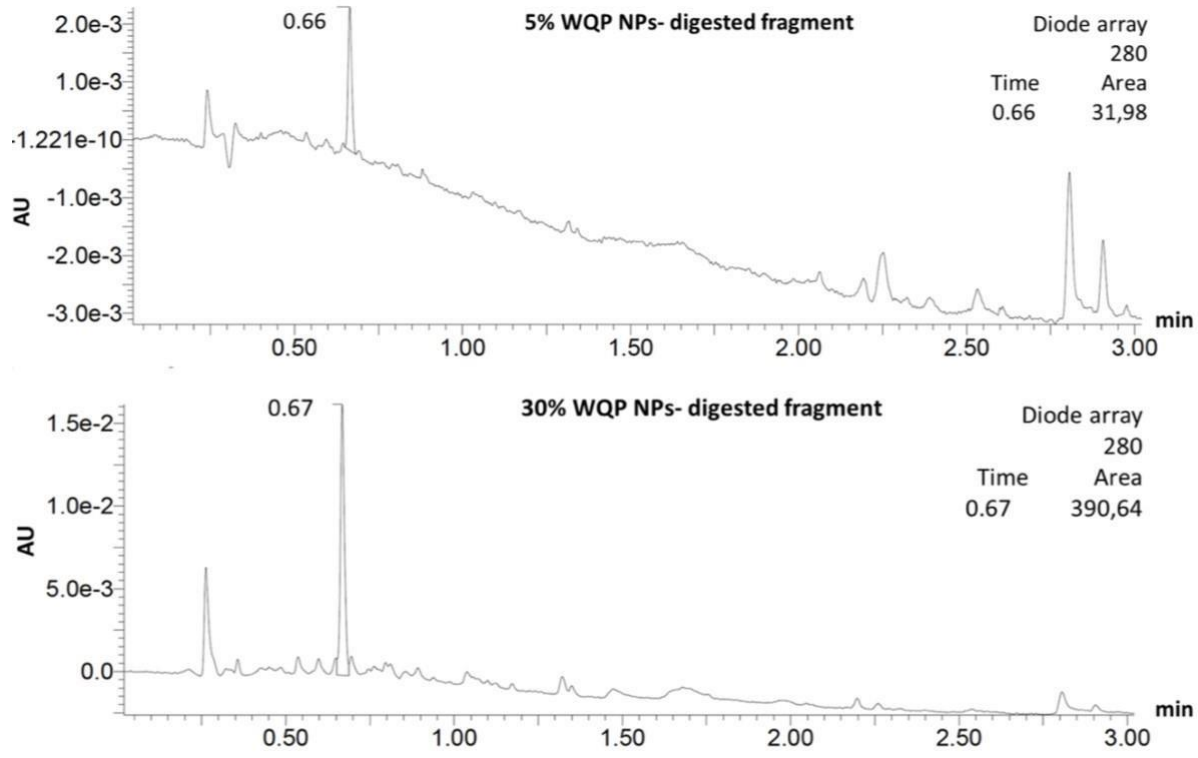

Figure A3.1 Integrated chromatograms of WQP-NPs with different surface valency. *Chromatograms with integrated area under curve values at 280nm obtained by UPLC-MS of peaks corresponding to digested WQP fragment of **A)** 5% WQP-NPs and **B)** 30% WQP-NPs*

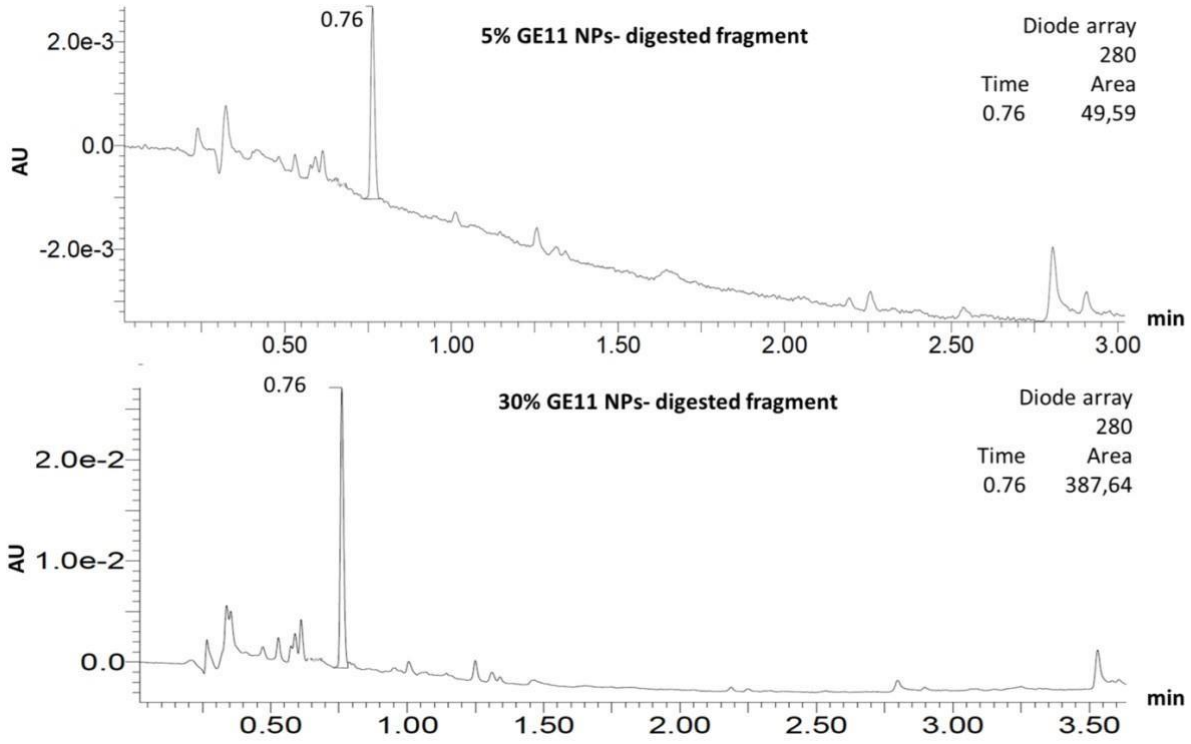

Figure A3.2. Integrated chromatograms of GE11-NPs with different surface valency. *Chromatograms with integrated area under curve values at λ=280nm obtained by UPLC-MS of peaks corresponding to digested GE11 fragment of* ***A)*** *5% GE11-NPs and* ***B)*** *30% GE11-NPs.*

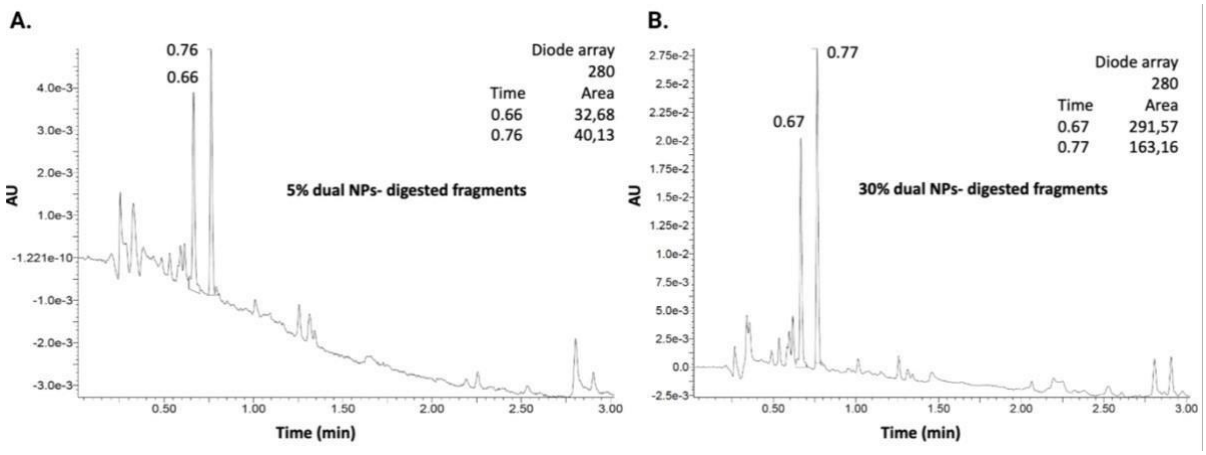

Figure A3.3 Integrated chromatograms of dual-peptide NPs having different surface valency. *Chromatograms with integrated area under curve values at λ=280nm obtained by UPLC-MS of peaks corresponding to digested fragments of both peptides of* ***A)*** *5% dual-NPs and* ***B)*** *30% dual-NPs.*

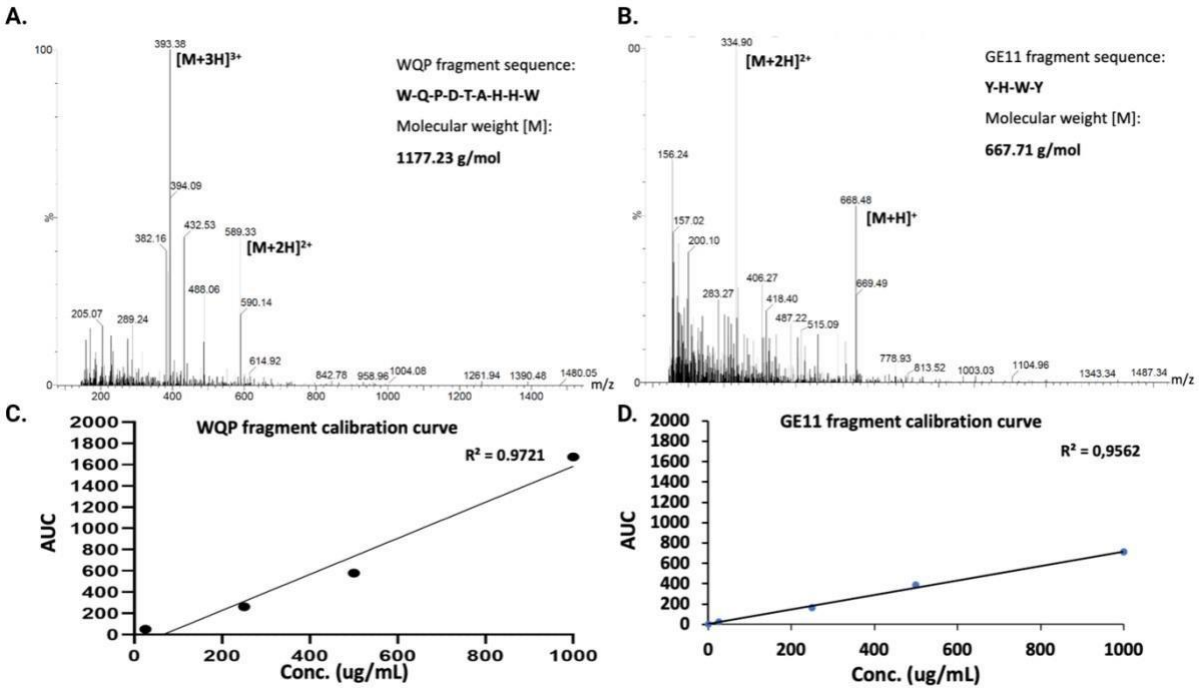

Figure A3.4 Surface characterisation by specific enzymatic digestion of 30% dual NPs. *Mass spectra of digested fragments of 30% dual-peptide NPs obtained as a ratio of its mass and charge (m/z) corresponding to* ***A)*** *WQP peptide* ***B)*** *GE11 peptide. Calibration curves were obtained by digesting fragments of known concentrations of* ***C)*** *WQP peptide and* ***D)*** *GE11 peptide to finally calculate the number of peptides on NP surface.*

Calculation of number of peptides on NP surface by enzymatic digestion:

As shown in the above figures, the digestion of single- and dual-peptide NPs having different surface valencies showed masses corresponding to the digested fragments of each peptide in the mass spectrum (Figure A3.4A and B). The peak obtained in the chromatogram at □=280nm was integrated (Figure A3.3A and B), and the area under curve value was used to calculate the concentration of individual peptides in 5% and 30% formulations, using the calibration curves (Figure A3.4C and D).

For calculation of theoretical (expected) number of peptides, we used the formula used in the previous chapters and list them in tabular form as follows:

Samples	Theoretical #peptide	Observed #peptide	Surface coverage (%)
2.5% dual WQP NPs	249	418	4,20
2.5% dual GE11 NPs	287	304	2,65
5% WQP NPs	498	410	4,12
5% GE11 NPs	574	380	3,31
15% dual WQP NPs	1494	1360	13,7
15% dual GE11 NPs	1723	1300	11,3
30% WQP NPs	2988	1730	17,3
30% GE11 NPs	3445	3110	27,1

Table A3.1 Calculation of number (#) of peptides on NP surface of single- and dual-peptide NPs having different surface valency. *For the dual-peptide formulations, the surface valency for each*

peptide is halved (since they are in 1:1 ratio), thus 5% dual NPs comprise 2.5% WQP and 2.5% GE11 as shown. The availability (valency and coverage) (%) of WQP on NP surface is calculated by dividing the number of expected versus observed WQP and getting a percentage of the formulated surface valency.

Samples	**Theoretical #peptide**	**Observed #peptide**	**Surface coverage (%)**
2.5% D-1 WQP NPs	249	283	2,84
3.75% D-2 WQP NPs	374	273	2,74
4.17% D-3 WQP NPs	415	304	3,06
4.5% D-4 WQP NPs	448	308	3,09
4.8% D-5 WQP NPs	478	244	2,45
2.5% D-1 GE11 NPs	287	313	2,73
1.25% D-2 GE11 NPs	144	112	0,97
0.83% D-3 GE11 NPs	95	56,9	0,49

0.5% D-4 GE11 NPs	57	26,7	0,23
0.24% D-5 GE11 NPs	28	1,89	0,16

Table A3.2 Calculation of number (#) of peptides on NP surface of dual-peptide NPs having different surface ratios. *For the dual-peptide formulations, the surface valency for each peptide is halved (since they are in 1:1 ratio), thus 5% dual NPs comprise 2.5% WQP and 2.5% GE11 as shown. The availability (valency and coverage) (%) of WQP on NP surface is calculated by dividing the number of expected versus observed WQP and getting a percentage of the formulated surface valency.*

Dual-NP formulations	**Expected ratio (GE11: WQP)**	**Observed ratio (GE11: WQP)**
D-1 NPs	1: 1	1: 1,04
D-2 NPs	1: 3	1: 2,83
D-3 NPs	1: 5	1: 6,17
D-4 NPs	1: 10	1: 13,3
D-5 NPs	1: 20	1: 14,9

Table A 3.3. Expected and observed stoichiometric ratios of 5% dual-NPs. *Obtained by dividing the surface coverage (%) obtained of GE11 to that of WQP for each of the formulations.*

Appendix 4

This Appendix section provides the results of a pilot study of one of the outlooks provided for this thesis: Dual peptide-based targeting in prostate tumor spheroid model. As it is a preliminary study, two main results are highlighted here. The generation and characterization of 22Rv1 tumor spheroids for their shape and viability depending on different culturing conditions is carried out, the optimization of which is finally achieved. Additionally, the formulation of dual peptide-NPs found to be the most optimal one for targeting studies using 22Rv1 cells in vitro, is tested for its selectivity using 3D tumor spheroid model using confocal imaging. Although there is a need for further optimization for uptake studies, these studies do provide a basis for understanding the role of NP surface ligand parameters for selective targeting in a more complex environment, thereby giving us a better understanding of the behavior of these systems in a model closer to an in vivo environment.

Background

Employing *in vitro* models closely mimicking the physiology of tumors offer several advantages for cancer research, enabling a better understanding of tumor biology, thus driving the rational design of potential anti-tumoral agents and drug delivery strategies. However, *in vitro* simulation of the numerous different factors and their complex interplay within the tumor environment poses some challenges. Three-dimensional (3D) tumor spheroids have gained increased attention since their development to better reproduce the *in vivo* behavior of malignant cells in comparison to the conventional two-dimensional (2D) cell cultures. Furthermore, it is now clearly established that tumors are not solely masses of abnormally proliferating cells, but rather comprise complex structures containing both cancer and healthy (or stromal) cells evolving together and embedded in an altered extracellular matrix (ECM), known altogether as the tumor microenvironment (TME). It plays a key role not only in tumor initiation, progression, and metastasis, but is also involved in therapy resistance and patients' relapse. Thus, implementing cancer models that combine 3D tumor spheroids and TME components offers a more realistic and physiological relevant context to carry tumor targeting studies *in vitro*. However, the appropriate characterisation and study of these complex models is rather challenging and requires thorough optimizations.

Here, we employed a previously developed reproducible method for generating and characterizing prostate tumor spheroids and further study their uptake of dual peptide-NPs using confocal microscopy. It provided valuable insights about the viability of cancer cells within the spheroid and their 3D architecture. In particular, our observations revealed the influence of the cell seeding density on the growth rate of the tumor spheroid. Furthermore, the uptake of dual peptide-NPs, with optimized surface peptide characteristics for targeting 2D monolayers of tumor cells, was found to be restricted to the outer layer of the spheroid, as opposed to penetrating within. This sheds light on the potential behavior of dual-peptide

NPs in a complex environment, calling for further optimizations for achieving efficient tumor penetration.

Generation and characterisation of 22Rv1 tumor spheroids:

The method of generation of the proposed 3D tumor model of 22Rv1 spheroids using ultralow attachment (ULA) plates was employed. The U-bottomed ULA plates permitted the culturing of 22Rv1 cells in a 3D configuration thanks to the inert substance coating their wells that prevented the attachment of cells to the plate surface to form a monolayer. Further, two seeding cell densities and incubation times were explored: 250 and 500 cells/well and 24 and 72h of incubation at 37ºC, 5% CO_2. Post spheroid culturing, they were embedded into collagen and seeded in an 8-well LabTek. In each case, the viability of cells was assessed using live/dead assay employing calcein/ propidium iodide (PI) and imaged using CLSM as depicted in Figure A 4.1. It was observed that the seeding density of 500 cells/well resulted in generation of a more densely compacted spheroid as compared to that from 250 cells/ well. This could be attributed to a greater number of cells resulting in higher aggressivity causing a compact spherical structure of the spheroid. Furthermore, at an incubation time of 72h, there were more cells present within the spheroid, as observed by an increase in the size of the spheroid and its compactness, in comparison to 24h of incubation. In both cases, majority of the cells were found to be viable (stained in green with Calcein AM). Thus, the parameters of 500cell/ well seeding density and 72h incubation were deemed optimal for 22Rv1 spheroid generation.

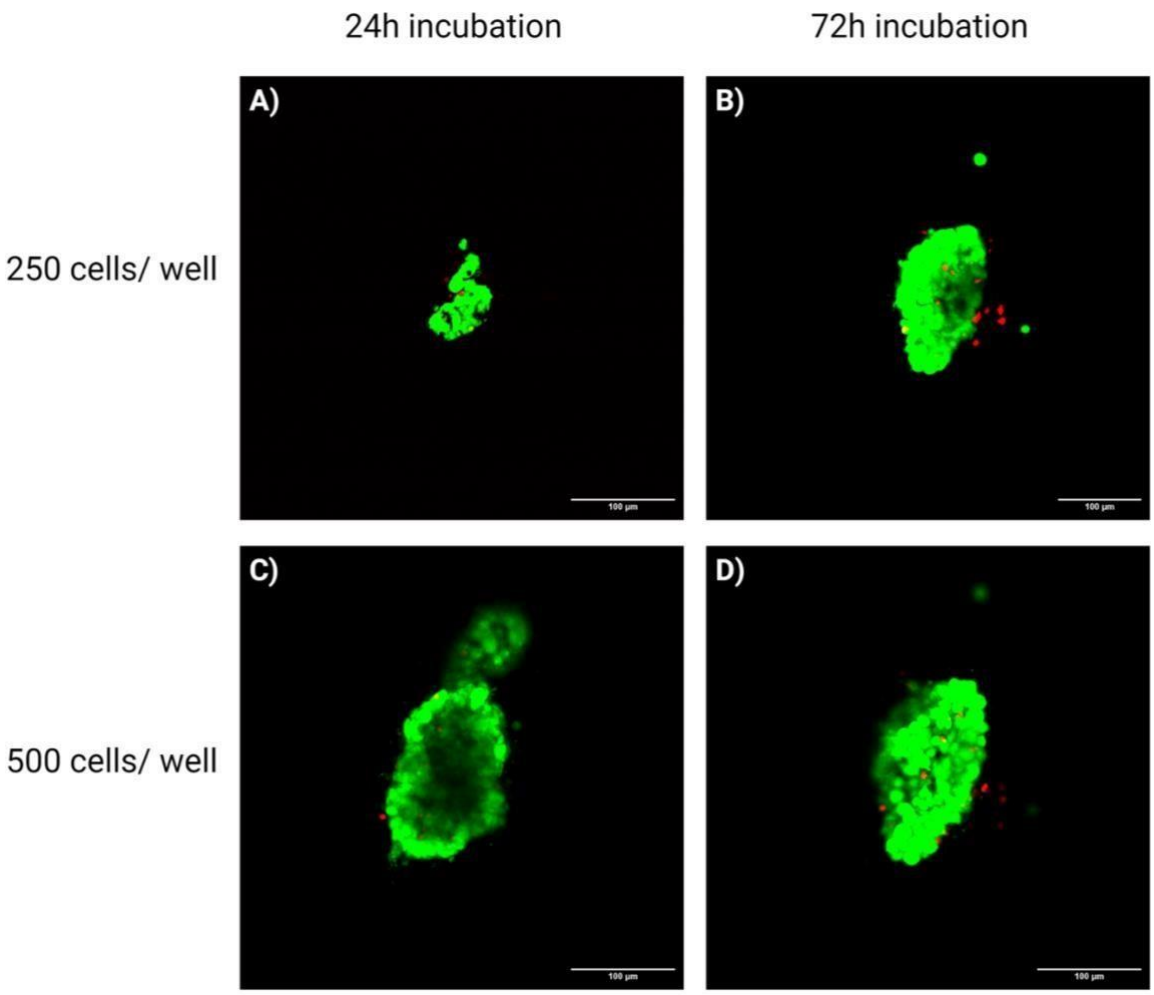

Figure A4.1 Viability characterization of generated 22Rv1 tumor spheroids by CLSM. *Representative confocal images of 22Rv1 tumor spheroids assessed for their viability using Calcein (Green) and PI (red) staining for live/dead assay with* ***A)*** *seeding density of 250 cells/well incubated for 24h,* ***B)*** *seeding density of 250 cells/well incubated for 72h, while* ***C)*** *seeding density of 500 cells/well incubated for 24h and D) seeding density of 500 cells/well incubated for 72h. Scale bar 100□m.*

<u>Uptake of dual peptide NPs in 22Rv1 tumor spheroids:</u>

For studying the uptake of previously formulated dual peptide (D-2 and D-3) NPs having 5% surface valency and surface peptide ratios of GE11: WQP as 1: 3 (D-2) and 1:5 (D-3), we incubated the 22Rv1 spheroids generated with previously optimized conditions, embedded in collagen with the same concentration of 50 g/mL of D-2 NPs for 24h at 37ºC, 5% CO_2, thus

maintaining the same conditions as those optimized for 2D cellular uptake studies. Nontagged 5% PLGA-PEG NPs were used as a negative control. Post 24h incubation, we imaged the spheroids at 37ºC, 5% CO_2 using CLSM using Z-stack feature and employed 3D projection at Y-axis using ImageJ software. As shown in Figure A4.2, at Z-stack corresponding to 100 m mean diameter, majority of the NPs, both dual peptide-tagged along with non-tagged control ones, were found along the circumference of the spheroid, with minimum/no penetration within the tumor spheroid. In case of D-2 and D-3 NPs, a higher adsorption of NPs was observed compared to the control NPs, possibly owing to the targeting from the dual peptides. However, the lack of tumor penetration could be possibly attributed to the employed ratios of peptide which offered insufficient specificity for accumulation of NPs within the spheroid, thereby shedding the light on the need for further optimizations of conditions such as surface ratios, NP concentration and incubation time for achieving selective uptake inside 22Rv1 tumor spheroids.

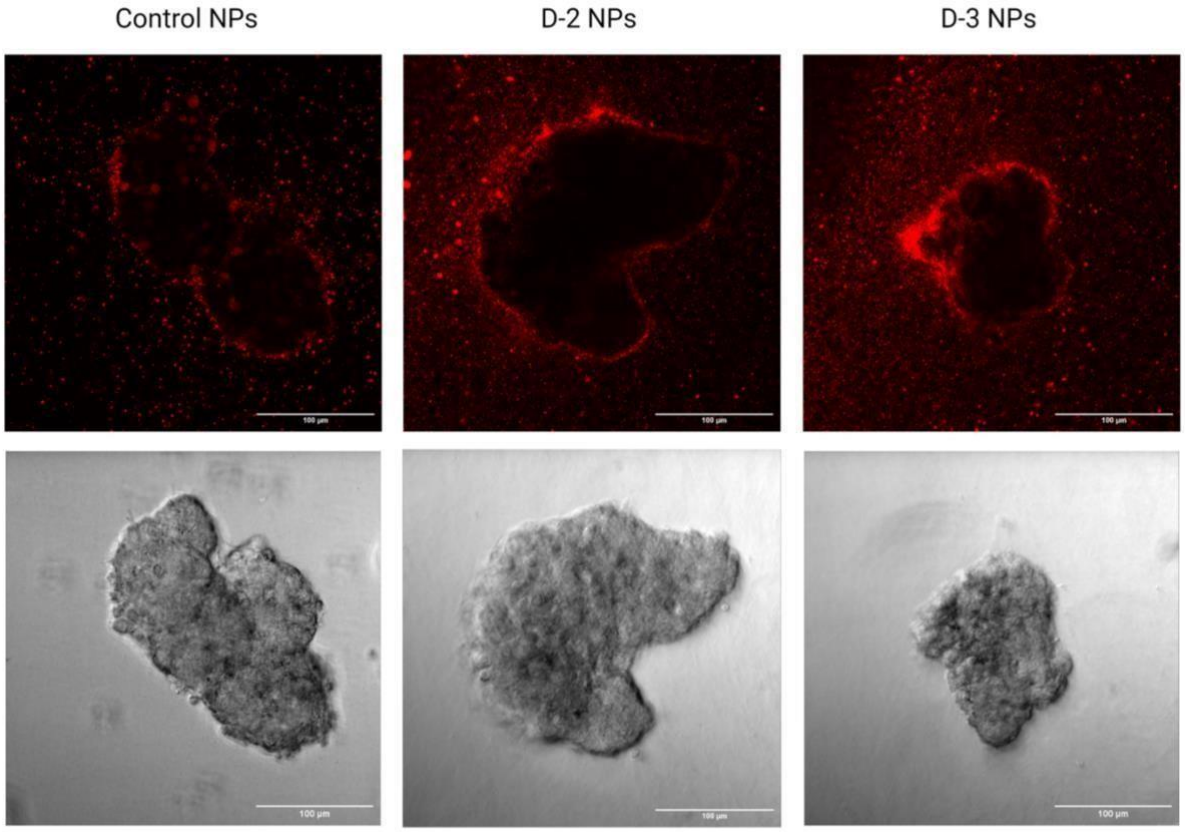

Figure A4.2 Uptake of dual peptide-NPs in 22Rv1 tumor spheroids by CLSM. *Representative confocal images of 22Rv1 tumor spheroids embedded in collagen assessed for the uptake of dual peptide (D-2 and D-3) NPs along with control (PLGA-PEG) NPs (stained with DiI-Red) post 24h incubation in the top panel with their corresponding bright field images in the bottom panel. Scale bar 100µm.*

Glossary

ACN- Acetonitrile

CE - Conjugation Efficiency

CLSM - Confocal Laser Scanning Microscopy

DAPI – 4´, 6´-diamidino-2-phenylindole

DiI - 1, 1'-dioctadecyl-3,3,3',3'-tetramethylindocarbocyanine perchlorate

DIEA – N, N-diisopropylethylamine

DLS - Dynamic Light Scattering

DMF – Dimethyl formamide

EPR- Endothelial Permeability and Retention

EDTA – Ethylenediaminetetraaceticacid

FBS - Fetal Bovine Serum

FDA - Food and Drug Administration

Fmoc/tBu - 9-fluorenylmethoxycarbonyl/tertbutyl

FMR – Ferromagnetic Resonance spectroscopy

FTIR – Fourier Transform InfraRed spectroscopy

HBTU- N,N,N´-Tertamethyl-O-(1H-benzatriazol-1-yl)uranium hexafluorophosphate, O(Benzotriazol-1-yl)-N,N,N´,N´-tetramethyluronium hexafluorophosphate.

HPLC-MS – High performance liquid chromatography/ mass spectrometry

LNCaP- Lymph Node Carcinoma of the Prostate

NMR – Nuclear Magnetic Resonance spectroscopy

NP - Nanoparticle

PCa – Prostate cancer

PC3 – Prostatic small cell carcinoma

PdI - Polydispersity Index

PEG - Polyethylene glycol

PFA - Paraformaldehyde

PI – Propidium iodide

PLGA - Poly(lactic-co-glycolic) acid **ppm**

– parts per million

RPMI-1640 – Rosewell Park Memorial Institute 1640 medium

RWPE-1 – Prostate epithelial cell line

SD – Standard deviation

TBTU - 2-(1H-Benzotriazole-1-yl)-1,1,3,3-tetramethylaminium tetrafluoroborate

TCEP - (tris(2-carboxyethyl) phosphine)

TEM - Transmission electron microscopy

ULA – Ultralow attachment

UPLC-MS – Ultra-high performance liquid chromatography/ mass spectrometry

XPS – X-ray Photoelectron Spectroscopy

ZP - Zeta Potential

Acknowledgements

The undertaking of this doctoral research has been an absolute rollercoaster ride that I will cherish in the years to come. From changing countries to facing a global pandemic, the past few years of PhD have been a goldmine of curiosity, opportunity, and a constant reminder to hold the unrelenting optimism. This work is not in any way an individual effort, but a teamwork interlaced with professional and personal encouragement from people around me, who have made this journey so memorable.

I would like to whole-heartedly thank my supervisors Silvia and Lorenzo for their constant support throughout this endeavor. Silvia, you have been a tremendous guiding force in all these years, and I cannot imagine being able to reach here without your encouragement and patience. Thank you for being so kind and welcoming, even outside the lab. Lorenzo, thank you for all the freedom and patience that allowed me to become self-reliant and of course, for giving me the opportunity to be a part of this wonderful group which feels like family. I would like to extend my deepest gratitude to my N4N group in Barcelona, for taking me in with such a warm embrace, making the move to a foreign country rather easy. My partner in science, crime, and gym, Teodora thank you for being such a wonderful colleague to share this experience with. Our travels together have been unforgettable and boisterously fun, I hope they will continue. You are an example to follow, and I wish you the best. Edgar, I am so happy that we got to do start (and end) this PhD together and to have learnt a lot from each other. I am grateful for all your help and unending (!) patience during these challenging years. Maria, you are one of the most helpful people I´ve encountered, thank you for all your support throughout these years, starting from my incorporation. Alis, your kindness and creativity are infectious, I hope you get to turn your passion for art into profession someday. Adrianna, I admire your professionalism, attention to detail, and sense of humor; it has been an interesting experience with you. Pietro and Natalia, I feel grateful having spent time, however briefly, with you. You are fantastic scientists, and I wish I could learn more from you. To N4N

Eindhoven team, thank you all for the support, encouragement, and inspiration, despite the distance. I have really enjoyed our time together, especially during the retreats, and I will always cherish the memories. I hope we get to stay in touch and wish you all the best. Outside the group, I would like to extend my warm gratitude to my fellow peers, for making my experience at IBEC so wonderful. Ines, you are one of the kindest, fierce, and most emotionally intelligent people I know. Thank you for your endless support, especially during the last months of writing, it has been very instrumental. Nimesh, your presence of mind is notable, I have really enjoyed our coffee sessions on all things science, Bangalore and Pune, they made my first months in a new city so smooth and easy. Julia, it has been a pleasure sharing the love for biology with you and learning about the intricacies of *in vivo* testing, I hope our paths cross in future, for good. To the administrative and technical staff at IBEC, PCB and UB, thank for all your support, guidance, and trust over these years. Fran, Sonia and Jaume, your sound technical knowledge of NMR, HPLC-MS and FACS, respectively, is commendable. Thank you for all the useful scientific discussions and inputs that have deeply contributed to the success of my research. Core facilities team, thank you for making life in the lab so smooth.

To my close friends scattered all over the world, thank for looking out for me, despite the distance. I deeply appreciate your valuable support and encouragement, especially during the times when things seemed bleak. I hope to see you soon. I would also like to acknowledge my Zumba family in Spain for being so open and welcoming, and for lifting my spirits and keeping me sane outside the lab and throughout the pandemic.

And lastly, none of this could have ever been possible without the unconditional support from my family. Aai and Baba, thank you for always encouraging me to carve my own path and supporting my life and career choices. I am immensely grateful for everything you have endured to make my life better. Shubhankar, your perseverance and hard work has always been so inspiring, making me strive harder, thank you for always being an example to follow. For all that has been, THANK YOU; For all that will be, YES!

Madhura.

Scientific activity

The list of publications and conference presentations from the work of this thesis are mentioned below:

Publications:

- **Murar, M.**; Albertazzi, L.; Pujals, S. Advanced Optical Imaging-Guided Nanotheranostics towards Personalized Cancer Drug Delivery. *Nanomaterials* **2022**, *12*, 399.
- **Murar, M.**; Pujals, S.; Albertazzi, L. Multivalent effect of WQP-peptide functionalized polymeric nanoparticles: towards selective targeting of prostate cancer. (*Under review in Nanoscale Advances)*
- **Murar, M.**; Pujals, S.; Albertazzi, L. A quantitative assessment of GE11 peptidemediated nanoparticle conjugation strategies: Impact on selective targeting of prostate cancer. (*Submitted to ACS Bio-conjugate chemistry).*
- **Murar, M.**; Pujals, S.; Albertazzi, L. Co-operative dual peptide-based strategy for selective prostate cancer targeting. *(To be submitted).*

Attendance to conferences with a poster or oral presentations:

- 3rd NALS (Nanomaterials applied to Life Sciences) International conference organized by Azul congresses (Santander, Spain), April 2022: ¨Co-operative dual peptide-based nanoparticle strategy for selective prostate cancer targeting¨. (Oral presentation).
- IBEC PhD Discussions (Barcelona, Spain) May 2022: ¨Co-operative dual peptide-based nanoparticle strategy for selective prostate cancer targeting¨. (Oral presentation).

- 2nd Material Science and Nanotechnology Conference, organized by Materials Research Society (MRS) (Virtual) December 2021: ¨Peptide based strategies for selective prostate cancer targeting using polymeric nanocarriers¨. (Oral presentation).
- International conference on Bio-inspired materials, organized by Nature journals, (Virtual) November 2021: ¨Peptide based strategies for selective prostate cancer targeting using polymeric nanocarriers¨. (Oral presentation).
- 14th IBEC Annual Symposium. (Virtual) October 2021: ¨Peptide based strategies for selective prostate cancer targeting using polymeric nanocarriers¨. (Poster presentation).
- 13th IBEC Annual Symposium. (Virtual) October 2020: Active targeting nanoparticles for personalized prostate cancer therapy¨ (Poster presentation).
- NanoBio&Med conference. (Barcelona) November 2019: ¨Multifunctional nanoparticles for personalized cancer therapy¨ (Poster presentation).
- 12th IBEC Annual Symposium. (Barcelona) July 2019: ¨Multifunctional nanoparticles for personalized cancer therapy¨ (Poster presentation).
- 11th IBEC Annual Symposium. (Barcelona) October 2018: (Poster presentation).

Curriculum Vitae

Madhura Murar was born on 26th September 1992 in Mumbai, India. She completed her BSc Biotechnology from University of Pune (2013). During this time, she was awarded with an undergraduate research scholarship to carry out her thesis project titled ´Effect of TiO_2 nanoparticles on multi-drug resistant *Pseudomonas aeruginosa´* at Department of Biotechnology, Pune university. She obtained her MSc Biotechnology degree in 2016 from Symbiosis International University Pune, India, during which she carried out her master thesis titled ´Structural studies on DOCK6

protein: Implications in cancer biology´ for six months at National Chemical Laboratory (NCL), Pune, India. She then joined National Centre for Cell Sciences (NCCS), Pune, India as a research assistant in the laboratory of Structural biology (2016-2017). In 2018, she received the International PhD fellowship and moved to IBEC, Barcelona to pursue a PhD in Nanosciences in the group of Nanoscopy for Nanomedicine on development of peptide functionalized nanocarriers for selective targeting of prostate cancer. The most significant results of her research are presented in this thesis.